

Aus dem Max-Planck-Institut für Hirnforschung
in Frankfurt am Main

The Neural Substrate of the Eureka Effect

vom Fachbereich Biologie der Technischen Universität Darmstadt
zur Erlangung des akademischen Grades
eines Doctor rerum naturalium
(Dr. rer. nat)

Dissertation von
Yiqing Lu
aus Zhejiang, China

1. Referent: Prof. Dr. Ralf Galuske
2. Referent: Prof. Dr. Bodo Laube
3. Referent: Prof. Dr. Wolf Singer

Darmstadt 2018

Yiqing Lu: The Neural Substrate of the Eureka Effect

Darmstadt, Technische Universität Darmstadt,

Jahr der Veröffentlichung der Dissertation auf TUPrints: 2018

URN: urn:nbn:de:tuda-tuprints-82185

Tag der mündlichen Prüfung: 16.11.2018

Veröffentlicht unter CC BY-NC-ND 4.0 International

<https://creativecommons.org/licenses/>

Summary

The Eureka effect, also known as Aha effect, insight or epiphany, refers to the common experience of suddenly solving a problem. Here we study this effect in a pattern recognition paradigm that requires the segmentation of complex scenes and recognition of objects on the basis of Gestalt rules and prior knowledge. In the experiments both sensory evidence and prior knowledge were manipulated in order to obtain trials that do or do not converge towards a perceptual solution. Subjects had to detect objects in blurred scenes and signal recognition with manual responses. Neural dynamics were analysed with high density Electroencephalography (EEG) recordings. We determined changes in spectral distribution, coherence, phase locking and fractal dimension. The Eureka effect was associated with increased coherent oscillations in the alpha and theta band over widely distributed regions of the cortical mantle predominantly in the right hemisphere. This increase in coherence was associated with a decrease of beta band activity over parietal and central regions, and with a decrease of alpha band activity over frontal and occipital areas. In addition, there was a lateralized reduction of fractal dimensionality for activity recorded from the right hemisphere. These results suggest that the transition towards the solution of a perceptual task is mainly associated with a change of network dynamics in the right hemisphere that is characterized by enhanced coherence and reduced complexity. We propose that the Eureka effect requires cooperation of cortical regions involved in working memory, creative thinking and the control of attention.

Zusammenfassung

Der Heureka Effektes, auch bekannt als Aha-Effekt oder Moment der Einsicht, beschreibt die subjektive Erfahrung einer plötzlichen Problemlösung. In der vorliegenden Untersuchung haben wir diesen Effekt anhand eines Mustererkennungs-Paradigmas untersucht, welches die Segmentierung komplexer Szenen, sowie das Erkennung von Objekten auf Basis von Gestalt-Prinzipien und Vorwissen erfordert. In den durchgeführten Experimenten wurden sowohl sensorische Evidenz, als auch das Vorwissen der Probanden so manipuliert, dass die perzeptuelle Lösbarkeit eines Reizes kontrolliert werden konnte. Im Experiment sollten Probanden Objekte in verschwommen Szenen erkennen und dieses Erkennen rückmelden. Dabei wurde die neuronale Dynamik mittels Elektroencephalographie (EEG) untersucht, um Veränderungen im Frequenzspektrum, in der Kohärenz, in der Phasenkongruenz und der fraktalen Dimensionalität zu quantifizieren. Dabei war der Eureka-Effekt mit erhöht kohärenter Aktivität im Alpha- und Theta-Band in weiten Regionen des Kortex, vor allem aber rechts-hemisphärisch, assoziiert. Die Zunahme der Kohärenz war dabei mit einer Abnahme der Aktivität im Beta-Band über parietalen und zentralen Regionen, sowie mit einer Abnahme der Aktivität im Alpha-Band über frontalen- und okzipitalen Regionen, assoziiert. Zusätzlich zeigte sich eine Reduktion der Lateralisierung der fraktalen Dimensionalität in der rechten Hemisphäre. Dies Ergebnisse legen nahe, dass ein Übergang in Richtung der Lösung einer perzeptuellen Aufgabe hauptsächlich mit einer Veränderung der Netzwerkdynamik, charakterisiert durch erhöhte Kohärenz und reduzierte Komplexität, der rechten Hemisphäre in Verbindung gebracht werden kann. Der Eureka-Effekt erfordert vermutlich die Koordination verschiedener kortikaler Regionen, die in Arbeitsgedächtnis, kreatives Denken und Aufmerksamkeitskontrolle involviert sind.

Table of Contents

Summary.....	1
Zusammenfassung.....	2
Table of Contents	3
1. Introduction.....	5
2. Materials and Methods.....	13
The selection of images	13
The procedure of manipulating the images.....	13
Participants.....	15
Visual stimuli	15
The recognition task (Experiment 1)	16
Selection of the suitable cut-off frequency for the image low-pass filter.....	17
The experimental task during EEG recording (Experiment 2)	18
Data acquisition	19
Behavioral analysis	20
Data analysis	20
Pre-processing.....	21
Spectral analysis.....	21
Coherence	22
Phase locking value (PLV)	24
Laterality index (LI).....	24
Dimensionality	25
Statistics	25
3. Results	27
The recognition of images with diverse degradation levels (Experiment 1)	27
The behaviour during the Eureka effect (Experiment 2)	29
Alpha band activity	31
Theta band activity.....	44
Beta band activity	51

Gamma band activity	54
Fractal dimensionality.....	54
Pupil size.....	57
Supplemental Figures.....	61
4. Discussion.....	77
Methodological considerations	77
The Eureka effect and gamma band.....	79
Right-hemisphere lateralized alpha and theta activity	79
Dissociation between alpha power and alpha phase locking	81
Right-hemisphere lateralized reduction of dimensionality	81
Decrease of beta activity	82
5. Conclusions and future directions.....	84
Bibliography	85
List of Abbreviations	98
List of Figures.....	99
Acknowledgements	102
Lebenslauf.....	103
Ehrenwörtliche Erklärung.....	104

1. Introduction

Nervous systems need to be able to distinguish activity patterns associated with the search for the solution of a computational problem from those representing a result. This distinction is necessary in order to terminate further search, to eventually convert the result into action, to permit synaptic plasticity for the storage of results, to allow initiation of a new search process and to permit access of results to awareness. Vertebrates seem in addition capable of judging the reliability of a particular result and to experience solution states as rewarding. It is pleasant to suddenly arrive at the solution of a perceptual problem, to understand a previously incomprehensible concept or to solve a puzzle. This sudden transition from searching for a solution to having found the solution has been termed one-shot learning, Aha experience, insight, epiphany, or Eureka effect (Kaplan and Simon, 1990; Sternberg and Davidson, 1995; Ahissar and Hochstein, 1997; Kounios and Beeman, 2014). Conditions inducing Eureka effects include verbal riddles (Shen et al., 2013; Zhao et al., 2013), matchstick arithmetic (Knoblich et al., 1999; Chi and Snyder, 2011), anagrams (Vartanian and Goel, 2005; Aziz-Zadeh et al., 2009), rebus puzzles (Luo et al., 2004), remote associates test (Mednick, 1962), and so on. The Eureka effect is often associated with the sudden availability of additional information that then triggers the insight. Some famous anecdotes of the Eureka effect include Archimede's discovery of how to measure the density of the king's crown, Newton's gravitational theory inspired by a falling apple and Kekule's sudden insight into the structure of the benzol ring after having dreamt of a snake biting its tail.

The Eureka effect can include the following features: mental impasse, restructuring, deeper understanding, and suddenness (Sandkuhler and Bhattacharya, 2008; Sprugnoli et al., 2017).

1) Mental impasse – During the process of problem solving, the solver becomes mentally stuck and unable to reach an answer, the mental block resulting from an overload of information provided by perception, memory, imagination, and logical reasoning (Bowden et al., 2005; Bowden and Jung-Beeman, 2007).

2) Restructuring – This process requires the retrieval of information from long-term memory and external cues. This convergence of information is necessary for the Eureka effect to occur. Whether this recombination of information occurs at the level of conscious or subconscious processing is an unresolved question (Ohlsson, 1984; Ansburg and Dominowski, 2000; Cunningham et al., 2009; Cranford and Moss, 2012).

3) Deeper understanding – The problem solving strategy leading to the Eureka effect involves deeper understanding, rather than merely a normal solution. This “understanding” can refer to the gain of internal solutions from the brain and/or the perception of external complicated stimuli from the environment (Dominowski and Dallob, 1995; Chu and MacGregor, 2011).

4) Suddenness – The Eureka effect occurs suddenly, and often unpredictably (Metcalf, 1986; Kounios and Beeman, 2014).

However, very little is known about the neuronal underpinnings of the Eureka effect. One of the reasons is that it is hard to predict under which circumstances and exactly when the Eureka effect occurs. Investigations of the Eureka effect are fraught with several methodological problems. First, measurements need to be performed with high temporal resolution because the moment when the Eureka effect occurs is often

unpredictable. Second, neurophysiological studies require sufficient and repeatable trials for analysis. Hence, the traditional strategies for triggering the Eureka effect, such as the Duncker Candle problem (Duncker, 1945; Fleck and Weisberg, 2004), the Nine-dot problem (Maier, 1930; Chein et al., 2010), and the Matchstick arithmetic problem (Ollinger et al., 2008), are inappropriate for neurophysiological studies of the Eureka effect because of the very limited number of trials in these tasks (Bowden et al., 2005). Consequently, several paradigms have been introduced to cope with the volatile nature of the Eureka effect. Riddles have been used because there are many of them and hundreds of trials can be completed in one experiment (Shen et al., 2013; Zhao et al., 2013). Another paradigm that resembles riddles is the remote associates test (RAT) (Mednick, 1962; Razumnikova, 2007; Cerruti and Schlaug, 2009). According to Mednick, ideas, knowledge, and experiences reside in a highly connected network and creativity results from the establishment of novel associations that eventually lead to the Eureka effect. Thus, creativity reflects the ability to combine “remote” nodes of the network. The Eureka effect can be induced by RAT. Each item of RAT includes three words that can be associated with a solution word in different ways. Participants must consider remote information which is connected to all three words and figure out the appropriate answer word. Here is an example: three remote items are “river”, “note” and “account”; the solution is “bank”. The RAT is still commonly used to study problem solving and creative thinking. Sandkuhler and Bhattacharya, 2008, combined the RAT with Electroencephalography (EEG) recordings and observed increased gamma power in parieto-occipital regions, increased alpha power in right temporal regions for trials with hint presentation, and decreased alpha power in the right prefrontal area for trials requiring extensive restructuring. In another RAT study, insight was found to be associated with increased hemodynamic activity and increased gamma power in the

right anterior superior temporal gyrus, and increased alpha power over the right posterior parietal cortex (Jung-Beeman et al., 2004).

However, the RAT paradigm has the disadvantage that it is difficult to control the time of occurrence of the Eureka event. Researchers therefore turned to visual paradigms which have been thoroughly studied in psychology and cognitive science. These paradigms have in common that manipulation of sensory evidence or prior knowledge leads to sudden solutions of perceptual problems. The advantage of these paradigms is that they can be controlled more precisely than non-visual paradigms, both temporally and spatially. Here, we list some of them:

1) White noise – The visibility of figures is gradually modified by varying the intensity of added noise. (James et al., 2000; Melloni et al., 2011; Mayer et al., 2016).

2) Panels – Long vertical panels covering images are gradually shrunk to more fully reveal underlying objects (James et al., 2000).

3) Dots – The original images were transformed to dot arrays. Subsequently, the perception of objects could be manipulated by varying the distribution of dots (Moca et al., 2011).

4) Blobs and shadow images – A more complicated visual degradation algorithm was introduced by Eger et al., 2007. In their algorithm, each image is subdivided into a 20 by 20 grid and the grid is then blurred by a Gaussian filter. The degradation level at which the image became identifiable was determined and fitted with an exponential function. Hence the stimuli used in this experiment resemble a mixture of blobs and shadows.

5) Mooney images, including Mooney faces – Black and white two-tone images

(Dolan et al., 1997; Tallon-Baudry and Bertrand, 1999; McKeeff and Tong, 2007; Giovannelli et al., 2010; Castelhana et al., 2013). The most interesting feature of Mooney images is that they are initially difficult to interpret, but can eventually lead to a stable percept of objects. This percept can also be facilitated by cues, which usually consist of original images (color or grayscale images) of the Mooney images (Hsieh et al., 2010; Goold and Meng, 2016). An example of a Mooney image is illustrated in Figure 1-1. This figure initially appears only has a bunch of black and white blobs and streaks. If you cannot recognize the object, please redirect your attention to Figure 1-2 (this is the relevant cue for Figure 1-1). It is easy to recognize an object in Figure 1-2. To achieve the correct answer, turn back to Figure 1-1. At this moment, the hidden object may become evident. The prior experience obtained from Figure 1-2 improves the perception of the seemingly “meaningless” stimuli in Figure 1-1.



Figure 1-1. Black and white image of a blurred stimulus. Please refer to page 11 for the related grayscale image in Figure 1-2.

In the present study, we applied Mooney images as the paradigm to induce the Eureka effect. There are advantages to use Mooney images. First, as a visual stimulus, Mooney images permit precise manipulations of parameters such as luminance, contrast, size, and pixels. Second, Mooney images can contain natural objects and complex backgrounds. The natural and complex stimuli allow induction of strong Eureka effects and highlight corresponding features of neural activity. To precisely manipulate Mooney images and to induce strong Eureka effects, we designed and fine-tuned a Mooney paradigm (experiment 1).

How are ambiguous inputs from Mooney images transformed to unambiguous perceptual solutions? It is suggested that prior experience, stored in memory, is used to modulate peripheral processing in order to facilitate scene segmentation, perceptual grouping and recognition (Dolan et al., 1997; Gorlin et al., 2012). The Bayesian hypothesis of perception posits that internal information, made available by top-down control is matched with external evidence (Kersten et al., 2004). Thus, the brain is assumed to perform a probabilistic inference that can optimize sensory information to minimize the mismatch between internal and external information. This function can be interpreted as perceptual closure which refers to the comprehensive perception of a degraded stimulus by completing missing parts (Grutzner et al., 2010). An example is the Gabor contour integration task, which creates a percept of an oval contour out of Gabor patches (van Stijn et al., 2016). As shown in Figure 1-3, a subset of Gabor elements can be rotated to create a closed figure. In this task, participants experience a sudden transition from searching for an oval contour to its identification. How can a group of elements form a complete recognition of an object? It has been suggested that objects are represented by simple components (Biederman, 1987). To recognize objects, the neural activities coding for component features need to be bound together. One proposal is that this is achieved through synchronization to transiently form a

coherently active assembly of neurons that generates the perception of a complete object (Singer and Gray, 1995).



Figure 1-2. The grayscale image. This is the cue of Figure 1-1.

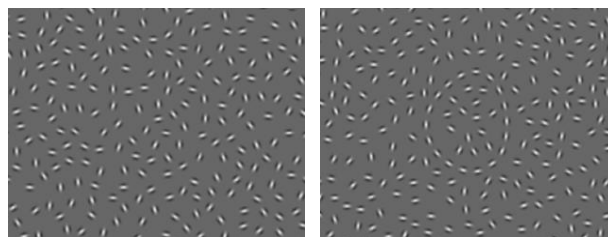


Figure 1-3. Gabor elements without (left) and with (right) a figure closed contour. Adapted from van Stijn et al., 2016.

Given that neural oscillatory and synchronized activities within and across cortical areas are associated with feature integration and perception (Gray et al., 1989; Singer, 1999; Sehatpour et al., 2008; Fries, 2009; Hipp et al., 2011; Volberg et al., 2013), we wondered whether and if so, how oscillatory and synchronized activities are involved in the Eureka effect. We hypothesized that solution states might be associated with enhanced coherence of neuronal activity as they are likely to result from successful

integration of distributed computational results. To examine this hypothesis, we designed a second experiment in which we presented Mooney stimuli identified as appropriate for the induction of the Eureka effect in the first experiment, captured neural activity with high density EEG recordings and then investigated how these neuronal responses were modulated during the Eureka effect.

The brain can be considered as a complex system with non-linear dynamics and hence parameters taken from complexity theory can be used to describe state transitions (Sporns et al., 2004; Bullmore and Sporns, 2012). We therefore also determined variables such as variance and dimensionality to characterize the phase transitions associated with the Eureka effect. One of these measures is fractal dimensionality (Nikolic et al., 2008).

The Eureka effect is associated with feelings of surprise and satisfaction, suggesting the involvement of the reward system. Somehow, the brain seems to be able to evaluate its internal state and to distinguish activity patterns associated with the search process from those representing a result. These result states in turn become associated with positive emotions such as happiness, ease, and certainty (Shen et al., 2016). These emotions are associated with changes in arousal and pupil diameter (Partala and Surakka, 2003; Bradley et al., 2008). Given that the Eureka effect goes along with surprise and positive emotions, we also measured pupil diameter as it reflects directly arousal and the balance between the cholinergic and noradrenergic modulatory projections (Murphy et al., 2011; Reimer et al., 2016). Recent evidence indicates that changes in pupil size are correlated with distinct brain states, neural responsiveness and behavioral performance (Reimer et al., 2014; McGinley et al., 2015a; McGinley et al., 2015b; Vinck et al., 2015). Thus, brain states can be tracked by pupil size (Reimer et al., 2016).

2. Materials and Methods

The selection of images

The original images used for the construction of the stimuli were taken from the Caltech-256 Object Category Dataset (<http://authors.library.caltech.edu/7694/>) (Griffin et al., 2007) and Flickr. More than 30,000 images were included in our initial database. We then manually chose images for further testing according to the following criteria. 1) Familiarity: we chose ordinary objects, such as animals, plants, furniture, tools, instruments, vehicles, and so on, 2) Natural and complex background: the images were taken from natural scenes, the target objects being embedded in a complex background, which can render identification difficult.

The procedure of manipulating the images

The original images were first converted to 256-level grayscale images. As the distribution of grayscale pixels varied widely and was non-normal and as luminance levels and contrast also differed, adjustments were required. Luminance and contrast were equated with histogram equalization which generates even contrast distributions (Lim, 1990).

To create Mooney images with different degradation levels, we applied a frequency-domain Gaussian filter on the grayscale images processed according to the methods described above (Haddad and Akansu, 1991). With this filter, the lower the cut-off frequency was, the harder it is to recognize the object in an image. The filters were

generated in three processing steps: 1) The spatial domain of the original image $f(x,y)$ is transformed to the frequency domain $F(u,v)$ by Fourier transformation; 2) $F(u,v)$ is this transform is low-pass filtered with a set cut-off frequencies to obtain a band passed representation $G(u,v)$; 3) $G(u,v)$ this representation is then transformed back to the spatial domain $g(x,y)$ (i.e. the blurred image) by an inverse Fourier transformation. In order to obtain images with different degradation levels, the low-pass filter was varied between a cut-off frequencies ranging from 10 Hz to 80 Hz (10 Hz per interval). The median gray level of each image was then chosen as the divide for the assignment of black or white pixels to the respective gray levels in order to obtain two tone Mooney images.

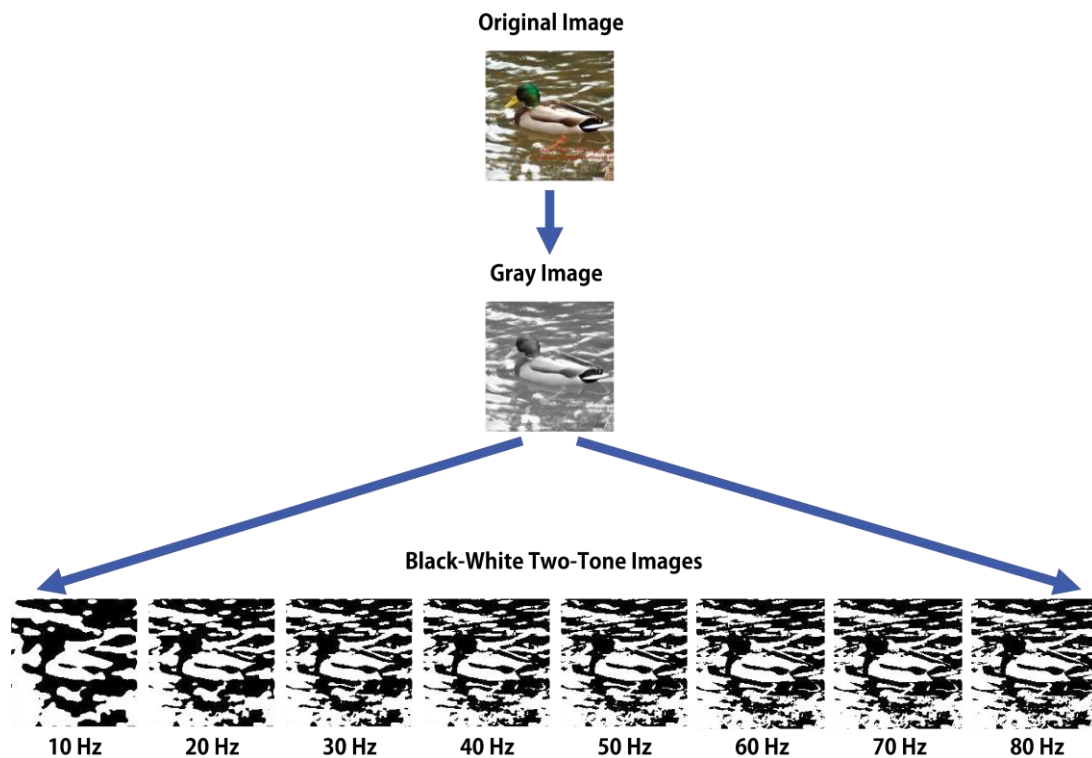


Figure 2-1. The procedure of image manipulating. The numbers of Hz represent the cut-off frequencies of the corresponding low-pass Gaussian filter.

Participants

Experiment 1: ten healthy subjects (Age 25.3 ± 1.3 y. Five males, 5 females). Experiment 2: twenty-nine healthy subjects (Age 25.2 ± 4.0 y. Sixteen males, 13 females). In the behavioral analysis of Experiment 1, all of the ten subjects were included. In the behavioral analysis of Experiment 2, twenty-five subjects were included, and four subjects were rejected due to insufficient correct responses. In the EEG analysis of Experiment 2, twenty-two subjects were included, and seven subjects were rejected due to insufficient valid data because of artefact rejection and insufficient correct responses. No subject took part in both experiments. All subjects were naïve to the experiment, were right-handed, had normal or corrected-to-normal vision and had no history of neurological or psychiatric disorders. They gave written informed consent before the experiment. The study was conducted in accordance with the Declaration of Helsinki. The subjects were recruited from local universities and got paid 15 Euro per hour for their participation.

Visual stimuli

Presentation® (Version 10.3, NeuroBehavioral Systems) was used for stimulus presentation and response collection. All stimuli were generated using MatLab. The stimuli were displayed as 150 x 150 pixel matrices at the center of a monitor screen with a refresh rate of 60 Hz and located 70 cm from the subjects' eye plane, subtending a visual angle of 4.4° , surrounded by gray background, with a gray level of 0.5 on a grayscale of [0, 1].

The recognition task (Experiment 1)

To select the appropriate low-pass spatial frequency for inducing the Eureka effect, the Mooney images were filtered at different spatial frequencies and then tested for the degree to which they were recognizable. The lower-frequency filtered images were more difficult to recognize. Hence they were arranged earlier in each trial than those with higher frequencies. Each trial contained 8 Mooney images (derived from one original image) with cut-off frequencies from 10 Hz to 80 Hz. Each Mooney image was presented for 2 seconds, at the center of the screen. If the subject could not identify the object within 2 s (button was not pressed), the next image would appear (i.e., if the subject could not identify the 10 Hz object, then the 20 Hz object would appear; then 30 Hz, 40 Hz, until the last one at 80 Hz).. Whenever the subject could identify the object in the image, they had to press the 'Yes' button as soon as possible. If the subject was unable to identify the 80 Hz object, the trial was aborted. Figure 2-2 shows the task procedure.

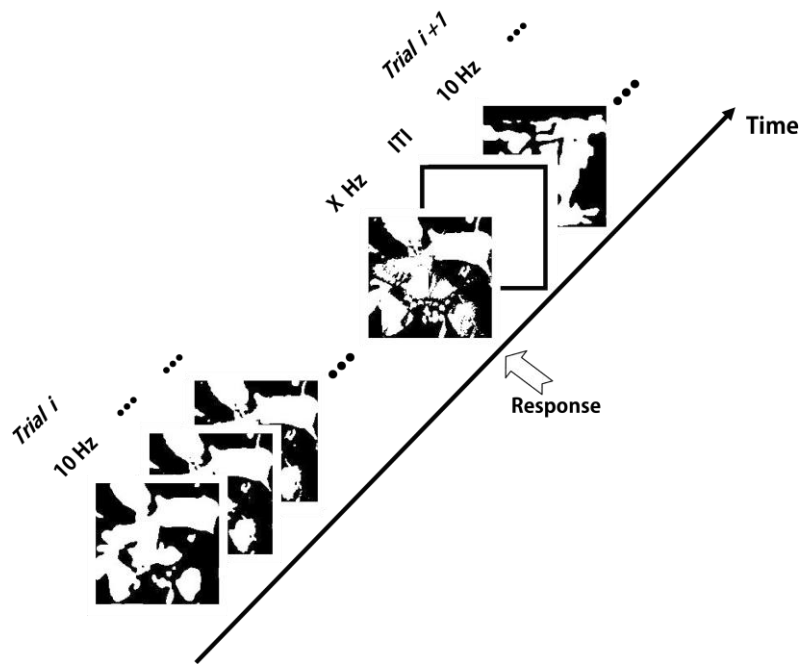


Figure 2-2. The recognition task stimulus (Experiment 1). Here, “*Trial i*” represents one trial. The 10 Hz filtered image was first presented for 2 seconds; then the 20 Hz filtered image for 2 seconds, and so on. The stimulus sequence was with the cut-off frequencies: 10 Hz, 20 Hz, 30 Hz, 40 Hz, 50 Hz, 60 Hz, 70 Hz and 80 Hz. When subject was able to recognize the object (it is a butterfly in this example), gave response as soon as possible. The “X Hz” in the figure illustrates the cut-off frequency from which the subject could recognize the object. There were inter-trial intervals (ITI), each lasted for one second.

Selection of the suitable cut-off frequency for the image low-pass filter

There are two conflicting requirements for the selection of the suitable cut-off frequency of the image low-pass filter. On the one hand the identification must be difficult enough to require cognitive resources, on the other hand the subjects must experience sufficient success to remain motivated and to exhibit the Eureka effect. According to the results from Experiment 1, 3.1% of the images can be recognized with 10 Hz cut-off frequency, which we considered to be too low to maintain high attention. And 10.6% of the images could be recognized with 20 Hz cut-off frequency

(the former 3.1% of the images are not included) (Figure 3-2). Because the images with 20 Hz cut-off frequency are easier to identify than those with 10 Hz cut-off frequency, we assumed that the former 3.1% of the images can also be recognized with 20 Hz cut-off frequency. So in total $3.1\% + 10.6\% = 13.7\%$ of the images should have been identifiable with a 20 Hz cut-off frequency, implying that subjects can recognize one image in approximately seven images (13.7%). This should have been sufficient to maintain the attention of subjects while being difficult enough to produce a Eureka effect. We therefore opted for a 20 Hz cut off frequency for all stimuli.

The experimental task during EEG recording (Experiment 2)

For each subject, 160 stimuli were used. At the beginning of each trial, a fixation cross was presented on gray background with a randomized duration between 2s and 3s. Then, a Mooney image was displayed for 8 s (We address this Mooney image presentation as the *first stage* of a trial). If the subject could identify the object in the image, they had to press the button “Yes” as soon as possible during this 8 s interval which terminated the trial. If they could not identify the object in the 8 s, the Mooney image disappeared. Then, a grayscale image appeared after a random interval of 1.5 s - 2 s. This image lasted for 4 s. In 50% of the trials, the grayscale images were congruent with the last Mooney images and served as cue for the subsequent identification. In the other 50% of the trials, they were incongruent (We address this grayscale image presentation as the *second stage* of a trial). Once the grayscale image had disappeared, the last Mooney image appeared again after a random interval of 2 - 3 s (We address this repeated Mooney image presentation as the *third stage* of a trial). At this third stage, subjects had to press the button “Yes” or “No”, indicating whether or not they could identify the object in the Mooney image. If subjects responded with a prompt “Yes” in the matching trials, we took this as evidence that they had experienced a Eureka effect, the sudden recognition of a pattern that they had been

unable to identify in the first stage. Figure 2-3 illustrates the task procedure. If the grayscale image was congruent with the Mooney image, the initially meaningless black and white contours could suddenly be bound into a clear percept, reflecting the information restructuring process of the Eureka effect. As the stimuli presented in the first and third stage were identical, we interpret any differences in the electrographic responses as related to the Eureka effect. Prior to the experiment, a training session with a different set of images was performed in order to allow each subject to practice. The order of trials and the order of experimental conditions were randomized.

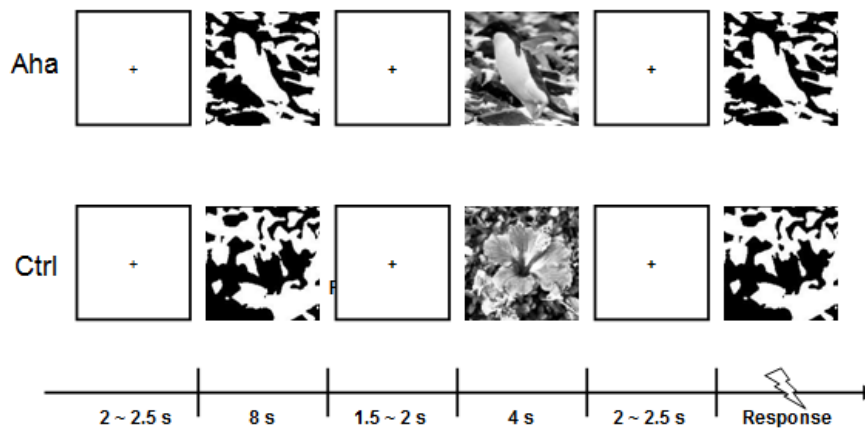


Figure 2-3. The procedure of Experiment 2. The upper row shows an example of Eureka (Aha) trials which were composed of grayscale images and their congruent Mooney images. The lower row shows an example of Control (Ctrl) trials which are composed of grayscale images and incongruent Mooney images.

Data acquisition

The experiment was implemented in an electrically shielded, sound-attenuated, dark room. Subjects watched the monitor which was outside the room through an electrically shielded window. The EEG was recorded with a HydroCel Geodesic

Sensor Net 130 (HCGSN) with 128 channels (Electrical Geodesics, Inc.). The electrodes were spaced over the head following the instructions. Data were sampled at 1000 Hz. Electrode impedances were kept <50 k Ω . Data were digitally saved on a Mac system for off-line analysis. EyeLink 1000 (SR Research Ltd.) was used in parallel to record eye movements and pupillary responses. This system is based on an infrared camera and a pattern recognition software that tracks diameter and position of the pupil. These data were recorded at a rate of 1000 Hz.

Behavioral analysis

In experiment 1, the degradation level at which each object could be identified was recorded. For each degradation level, we then calculated the percentage of correct identifications. The degradation criteria used in experiment 2 were selected from the result of experiment 1 in order to induce Eureka effect. In experiment 2, response across all stages of the trial were recorded. Then we subdivided trials into two groups: An Eureka group (Aha) and a control (Ctrl) group. The Aha group consisted of trials (with congruent cue) and “Yes” responses at the third stage. The Ctrl group consisted of trials (with incongruent cue) and “No” responses at the third stage. Trials that did not meet these requirements were discarded from further analysis. We then compared the distributions of reaction times (RTs) for trials of the two groups.

Data analysis

All EEG data was analyzed using the MatLab toolboxes Fieldtrip (Oostenveld et al., 2011), EEGLAB (Delorme and Makeig, 2004), and our customized scripts. All pupil size data was analyzed using our customized scripts.

Pre-processing

The continuous EEG signal was high-pass filtered (0.3 Hz) and notch filtered (50Hz). The filtered signal was then segmented into a series of 2 - 10 s long trials (dependent on the reaction time). Each trial segment started 1 s before the onset of the third stage, and ended 1 s after the response during the third stage. The semi-automatic artefact rejection was supplemented by visual inspection, Fieldtrip scripts and independent component analysis (ICA) to detect electrode drifts, eye movements, electromyographic and electrocardiographic interference (Bell and Sejnowski, 1995; Amari et al., 1996; Lee et al., 1999; Anemuller et al., 2003). Rejected channels were interpolated using spherical splines. To avoid contamination of neural activity induced by stimulus onset rather than Eureka effects, only the trails with reaction times longer than 0.5 s were analyzed.

Spectral analysis

Time-frequency distributions were computed using the fast Fourier transform (FFT) (Frigo and Johnson, 1998) with 5 cycles per time-window and variable width of frequency smoothing depending on the frequency, between 30 and 100 Hz, in 1 Hz steps. The FFT was also performed with 7 cycles per time-window and a Hanning taper, between 1 and 30 Hz, in 1 Hz steps. For baseline correction, a time period after stimulus onset of the first stage was used that had the same length as the analysis window used in the third stage, whose duration was determined by the respective reaction time. Finally, we calculated grand averages for each condition and participant.

Coherence

Brain networks are defined both anatomically and functionally. Given the high degree of anatomical connectedness among processing streams, any cognitive and executive task requires fast and flexible formation of functional networks. One suitable measure for functional connectivity is coherence (Rosenberg et al., 1989). It takes into account both phase and amplitude components of signals and provides information about the functional coupling of network nodes. We therefore calculated coherence in specific frequency bands in selected time windows using two different methods.. First, coherence was calculated between 20 electrode positions (Fp1, Fp2, F7, F3, Fz, F4, F8, T3, C3, E55, C4, T4, T5, P3, Pz, P4, T6, O1 and O2). This resulted in 190 coherence values. Second, coherence was calculated between clusters of channels which were selected depending on their positions. Ten clusters were formed according to the proposal by Marie and Trainor, 2013. The clusters cover left frontal (LF), left central (LC), left parietal (LP), left temporal (LT), left occipital (LO), right frontal (RF), right central (RC), right parietal (RP), right temporal (RT), and right occipital (RO) areas (Figure 2-4).

Each cluster included 9 or 10 channels. Coherence values for each cluster pair therefore represent the average coherence of all channel pairs crossing the two clusters. Ten clusters yield 45 cluster pairs, i.e., 45 coherence values. In order to avoid the bias that may be introduced by an unequal numbers of trials, the number of trials for Aha and control groups was equalized before the comparison by randomly discarding trials from the condition with a higher number of trials. Coherence has been calculated according to the formula below:

$$C(f) = \frac{\left| \sum_k A_k(f) B_k(f) e^{j(\phi_k(f) - \theta_k(f))} \right|}{\sqrt{\sum_k A_k(f)^2} \sqrt{\sum_k B_k(f)^2}}$$

where $A_k(f)e^{j\phi_k(f)}$ and $B_k(f)e^{j\theta_k(f)}$ describe the Fourier transformed signals, and k is the trial number (Srinath and Ray, 2014). The coherence values are real-valued numbers from 0 to 1. One means that two signals have perfect coupling, while zero indicates independence.

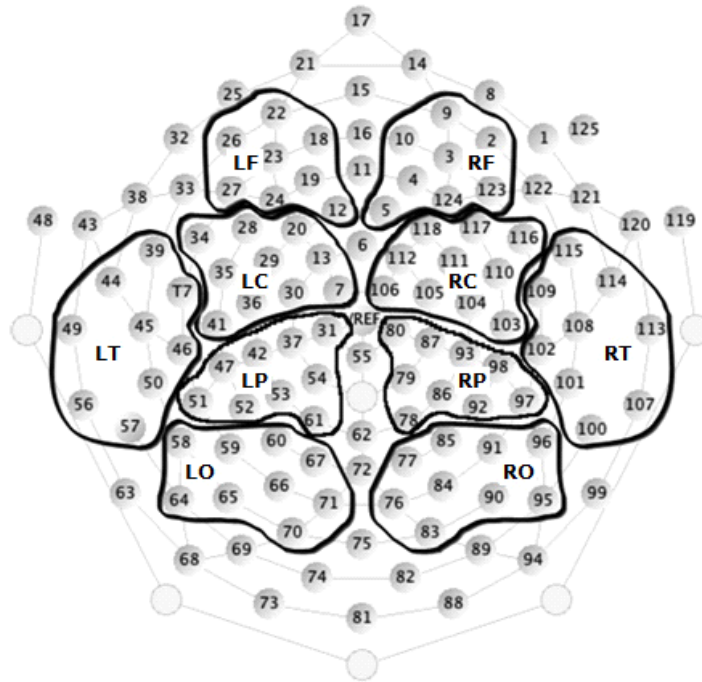


Figure 2-4. The position of ten clusters on HCGSN-128 EEG recording system.
Adapted from Marie and Trainor, 2013.

Phase locking value (PLV)

As coherence values are sensitive to amplitude variations, we calculated in addition phase locking values. These values reflect phase correlations between two oscillatory signals (Lachaux et al., 1999; Srinath and Ray, 2014) and serves as an index for quantification of neural synchronization between different neuron groups. The key factor distinguishing the PLV from coherence is that the PLV does not take amplitude into account. It only measures the phase component. Similar to coherence, PLV also has a real-valued number from 0 to 1. The value 1 indicates that two signals have strict phase locking, while 0 indicates that their phase relations are random. The PLV can be represented as

$$P(f) = \frac{1}{N} \left| \sum_k e^{j(\phi_k(f) - \theta_k(f))} \right|$$

where $e^{j\phi_k(f)}$ and $e^{j\theta_k(f)}$ are the imaginary parts of the signals, N is the amount of trials, and k is the trial number.

Laterality index (LI)

In order to capture lateralization effects, we calculated lateralization indices (LI) (Jansen et al., 2006; Wilke and Schmithorst, 2006; Seghier, 2008). LIs were calculated by evaluating differences between right and left hemispheres. We used the following formula to determine the LI:

$$LI = \frac{V_R - V_L}{V_R + V_L}$$

where V_R and V_L refer to averaged values (e.g. coherence value) within the right and left hemisphere, or the right and left electrode cluster. A positive or negative value of LI means a lateralization of neural activity to the right or left side, respectively.

Dimensionality

In order to assess changes in the complexity of network dynamics we determined the fractal dimension of the recorded high dimensional time series. The EEG data were normalized to z -scores and then analyzed for fractal structure. The principle of the analysis is based on scale-versus-count relationships for dimension D , which can be given by

$$C(\delta) = \lim_{n \rightarrow \infty} \frac{1}{n^2} |(x_i, x_j)|$$

$$D = \ln(C(\delta)) / \ln(\delta)$$

where n is the number of measurements, (x_i, x_j) are pairs of points ($|x_i - x_j| < \delta$, $i \neq j$), δ is spheres of a certain size and $C(\delta)$ is the count of the size (Grassberger and Procaccia, 1983).

Statistics

To evaluate the significance of differences between trials with the Eureka effect and the control condition, we performed a Wilcoxon signed-rank test when samples were not normally distributed; or a t -test (two-tailed) when samples were normally distributed. A cluster-based nonparametric randomization test was used to solve the multiple comparisons problem (MCP) (Maris and Oostenveld, 2007). For each paired sample, an independent samples t -test was computed. All samples with the p value lower than threshold 0.05 were selected and then clustered on the basis of spatial and temporal adjacency. The sum of the clustered t values was calculated. These samples were then randomized across Aha and Ctrl conditions, and the cluster t value was

analyzed. This step was repeated 1000 times. We then obtained a new distribution of cluster t values. On the basis of this distribution, the t value from the original data was evaluated. Here, we used the threshold 0.05 for significance. Similarly, the cluster-based nonparametric randomization test was also used to correct the z value of the Wilcoxon signed-rank test.

3. Results

The recognition of images with diverse degradation levels (Experiment 1)

The degradation of the Mooney images led to diverse behavioral outcomes. Figure 3-1 shows examples of images with different levels of degradation and the effects on identification (Figure 3-2).

The identification rates for the various degradation levels were 3.1%, 10.6%, 8.5%, 8.8%, 7.6%, 6.4%, 6.2%, and 4.1%, for cut-off frequencies ranging from 10 Hz to 80 Hz (Figure 3-2). There were 44.7% trials without a response (i.e., unrecognized). According to the two requirements (keep difficulty & attract attention) for Experiment 2, and together with the results of Experiment 1, the 20 Hz degradation level was selected to manipulate the stimuli (for details of selection, see Methods “Selection of the suitable cut-off frequency for the image low-pass filter”).

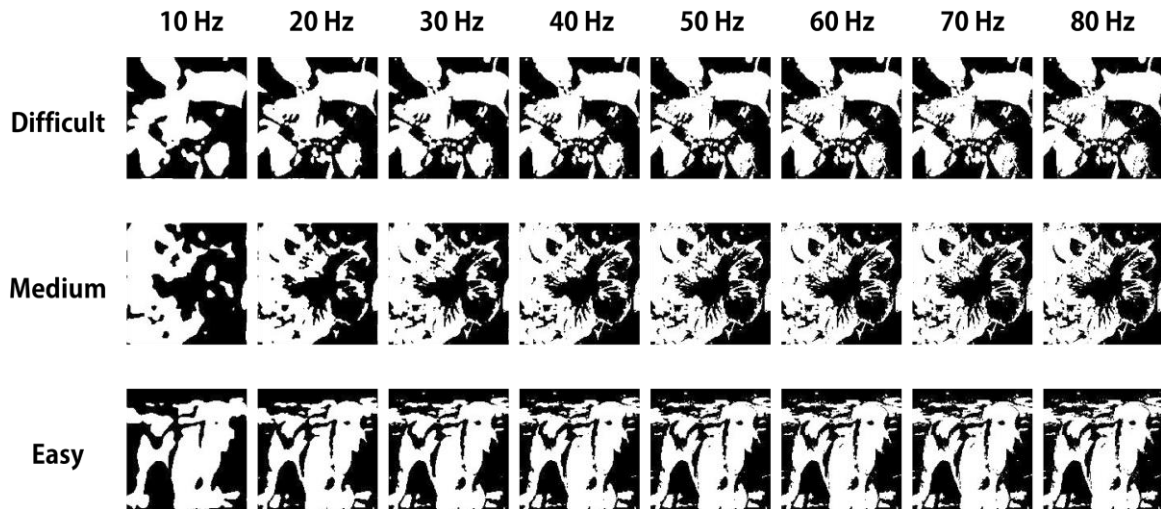


Figure 3-1. Examples of images with different recognition difficulty in Experiment 1. From top row to bottom row: difficult, medium and easy images. Each row represents the images filtered with low-pass cut-off frequencies from 10 Hz to 80 Hz. The images of each row are derived from one original image, and shown from low (left) to high (right) cut-off frequencies. For the difficult images (top row), most of subjects can either recognize only the higher spatial frequency filtered image (right), or recognize none of them. For the medium images (middle row), most subjects can recognize object from the middle area of the row to the right area. For the easy images (bottom row), most subjects can recognize object easily from the lower spatial frequency filtered image (left side), to the high spatial frequency filtered image (right side).

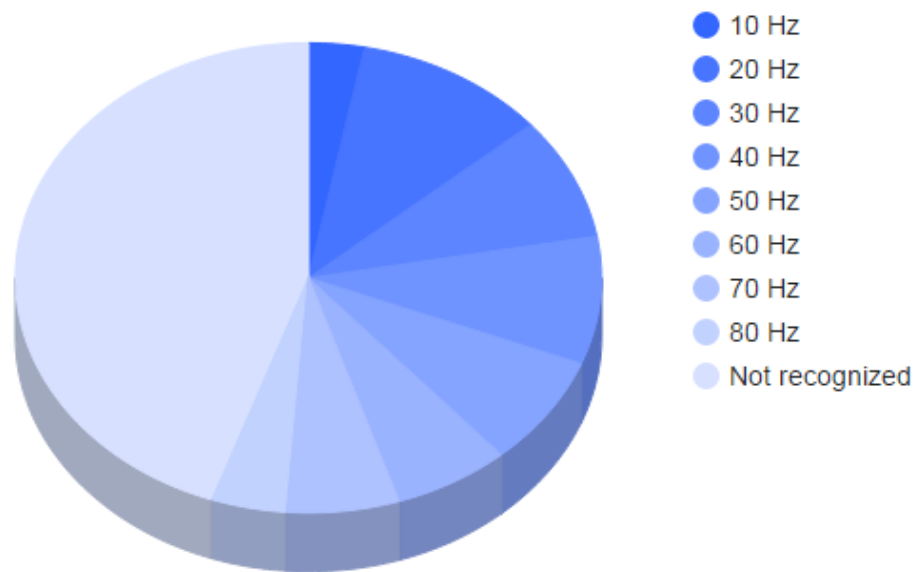


Figure 3-2. The response percentages per degradation level (per cut-off frequency). The lighter colors represent higher frequency filtered images. The slices show that most of the responses are from the “lighter blue area”. On other words, most of the images are difficult to be recognized at the low cut-off frequencies.

The behaviour during the Eureka effect (Experiment 2)

We observed that 83.9% trials were continued till the third stage and 90.5% of them had correct responses. “Correct meant “Yes” response to congruent trials or “No” responses to incongruent trials. This result suggests that the subjects really experienced the Eureka effect and that the comparison between Aha and Ctrl conditions was valid.

The reaction times (RTs) of Aha and Ctrl trials are summarized in Figure 3-3. The RTs in Aha trials are faster than the RTs in Ctrl trials. The smoothed distribution of RTs shows that the peak of the Aha RTs distribution is at 0.90 s, while the peak of the Ctrl RTs distribution is at 1.50 s. The Aha RTs distribution has a narrow peak, while

the Ctrl RTs distribution is wide. The median of the Aha trial RTs is 1.13 s, and that of the Ctrl trials is 2.00 s (Figure 3-3). The Aha RTs is significantly shorter than the Ctrl RTs ($p = 3.2229e-005$, Wilcoxon signed rank test). We found that 92.9% of the Aha trials and 99.3% of the Ctrl trials have RTs longer than 0.5 s. These trials were kept for further analysis.

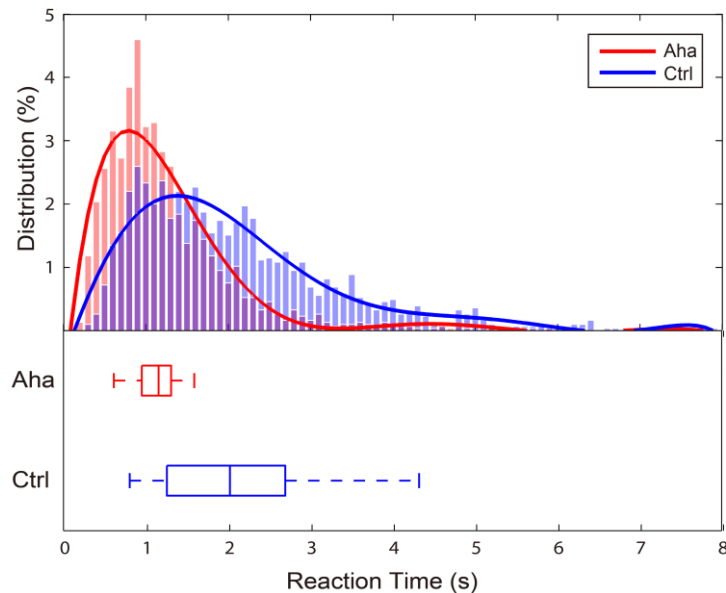


Figure 3-3. The distribution of reaction times (RTs). The upper panel: distribution of RTs for all trials. Each bar represents a 0.1 s time window. The height of each bar is the percentage distribution of the RTs for the specific time window. The fitting values are marked by the red and blue curves. The lower panel: distribution of RTs for subjects. The boxes show the median values, the 25th, and the 75th percentiles. The ends of whiskers show extremums. Red and blue colors represent Aha and Ctrl trials, respectively.

Alpha band activity

In Aha and Ctrl trials aligned to stimulus onset (“stimulus locked epochs”) there was no significant difference in alpha band (8-12 Hz) power. (The analyses for theta, beta and gamma bands are described in subsequent chapters.)

To analyze the characteristics of between-channel synchronization in the low frequency range, we calculated coherence. The averaged value of alpha coherence from stimulus onset (0 ms) to 500 ms after onset was then plotted on a coherence matrix in order to assess the topology of coherence (Figure 3-4). Interestingly, the topographical distribution of alpha coherence revealed interhemispheric asymmetries (Figure 3-5). Alpha band coherence increased during the Eureka effect especially within the right hemisphere. Figure S1 shows the coherence for channel pairs (Aha minus Ctrl). Due to a large number of channel pairs, Figure S1 was separated into 3 sub-figures. Each single panel shows the coherence between two different channels.

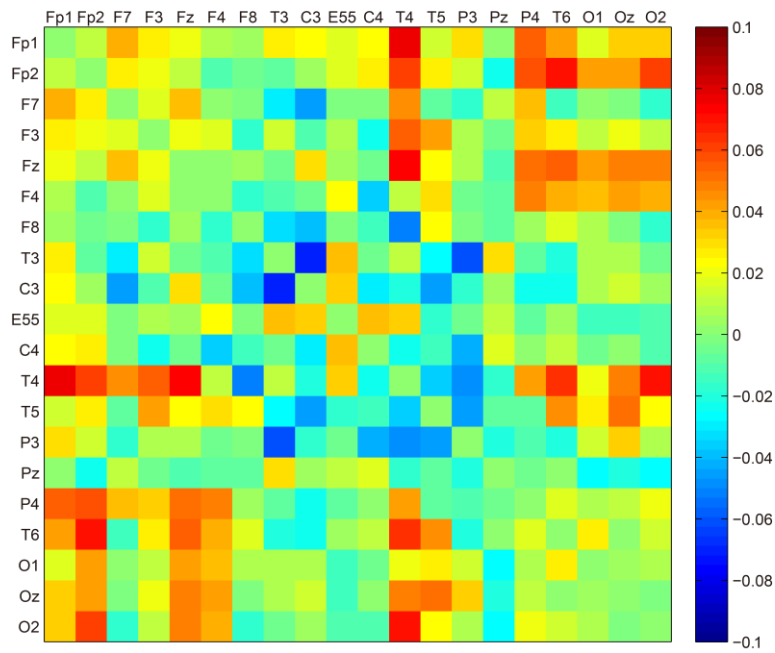


Figure 3-4. The alpha coherence matrix of channels (stimulus locked epochs). Each square represents the average alpha coherence of each channel pair during the time window from stimulus onset to 500 ms after onset (0 - 500 ms). The matrix represents the difference of alpha coherence between Aha and Ctrl (Aha minus Ctrl).

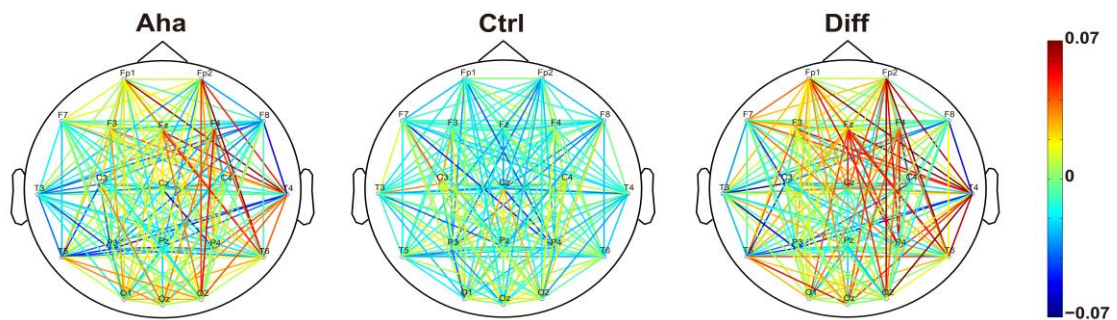


Figure 3-5. The topographic distribution of alpha coherence of channels (stimulus locked epochs). Diff is the difference between Aha and Ctrl (Aha minus Ctrl). Each colored solid line represents the alpha coherence value between the two connected channels, during the time window from stimulus onset to 500 ms after onset (0 - 500 ms).

To quantify the lateralization of alpha coherence, we calculated the laterality index (LI) of alpha coherence for channel pairs in both hemispheres. The results are shown in Figure 3-6. The curves in Figure 3-6A represent the LI for Aha and Ctrl conditions, respectively. Aha LIs show a right hemispheric lateralization of enhanced coherence that is absent in Ctrl. The right hemisphere increase in alpha coherence is significant in the interval from 345 ms to 450 ms post-stimulus ($p < 0.05$). The distribution of changes in alpha coherence across subjects is shown in Figure 3-6B. The majority (15 of 22) of subjects show an increased LI of alpha coherence.

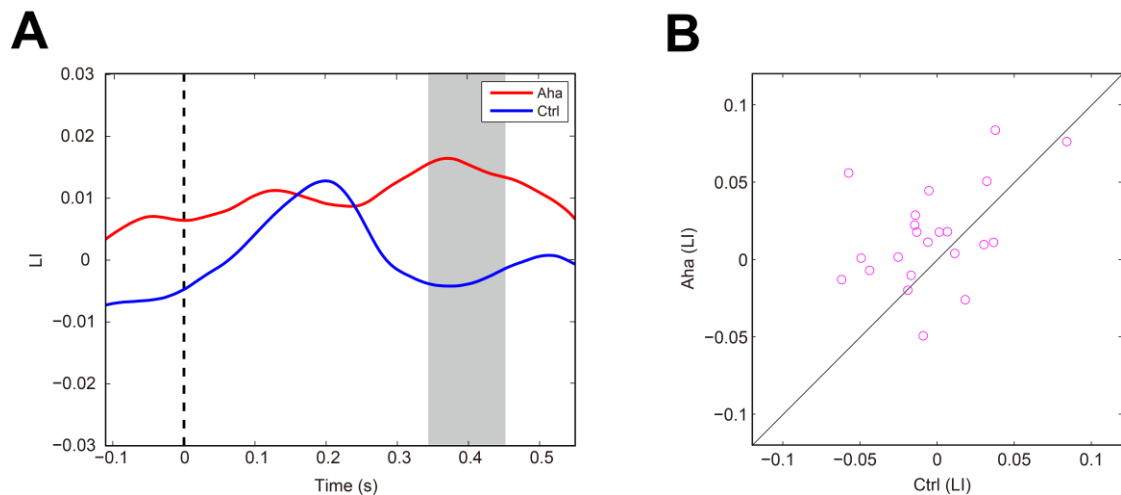


Figure 3-6. The laterality index (LI) of alpha coherence of channels (stimulus locked epochs). (A) The averaged LI across all subjects. The values for Aha and Ctrl are indicated by red and blue curves, respectively. Significantly different values between conditions are marked by gray bars. Zero second is stimulus onset. (B) The LI between the two conditions for each subject. Each subject is marked by a small circle.

To assess changes in phase locking associated with the Eureka effect, we analyzed the phase locking values (PLV) for channel pairs in the alpha band (Figure S2) (The theta, beta and gamma activities are described in subsequent chapters.) The averaged alpha band PLV from 0 ms to 500 ms after stimulus onset is summarized by the PLV matrix in Figure 3-7. Interestingly, the topography of the alpha PLV closely resembles

that of alpha coherence (Figure 3-8). Alpha band PLV also increased during the Eureka effect especially within the right hemisphere and the results of LI quantification are similar as for coherence (Figure 3-9). LIs show that alpha PLV during the Eureka effect is significantly increased in the right hemisphere, in the interval from 385 ms to 445 ms post stimulus ($p < 0.05$) (Figure 3-9A). This time window overlaps with the interval of enhanced coherence (335 - 425 ms). Figure 3-9B shows the LIs of the alpha PLV for all subjects, confirming that the majority of subjects (16 of 22) exhibit an increased LI of the alpha PLV associated with the Eureka effect. Taken together these results suggest that the Eureka effect is associated with enhanced coherence of oscillatory activity in the alpha band.

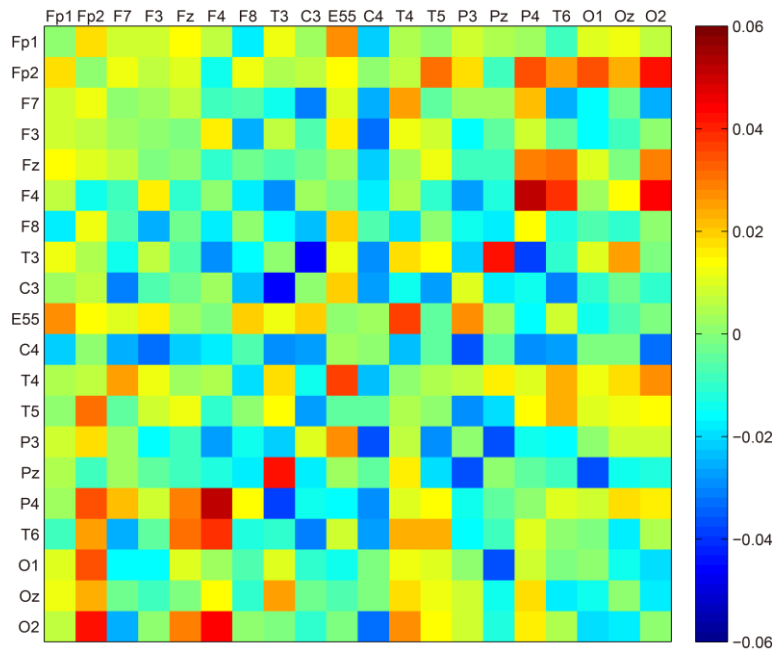


Figure 3-7. The alpha PLV matrix of channels (stimulus locked epochs). Each square represents the average alpha PLV of each channel pair during the time window from stimulus onset to 500 ms after onset (0 - 500 ms). The matrix represents the difference of alpha PLV between Aha and Ctrl (Aha minus Ctrl).

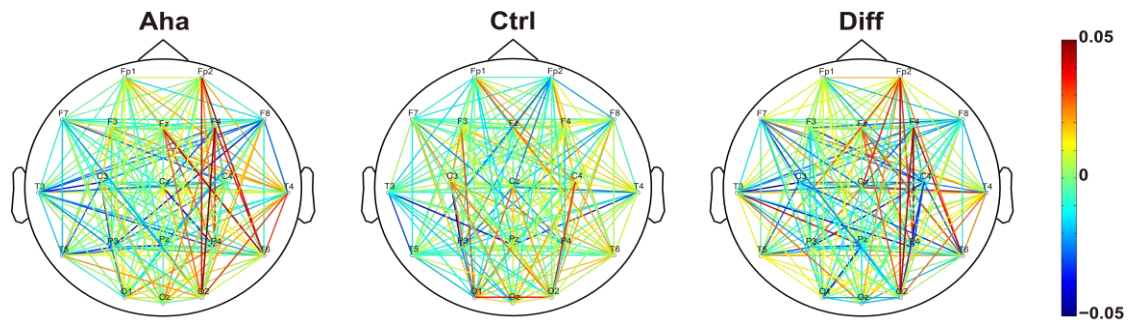


Figure 3-8. The topographic distribution of alpha PLV of channels (stimulus locked epochs). Each colored solid line represents the alpha PLV between the two connected channels, during the time window from stimulus onset to 500 ms after onset (0 - 500 ms).

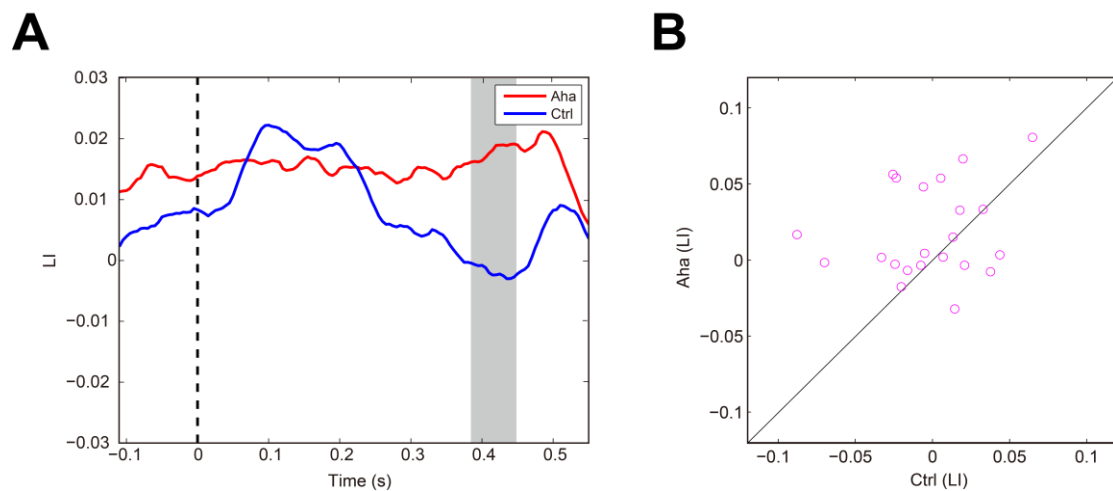


Figure 3-9. The laterality index (LI) of alpha PLV of channels (stimulus locked epochs). (A) The averaged LI across all subjects. The values for Aha and Ctrl are indicated by red and blue curves, respectively. Significantly different values between conditions are marked by gray bars. Zero second is stimulus onset. (B) The LI between the two conditions for each subject. Each subject is marked by a small circle.

Due to the variable reaction time across trials, we also aligned the epochs with the responses (“response locked epochs”) and repeated the analyses of power, coherence, and PLV in the alpha band. (Same as above, the analyses for theta, beta and gamma bands are described in subsequent chapters). In this response segment alpha power was found to be lower for Aha than for Ctrl trials (Figure 3-10). As shown in Figure 3-10A, two clusters of reduced alpha power were found ($p < 0.05$). One was in the frontal region, mostly in the left hemisphere, from 150 ms before response to response (-150 - 0 ms). In this cluster, alpha power was significantly decreased before the response, as shown in Figure 3-10. The second cluster was in the occipital region, from 335 ms before response to response (-335 - 0 ms). Interestingly, this cluster exhibited a gradual shift from the left to the right hemisphere across time. Before -220 ms, this cluster was mainly located in the left occipital area; after -220 ms, it moved to the right occipital and right superior parietal areas (Figure 3-10).

Also in the response locked datasets alpha coherence was enhanced in Aha conditions in the right hemisphere (Figure S3). The average values of alpha coherence from 500 ms before the response (-500 ms) to the response (0 ms) were plotted in a coherence matrix (Figure 3-11) as before and this showed again a lateralization to the right hemisphere of the Aha associated increase in coherence (Figure 3-12) resembling the pattern obtained with stimulus locked epochs.

To examine the lateralized distribution of alpha coherence, the LI was also calculated, shown in Figure 3-13. There was a significant positive cluster from -355 ms to -275 ms ($p < 0.05$), i.e., the alpha coherence during Eureka effect was significantly increased in the right hemisphere for this period before the response (0 ms) (Figure 3-13A). The LIs of alpha coherence during this interval were calculated individually for all subjects and are plotted in Figure 3-13B. The majority of subjects (16 of 22) show an increased LI.

We then calculated coherence between channel clusters for response locked epochs, shown in Figure S5 (Aha minus Ctrl). The matrix plot in Figure 3-14 shows the averaged values of alpha coherence from 500 ms before the response to the response for each cluster pair. The topographical distribution of the inter cluster coherence reflects again the lateralization of increased alpha coherence during the Eureka effect to the right hemisphere (Figure 3-15).

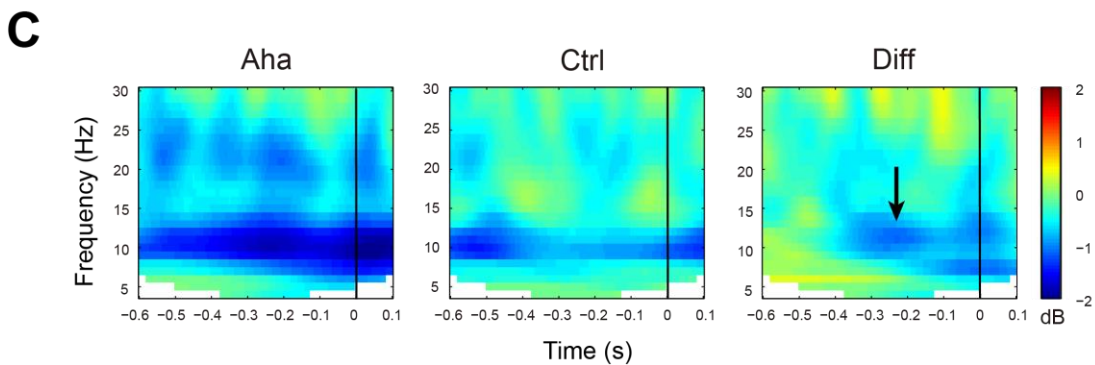
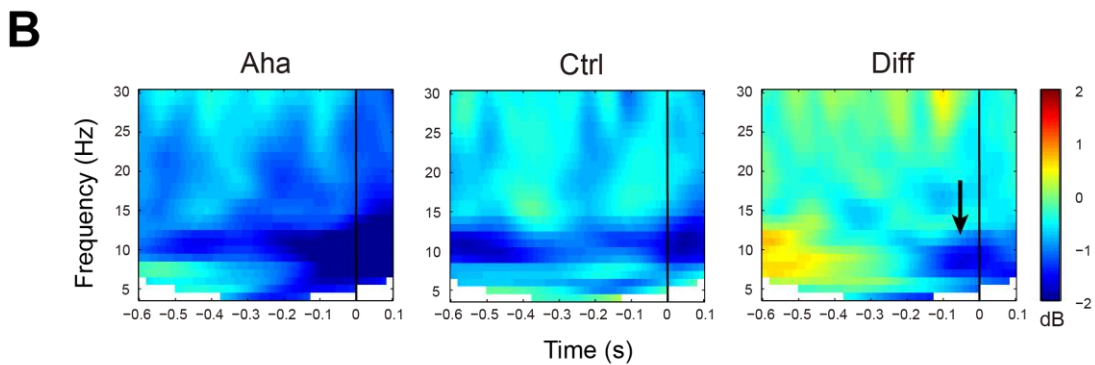
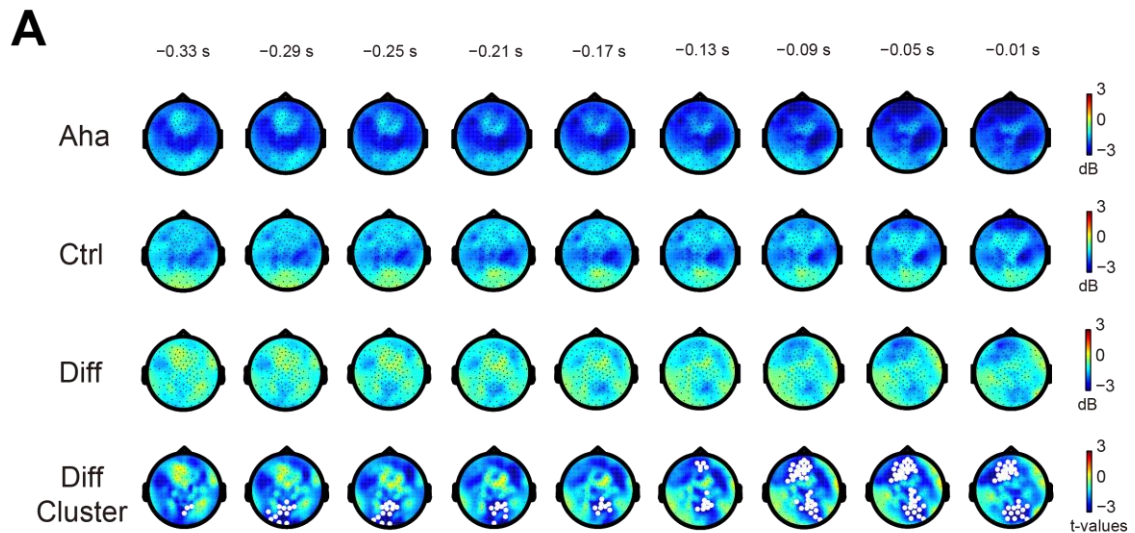


Figure 3-10. The alpha power before response. (A) The Aha, Ctrl and Diff graphs represent the alpha power for the Eureka effect, control and the difference between them, respectively. The Diff Cluster row represents the t -values of cluster analysis for the difference between the Eureka effect and control conditions. The white dots show the significant negative clusters, which match the negative regions in the Diff row. (B) The time-frequency plot of the cluster 1 (the frontal cluster). (C) The time-frequency plot of the cluster 2 (the occipital cluster). The arrows in B and C show the decreased alpha power. The vertical black lines in B and C at 0 s indicate response.

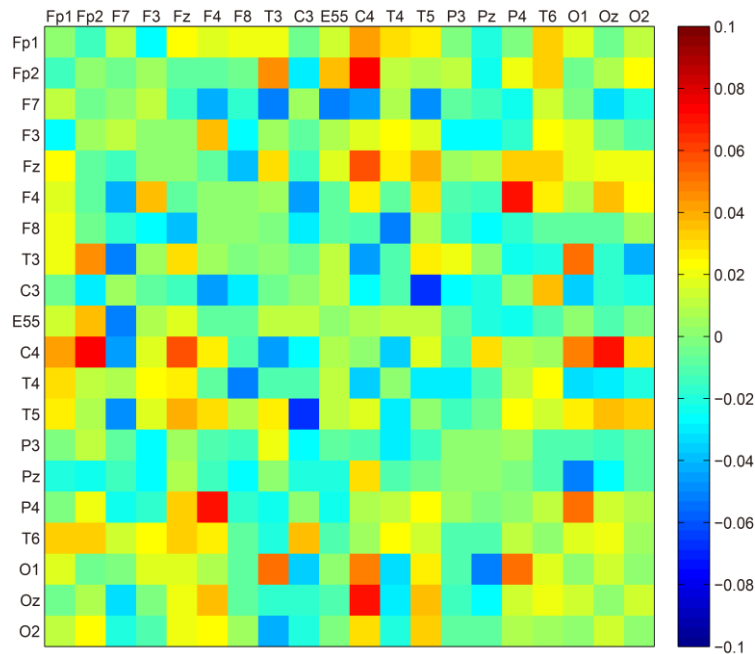


Figure 3-11. The alpha coherence matrix of channels (response locked epochs). Each square represents the average alpha coherence of each channel pair during the time window from 500 ms before response to response (-500 - 0 ms). The matrix represents the difference of alpha coherence between Aha and Ctrl (Aha minus Ctrl).

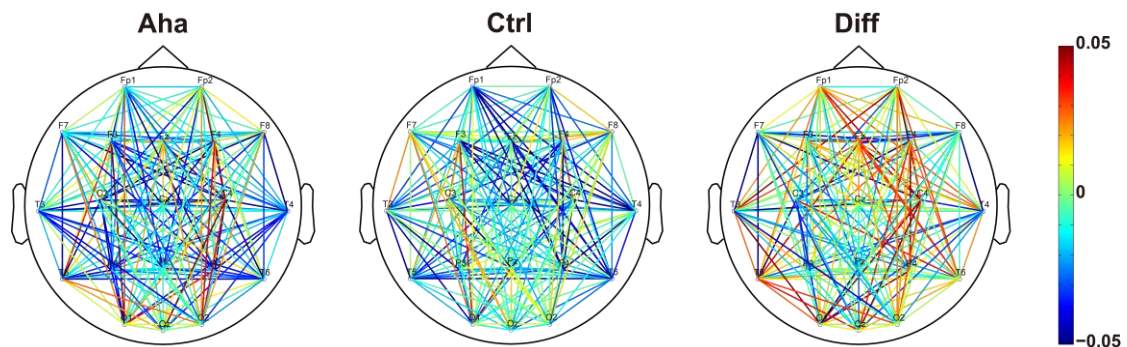


Figure 3-12. The topographic distribution of alpha coherence of channels (response locked epochs). Each colored solid line represents the alpha coherence value between the two connected channels, during the time window from 500 ms before response to response (-500 - 0 ms).

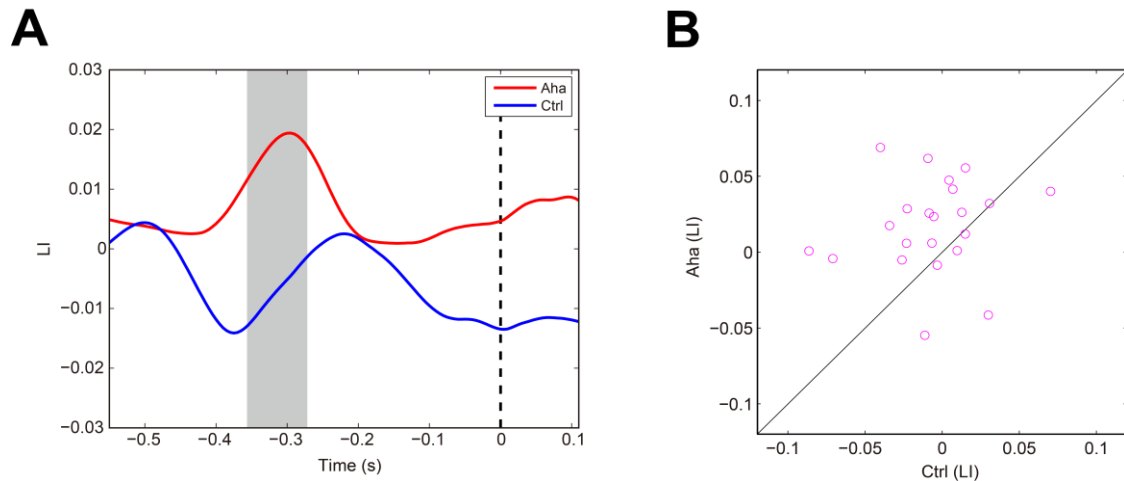


Figure 3-13. The laterality index (LI) of alpha coherence of channels (response locked epochs). (A) The averaged LI across all subjects. The values for Aha and Ctrl are indicated by red and blue curves, respectively. The significant different values between conditions are marked by gray bars. Zero second is the response. (B) The LI between two conditions for each subject. Each subject is marked by a small circle.

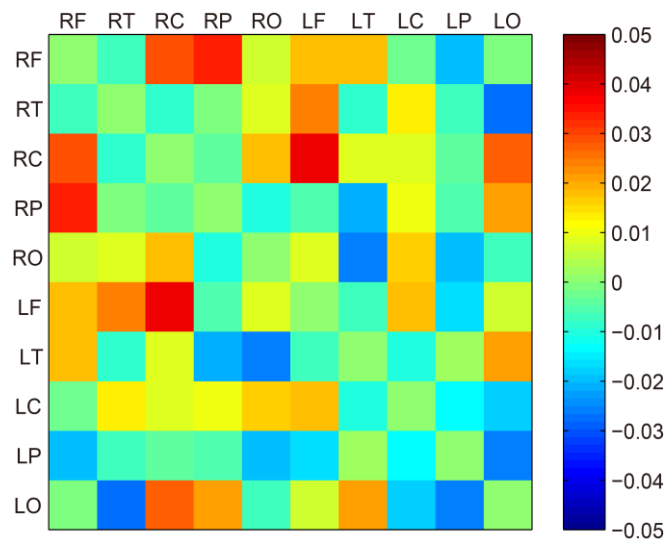


Figure 3-14. The alpha coherence matrix of channel clusters (response locked epochs). The alpha coherence values for each cluster pairs were calculated during the time window from 500 ms before response until response point. The matrix represents the difference of alpha coherence between Aha and Ctrl (Aha minus Ctrl). The clusters cover left frontal (LF), left central (LC), left parietal (LP), left temporal (LT), left occipital (LO), right frontal (RF), right central (RC), right parietal (RP), right temporal (RT), and right occipital (RO) areas.

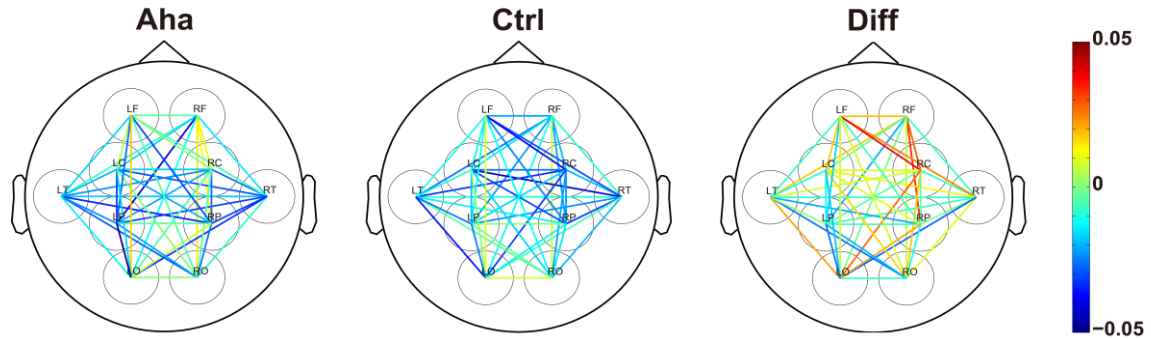


Figure 3-15. Topographic distribution of alpha coherence of channel clusters (response locked epochs). Each colored solid line represents the alpha coherence value between the two connected channel clusters, during the time window from 500 ms before the response to the response (-500 - 0 ms).

Similarly, also the cluster analysis of response locked epochs shows a right hemisphere lateralized increase in alpha coherence in Aha condition, but not the Ctrl condition. The cluster difference was significant in the interval from -340 ms to -285 ms (Figure 3-16A), resembling the period of -355 ms to -275 ms during which channel pair coherence was enhanced. The LI values of all subjects are shown in Figure 3-16B, and the majority of subjects (14 of 22) show an increased LI.

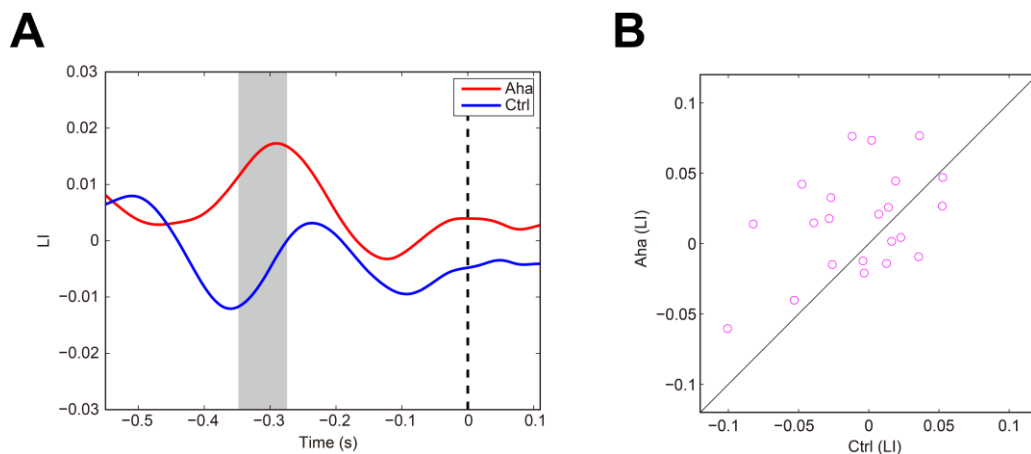


Figure 3-16. Laterality index (LI) of alpha coherence of channel clusters (response locked epochs). (A) The averaged LI across all subjects. The values for Aha and Ctrl are indicated by the red and blue curves, respectively. The time period with significantly different values between conditions is marked by gray bars. Zero second is the response point. (B) The LI between the two conditions for each subject. Each subject is marked by a small circle.

We also calculated PLV for response locked epochs (Figure S4, S6). The PLV analysis for response locked epochs confirmed the results from coherence analysis. The matrix in Figure 3-17 shows the averaged values of alpha PLV from 500 ms before the response to the response point (0 ms). The topographical distribution of cluster results confirmed the right hemispheric lateralization of increased alpha PLV during the Eureka effect (Figure 3-18). The LIs of alpha PLV were significantly enhanced in the right hemisphere from -305 ms to -275 ms and thus in a similar interval as the enhanced coherence (-340 ms to -285 ms) (Figure 3-19A). The LIs of all subjects were plotted in Figure 3-19B and the majority of subjects (17 of 22) show an increased LI.

In conclusion the analysis of alpha band activity suggests that the Eureka effect is associated with an increase in coherence and phase synchrony in a widely distributed network, mainly within the right hemisphere.

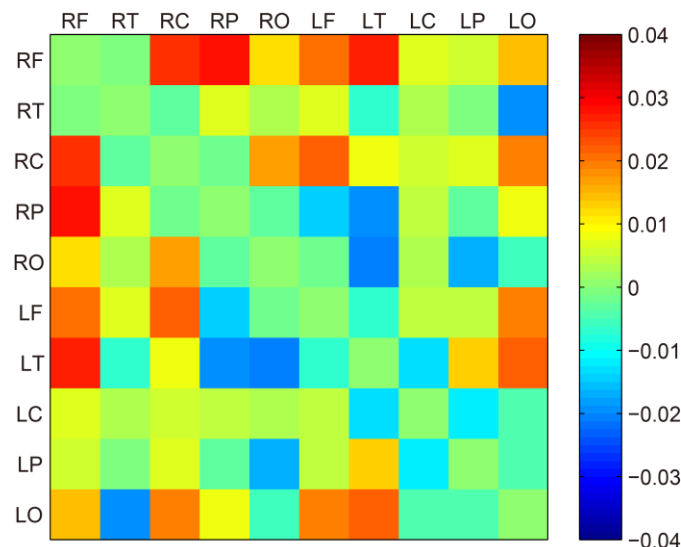


Figure 3-17. The alpha PLV matrix of the channel clusters (response locked epochs). The alpha PLV for each cluster pairs was calculated during the time window from 500 ms before response until response point. The matrix represents the difference of alpha PLV between Aha and Ctrl (Aha minus Ctrl).

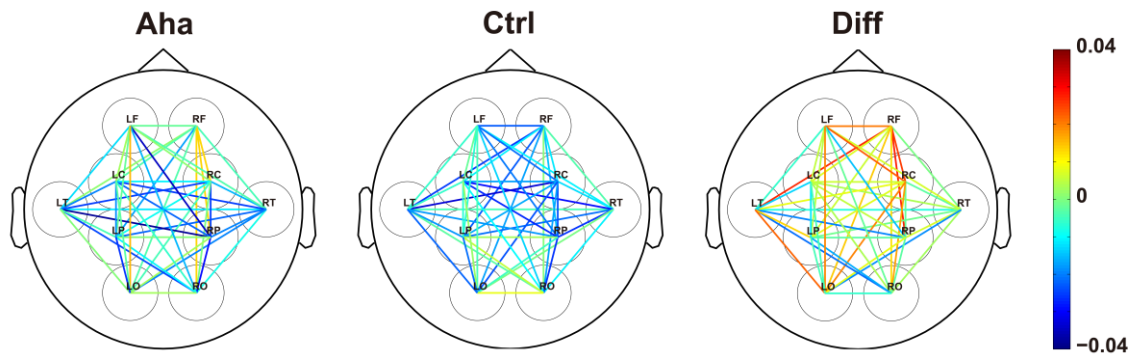


Figure 3-18. Topographic distribution of alpha PLV of channel clusters (response locked epochs). Each colored solid line represents the alpha PLV between the two connected channel clusters, during the time window from 500 ms before response to response (-500 - 0 ms).

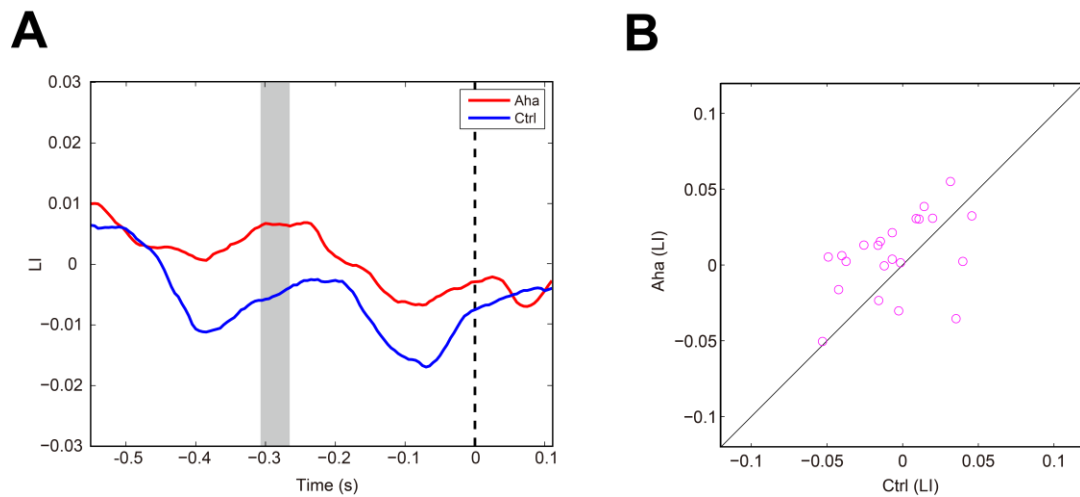


Figure 3-19. Laterality index (LI) of alpha PLV of channel clusters (response locked epochs). (A) The averaged LI across all subjects. The PLVs for Aha and Ctrl are indicated by the red and blue curves, respectively. The time period with significantly different values between conditions is marked by gray bars. Zero second is the response point. (B) The LI between two conditions for each subject. Each subject is marked by a small circle.

Theta band activity

To analyze the theta band (4-7 Hz) activity, the same methods were used as above for the alpha band. In epochs aligned with stimulus onset there were no significant differences in power between Aha and Ctrl conditions. However, coherence analysis revealed again a right lateralized increase in coherence for the interval 0 – 500 ms after stimulus onset for the Eureka condition (Figure 3-20/21). The LI analysis showed that the theta coherence during Eureka effect was significantly increased in revealed that this effect was significant in two time windows: from 125 ms to 260 ms ($p < 0.05$) and from 375 ms to 395 ms ($p < 0.05$), after stimulus onset (Figure 3-22A). This effect was again seen in the majority (17 of 22) of subjects (Figure 3-22B, C).

The cluster analysis fully confirmed these changes in the theta band coherence (Figures S7 and 3-23/24). The right lateralized increase in theta coherence was significant from 250 ms to 365 ms after stimulus onset (Figure 3-25A, B).

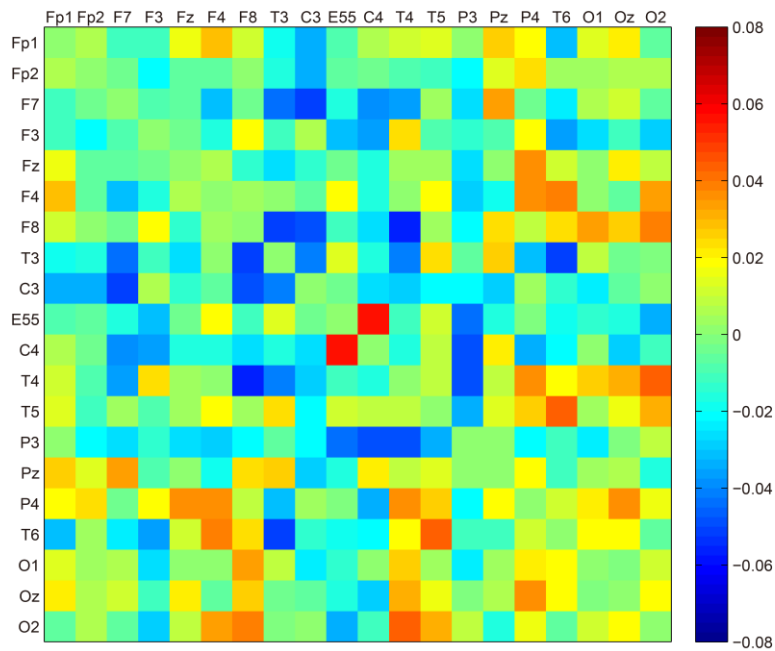


Figure 3-20. The theta coherence matrix of channels (stimulus locked epochs). Each square represents the average theta coherence of each channel pair during the time window from stimulus onset to 500 ms after onset (0 - 500 ms). The matrix represents the difference of theta coherence between Aha and Ctrl (Aha minus Ctrl).

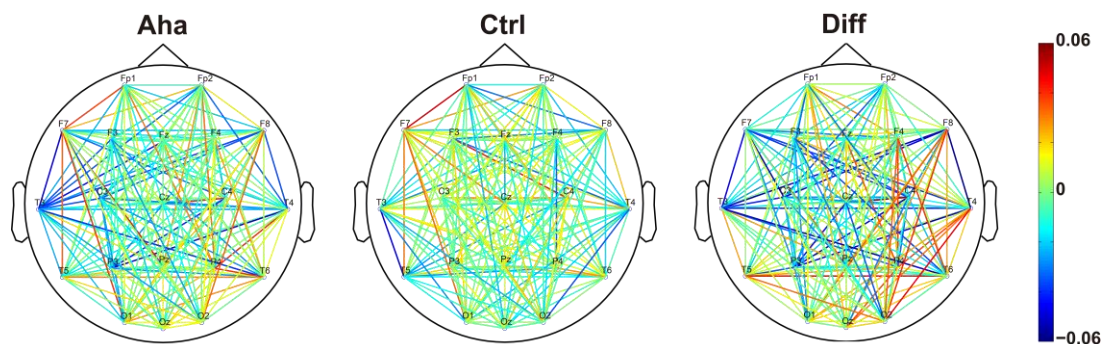


Figure 3-21. The topographic distribution of theta coherence of channels (stimulus locked epochs). Each colored solid line represents the theta coherence value between the two connected channels, during the time window from stimulus onset to 500 ms after onset (0 - 500 ms).

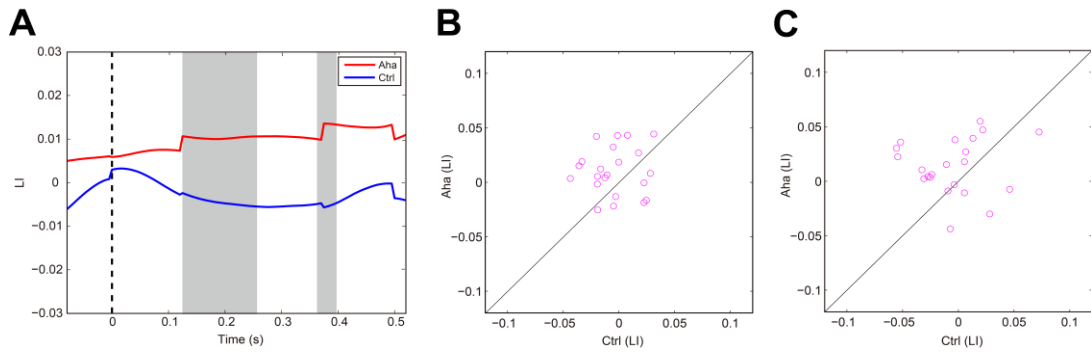


Figure 3-22. The laterality index (LI) of theta coherence of channels (stimulus locked epochs). (A) The averaged LI across all subjects. The values for Aha and Ctrl are indicated by red and blue curves, respectively. The significant different values between conditions are marked by gray bars. Zero second is the stimulus onset. (B) and (C) The LI between two conditions for each subject. Each subject is marked by a small circle. Panel B represents the LI of cluster 1 (125 - 260 ms). Panel C represents the LI of cluster 2 (375 - 395 ms).

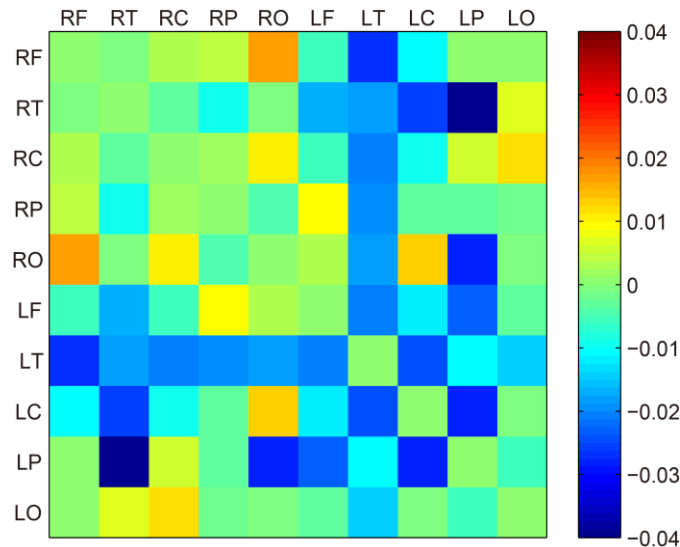


Figure 3-23. The theta coherence matrix of channel clusters (stimulus locked epochs). The theta coherence values for each cluster pairs were calculated during the time window from stimulus onset to 500 ms after onset (0 - 500 ms). The matrix represents the difference of theta coherence between Aha and Ctrl (Aha minus Ctrl).

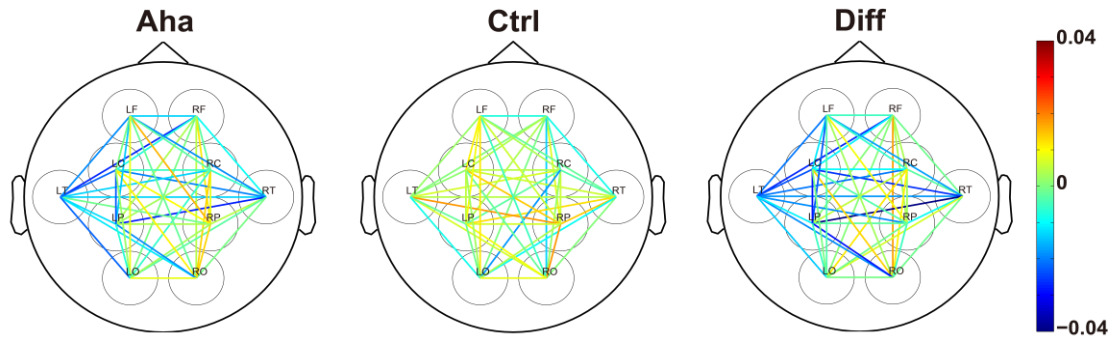


Figure 3-24. Topographic distribution of theta coherence of channel clusters (stimulus locked epochs). Each colored solid line represents the theta coherence value between the two connected channel clusters, during the time window from stimulus onset to 500 ms after onset (0 - 500 ms).

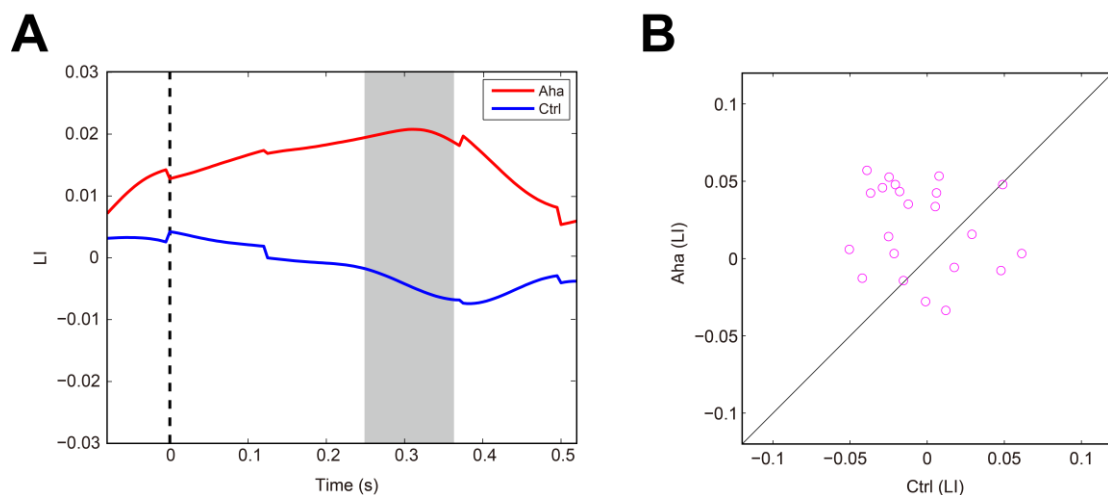


Figure 3-25. The laterality index (LI) of theta coherence of channel clusters (stimulus locked epochs). (A) The averaged LI across all subjects. The values for Aha and Ctrl are indicated by red and blue curves, respectively. Significant different values between conditions are marked by gray bars. Zero second is the stimulus onset. (B) The LI between the two conditions for each subject. Each subject is marked by a small circle.

The PLV analysis for channel pairs again showed a right lateralized increase in theta synchrony (Figure S2 and Figure 3-26, 27). And LI analysis (Figure 3-28) indicated that this effect was significant in the time window from 375 ms to 420 ms ($p < 0.05$)

which overlaps with the interval of enhanced theta (375 - 395 ms) and alpha (385 - 445 ms) coherence. The LIs of theta PLV for all subjects are plotted in Figure 3-28B and show, that the effects were present in the majority of subjects (15 of 22).

The corresponding PLV results of the cluster analysis are shown in Figures S8 and 3-29/30, confirming a right lateralized increase in PLV with the Eureka effect that was significant in the interval from 325 ms to 400 ms ($p < 0.05$) post stimulus (Figure 3-31A/B). In summary, the Eureka effect is also associated with enhanced theta coherence and phase synchronization within a widely distributed network located mainly in the right hemisphere.

However, for the analysis of theta activity in epochs aligned with response, we did not find significant lateralization.

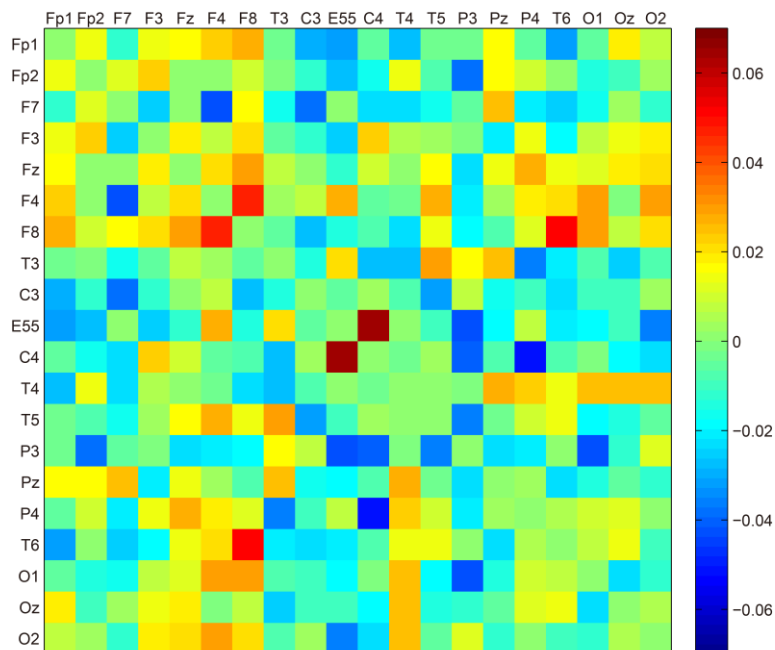


Figure 3-26. The theta PLV matrix of channels (stimulus locked epochs). Each square represents the average theta PLV of each channel pair during the time window from stimulus onset to 500 ms after onset (0 - 500 ms). The matrix represents the difference of theta PLV between Aha and Ctrl (Aha minus Ctrl).

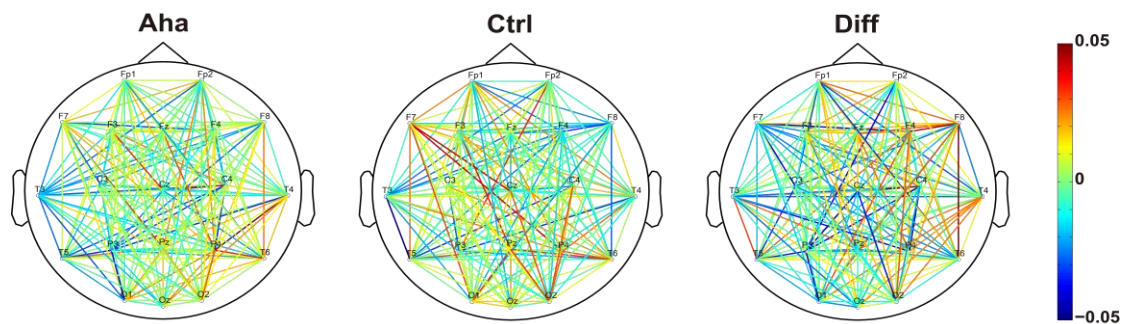


Figure 3-27. The topographic distribution of theta PLV of channels (stimulus locked epochs). Each colored solid line represents the alpha PLV between the two connected channels, during the time window from the stimulus onset to 500 ms after onset (0 - 500 ms).

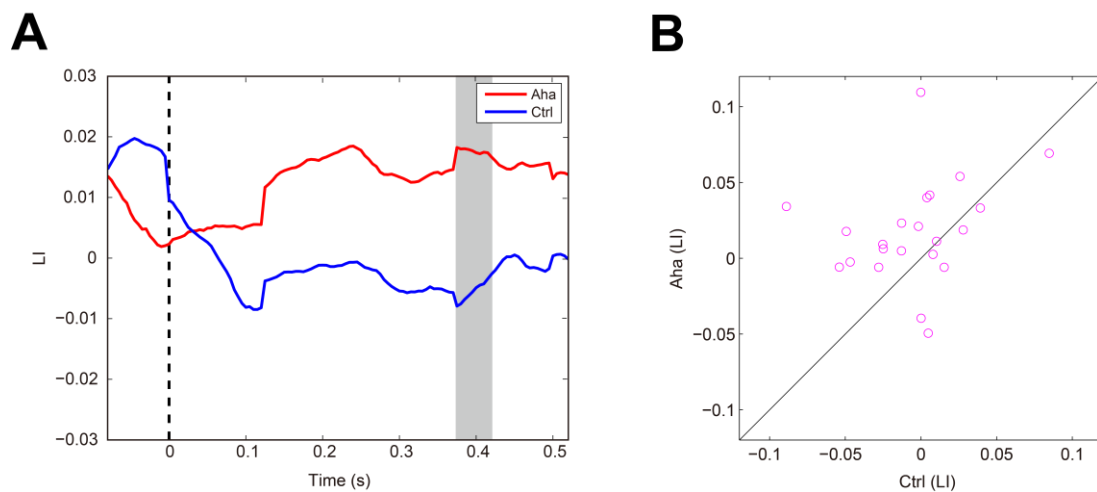


Figure 3-28. The laterality index (LI) of theta PLV of channels (stimulus locked epochs). (A) The averaged LI across all subjects. The values for Aha and Ctrl are indicated by red and blue curves, respectively. Significantly different values between conditions are marked by gray bars. Zero second is the stimulus onset. (B) The LI between the two conditions for each subject. Each subject is marked by a small circle.

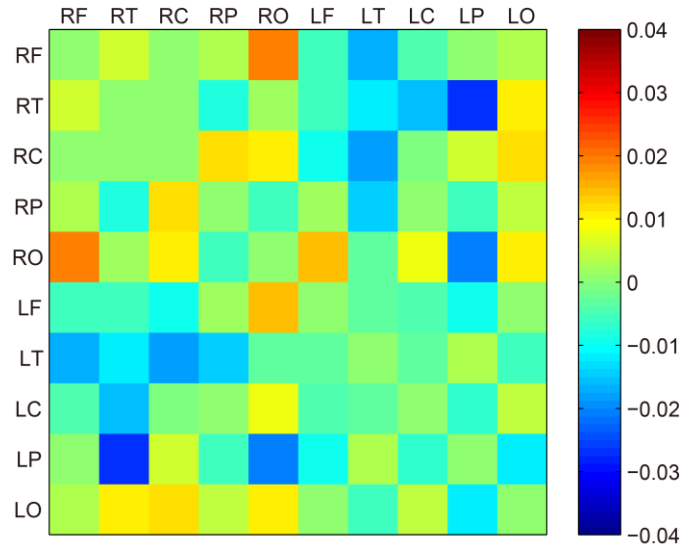


Figure 3-29. The theta PLV matrix of channel clusters (stimulus locked epochs). The theta PLVs for each cluster pairs were calculated during the time window from stimulus onset to 500 ms after onset (0 - 500 ms). The matrix represents the difference of theta PLV between Aha and Ctrl (Aha minus Ctrl).

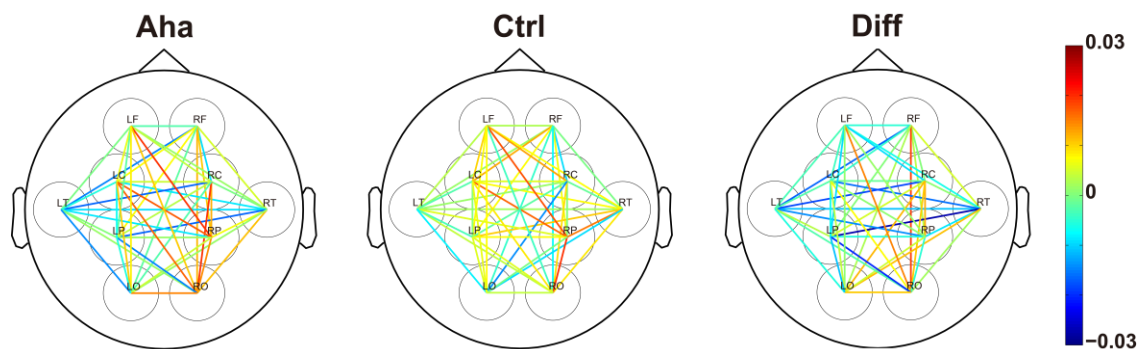


Figure 3-30. Topographic distribution of theta PLV of channel clusters (stimulus locked epochs). Each colored solid line represents the theta PLV between the two connected channel clusters, during the time window from stimulus onset to 500 ms after onset (0 - 500 ms).

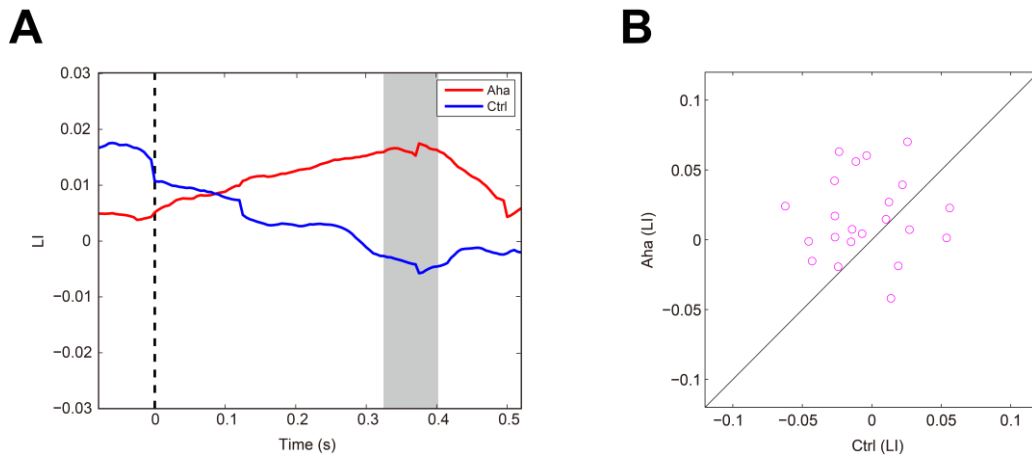


Figure 3-31. The laterality index (LI) of theta PLV of channel clusters (stimulus locked epochs). (A) The averaged LI across all subjects. The values for Eureka (Aha) and control conditions are indicated by red and blue curves, respectively. The significant different values between conditions are marked by gray bars. Zero sec is the onset of stimuli. (B) The LI between two conditions for each subject. Each individual is marked by a small circle.

Beta band activity

In responses aligned to stimulus onset the Eureka effect was associated with a decrease in beta power (13–30 Hz) (Figure 3-32). As shown in Figure 3-32A, this decrease was again lateralized to the right hemisphere and significant in the interval from 240 ms to 360 ms after stimulus onset ($p < 0.05$). This decrease was most prominent for clusters comprising the right parietal cortex and central gyrus, close to the midline.

In epochs aligned to the response (Figure 3-33A/B) the decrease of beta power was also present although not significant for clusters in the right parietal and right occipital cortices in the time window of -380 – -285 ms before the response ($p = 0.0789$).

Here we show the beta band power which was calculated on single channels. The beta coherence and PLV analysis (channel pairs and clusters) did not show significant results.

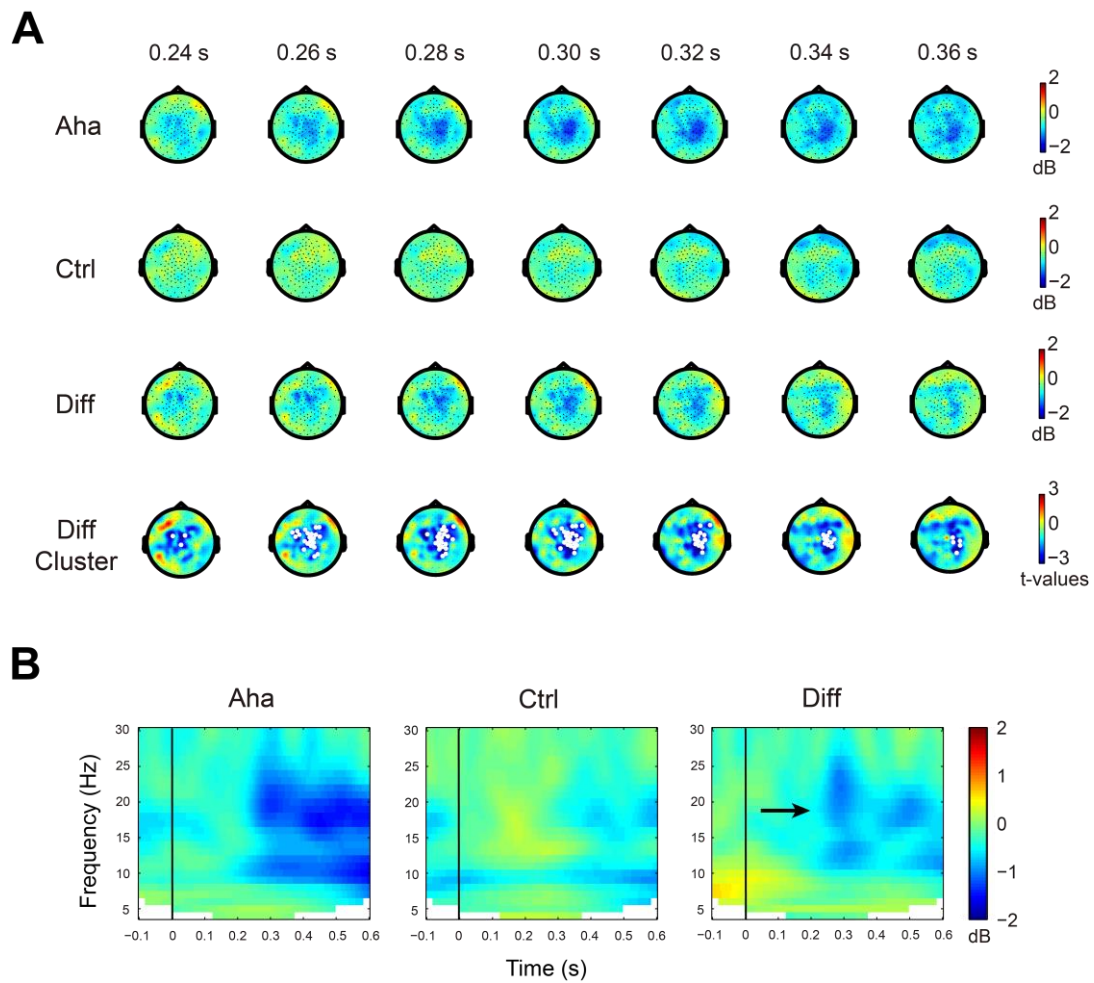


Figure 3-32. The beta power after stimulus onset. (A) The Aha, Ctrl and Diff graphs represent the beta power for the Eureka effect, control and the difference between them, respectively. The Diff Cluster row represents the t -values of cluster analysis for the difference between Aha and Ctrl. The white dots show the significant negative clusters which match the negative regions in the Diff row. (B) The time-frequency plot of the cluster. The arrow shows decreased beta power. The vertical black lines at the 0 s indicate stimulus onset.

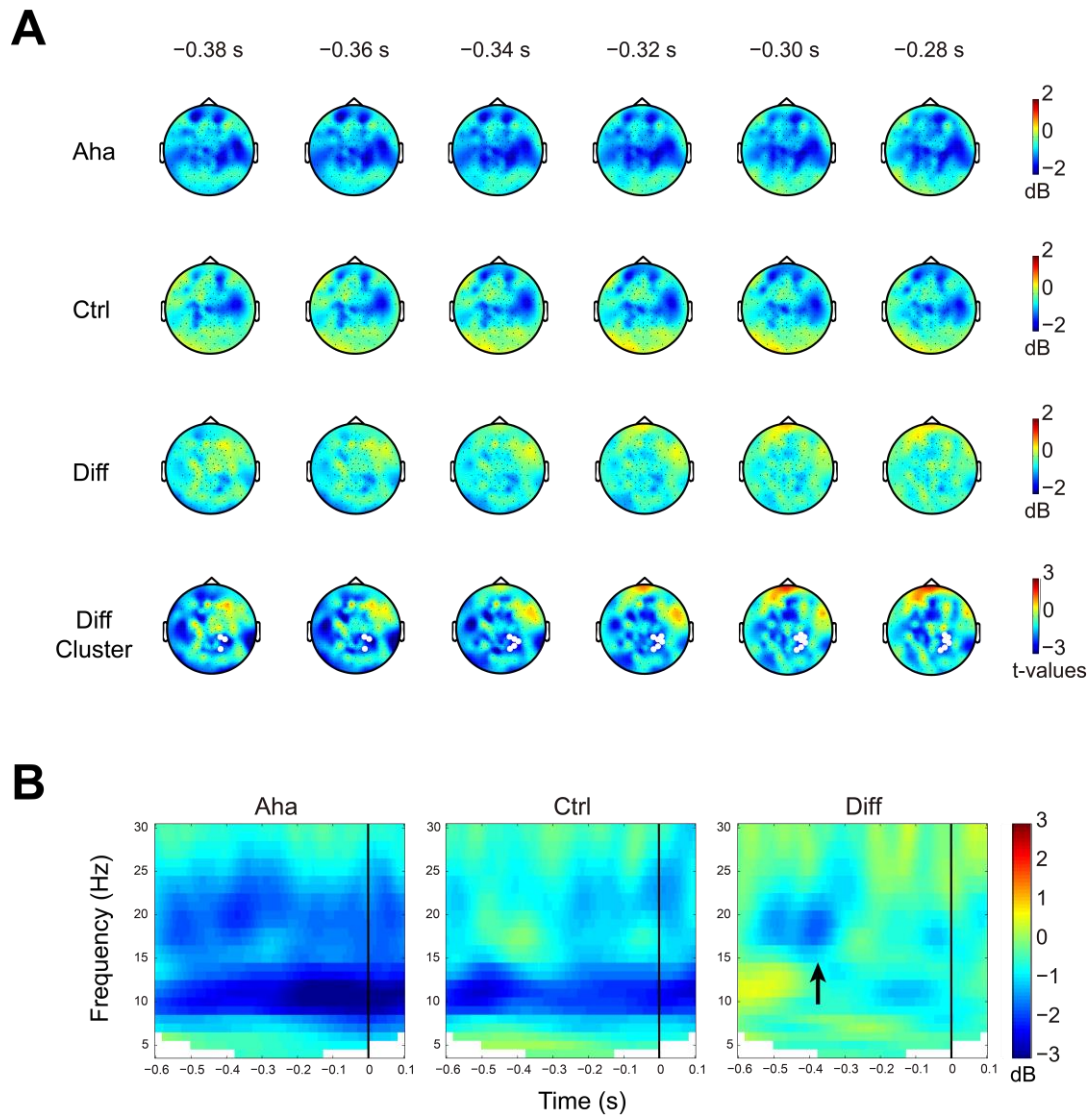


Figure 3-33. The beta power before response. (A) The Aha, Ctrl and Diff graphs represent the beta power for the Eureka effect, control and the difference between them, respectively. The Diff Cluster row represents the t -values of cluster analysis for the difference between Aha and Ctrl. The white dots show the significant negative clusters, which match the negative regions in the Diff row. (B) The time-frequency plot of the cluster. The arrow shows decreased beta power. The vertical black lines at the 0 s indicate response.

Gamma band activity

We observed no Eureka associated changes in the gamma band for any of the tested measures (power, coherence, PLV) neither in the stimulus nor in the response aligned epochs.

Fractal dimensionality

We analyzed dimensionality for the time window from 0 - 500 ms after stimulus onset, for 10 clusters of channels. The method for channel clustering was the same as applied previously for coherence and PLV analysis. We observed significant reductions of dimensionality over right central and left parietal areas, and a significant increase over the right occipital area (Figure 3-34A) in the Eureka trials. Furthermore, LI analysis showed that the dimensionality reduction was more pronounced ($\ln(\delta)$ from 1.47 to 1.65, $p < 0.05$) in the temporal region of the right hemisphere (Figure 3-34B). Similar results were obtained for response aligned activity patterns. In the time window from 500 ms before response to the response there was a significant reduction of dimensionality over the right temporal area, and an increase of dimensionality over the left frontal area; however, only 3 scale bins showed a significant difference (Figure 3-35A). Here, the scale bins refer to the data scales used for dimensionality analysis. The LI analysis confirmed the right lateralization of the dimensionality reduction ($\ln(\delta)$ from 0.94 to 1.26, $p < 0.05$) over temporal areas (Figure 3-35B).

Taken together, in both the stimulus and response aligned epochs the Eureka effect was associated with a reduction of fractal dimensionality in the right temporal cortex. In the Discussion we shall offer an interpretation of the relation between dimensionality, the Eureka effect and synchronization.

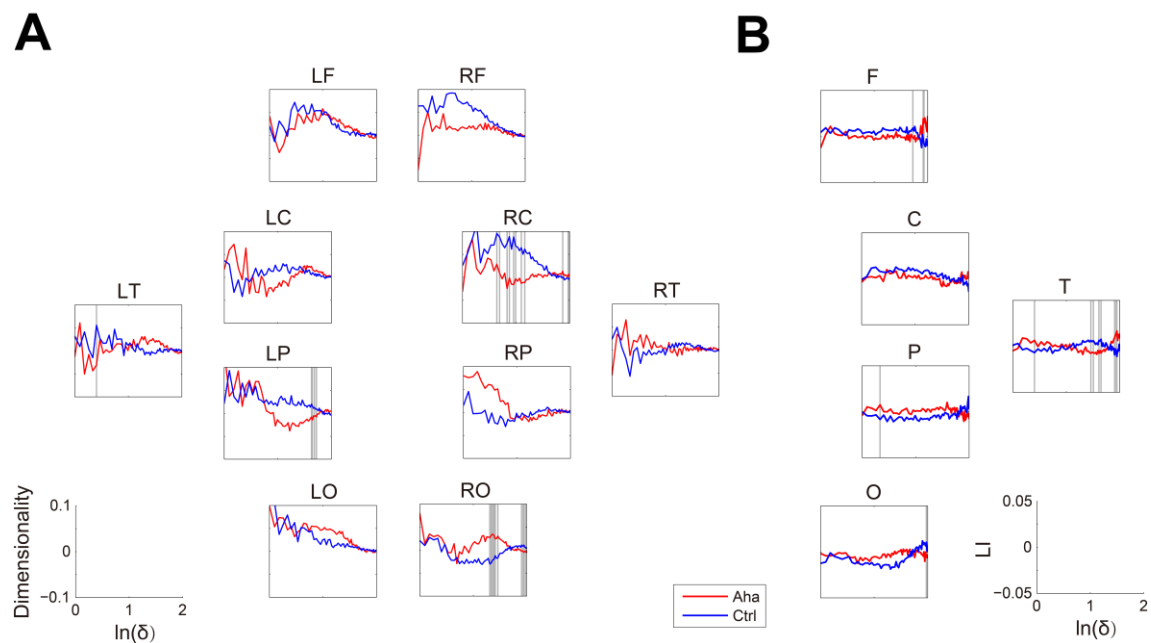


Figure 3-34. The dimensionality for ten channel clusters, in the time window: 0 s – 0.5 s. Zero is stimulus onset. The bins with significant difference between Aha and Ctrl are marked by gray lines. (A) The axis Y shows the dimensionality. The axis X shows the natural logarithm of scale size. The panels are arranged as the cluster positions. The title of each panel represents the cluster. (B) The axis Y shows the LI of dimensionality. The axis X shows the natural logarithm of scale size. The title of each panel represents the cluster pair for LI analysis.

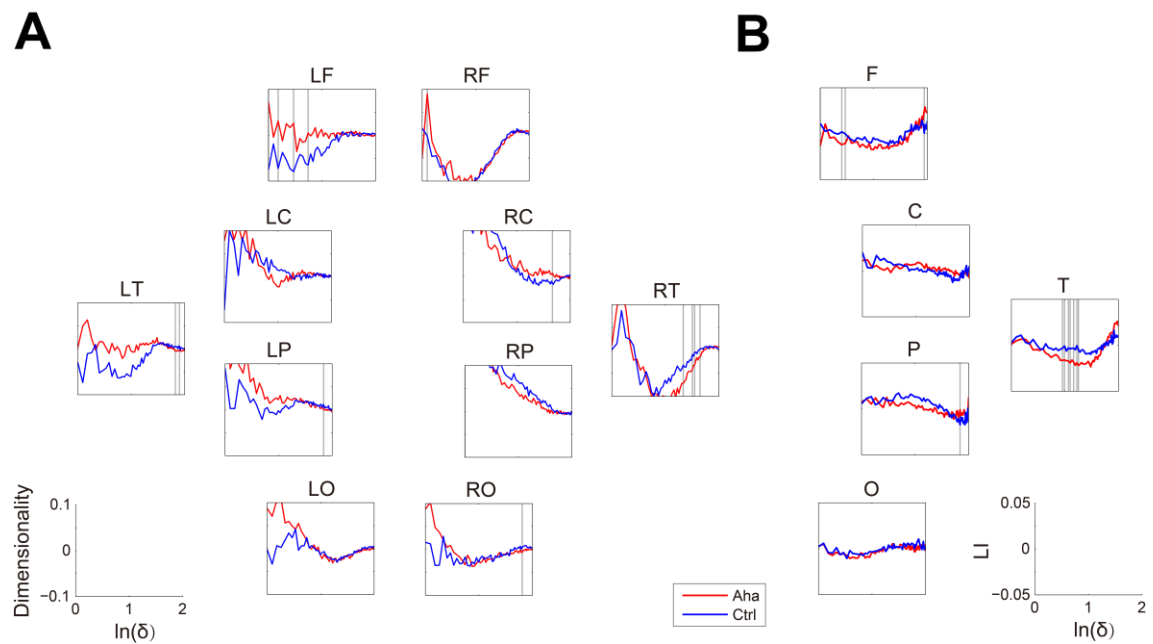


Figure 3-35. The dimensionality for ten channel clusters, in the time window: -0.5 s – 0 s. Zero is the response point. The bins with significant difference between Aha and Ctrl are marked by gray lines. (A) The axis Y shows the dimensionality. The axis X shows the natural logarithm of scale size. The panels are arranged as the cluster positions. The title of each panel represents the cluster. (B) The axis Y shows the LI of dimensionality. The axis X shows the natural logarithm of scale size. The title of each panel represents the cluster pair for LI analysis.

Pupil size

Pupil size changes were again assessed separately in the stimulus and response aligned epochs. In addition, trials were sorted according to reaction times (RTs). Baseline values were obtained from the first stage of trials and time windows had the same length as the time windows analysed during the third stage of trials.

After baseline correction only very few bins of the stimulus aligned epochs showed significant Eureka associated changes of pupil size. Only in the trials with RTs > 2.0 s, the pupil sizes were significantly larger in the Aha than the Ctrl condition. (Figure 3-39C).

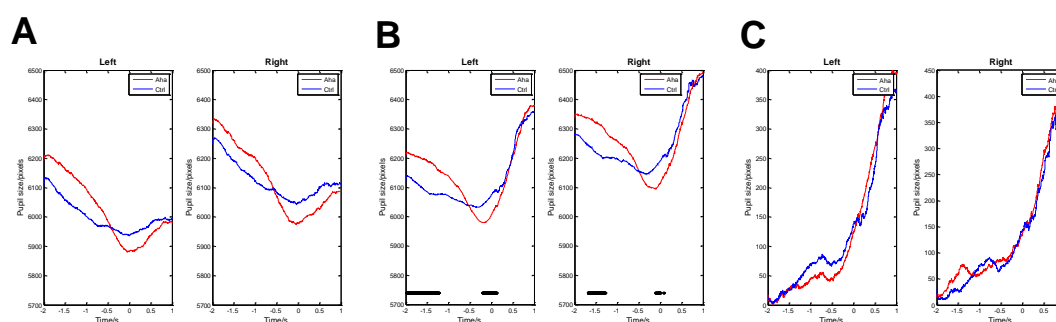


Figure 3-36. The pupil size for trials with RTs > 0.5 s (stimulus locked epochs). All data aligned with response (0 s). Panels A, B and C show baseline data, raw experiment data, and baseline corrected experiment data, respectively. The bins with significant difference between Aha and Ctrl are marked by black lines.

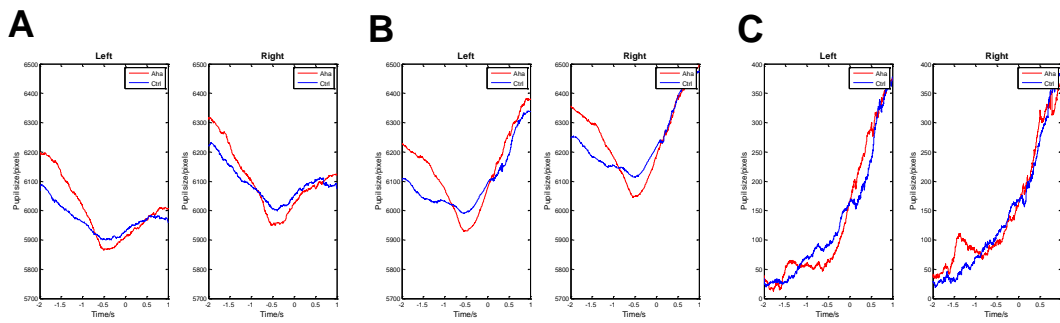


Figure 3-37. The pupil size for trials with RTs > 1.0 s (stimulus locked epochs). All data aligned with response (0 s). Panels A, B and C show baseline data, raw experiment data, and baseline corrected experiment data, respectively.

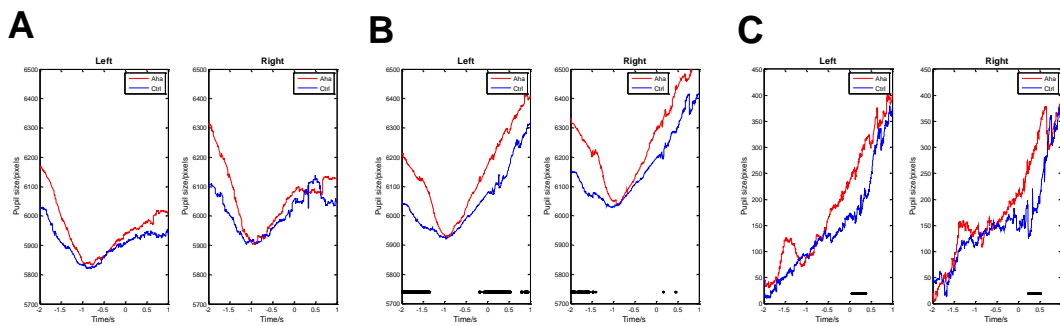


Figure 3-38. The pupil size for trials with RTs > 1.5 s (stimulus locked epochs). All data aligned with response (0 s). Panels A, B and C show baseline data, raw experiment data, and baseline corrected experiment data, respectively.

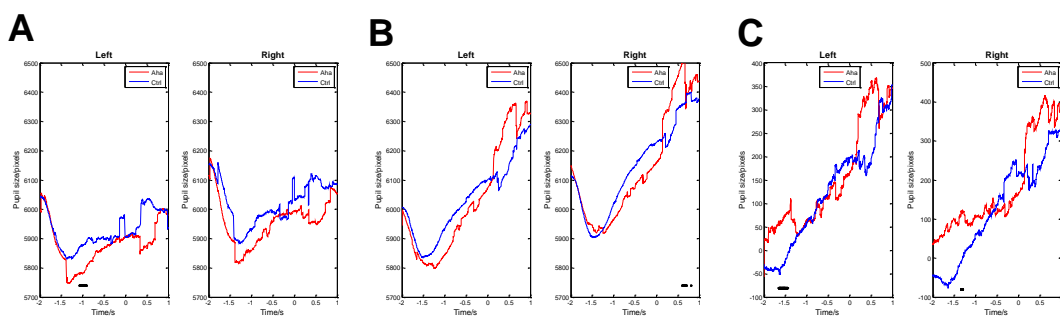


Figure 3-39. The pupil size for trials with RTs > 2.0 s (stimulus locked epochs). All data aligned with response (0 s). Panels A, B and C show baseline data, raw experiment data, and baseline corrected experiment data, respectively.

In the response aligned epochs pupil size was larger in the Eureka condition but this effect was significant only in trials with RTs < 2.0 s. The significant differences are represented in Figure 3-40C, Figure 3-41C and Figure 3-42C (RTs > 0.5 s, RTs > 1.0 s and RTs > 1.5 s, respectively).

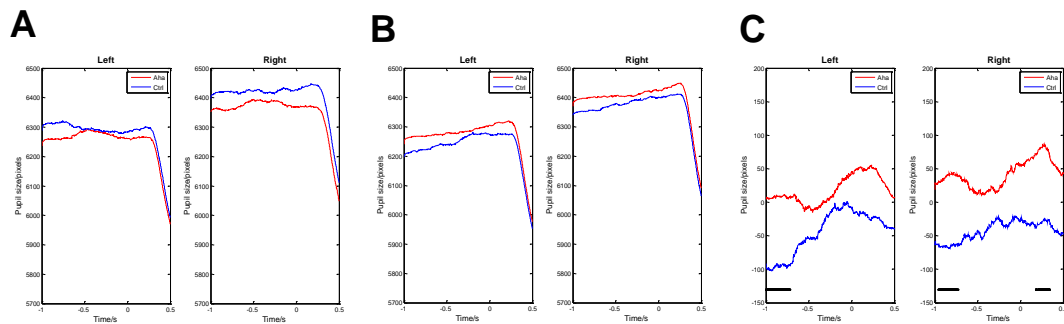


Figure 3-40. The pupil size for trials with RTs > 0.5 s (response locked epochs). All data aligned with stimulus onset (0 s). Panels A, B and C show baseline data, raw experiment data, and baseline corrected experiment data, respectively.

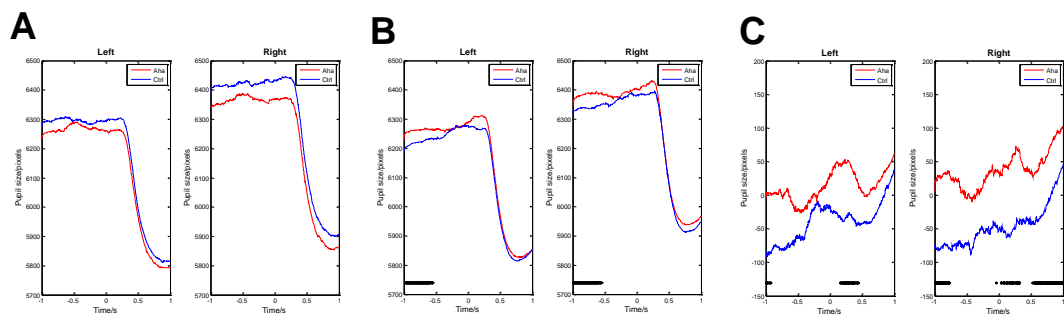


Figure 3-41. The pupil size for trials with RTs > 1.0 s (response locked epochs). All data aligned with stimulus onset (0 s). Panels A, B and C show baseline data, raw experiment data, and baseline corrected experiment data, respectively.

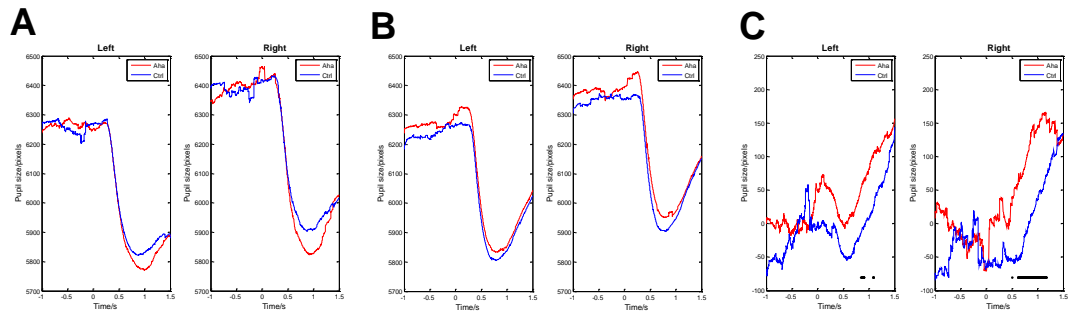


Figure 3-42. The pupil size for trials with RTs > 1.5 s (response locked epochs). All data aligned with stimulus onset (0 s). Panels A, B and C show baseline data, raw experiment data, and baseline corrected experiment data, respectively.

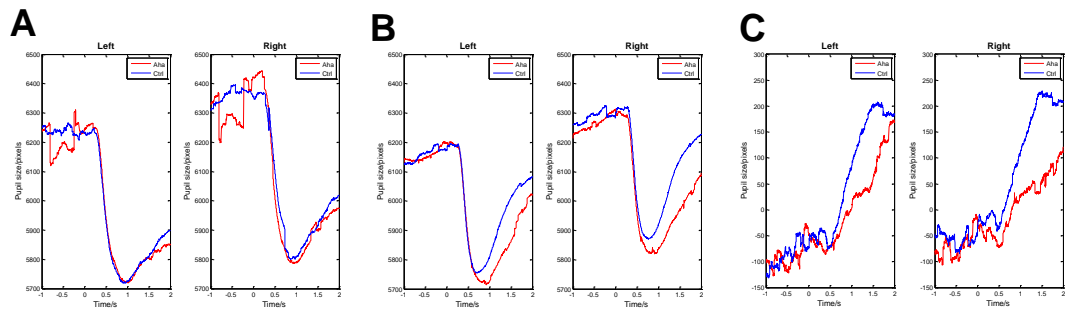


Figure 3-43. The pupil size for trials with RTs > 2.0 s (response locked epochs). All data aligned with stimulus onset (0 s). Panels A, B and C show baseline data, raw experiment data, and baseline corrected experiment data, respectively.

Supplemental Figures

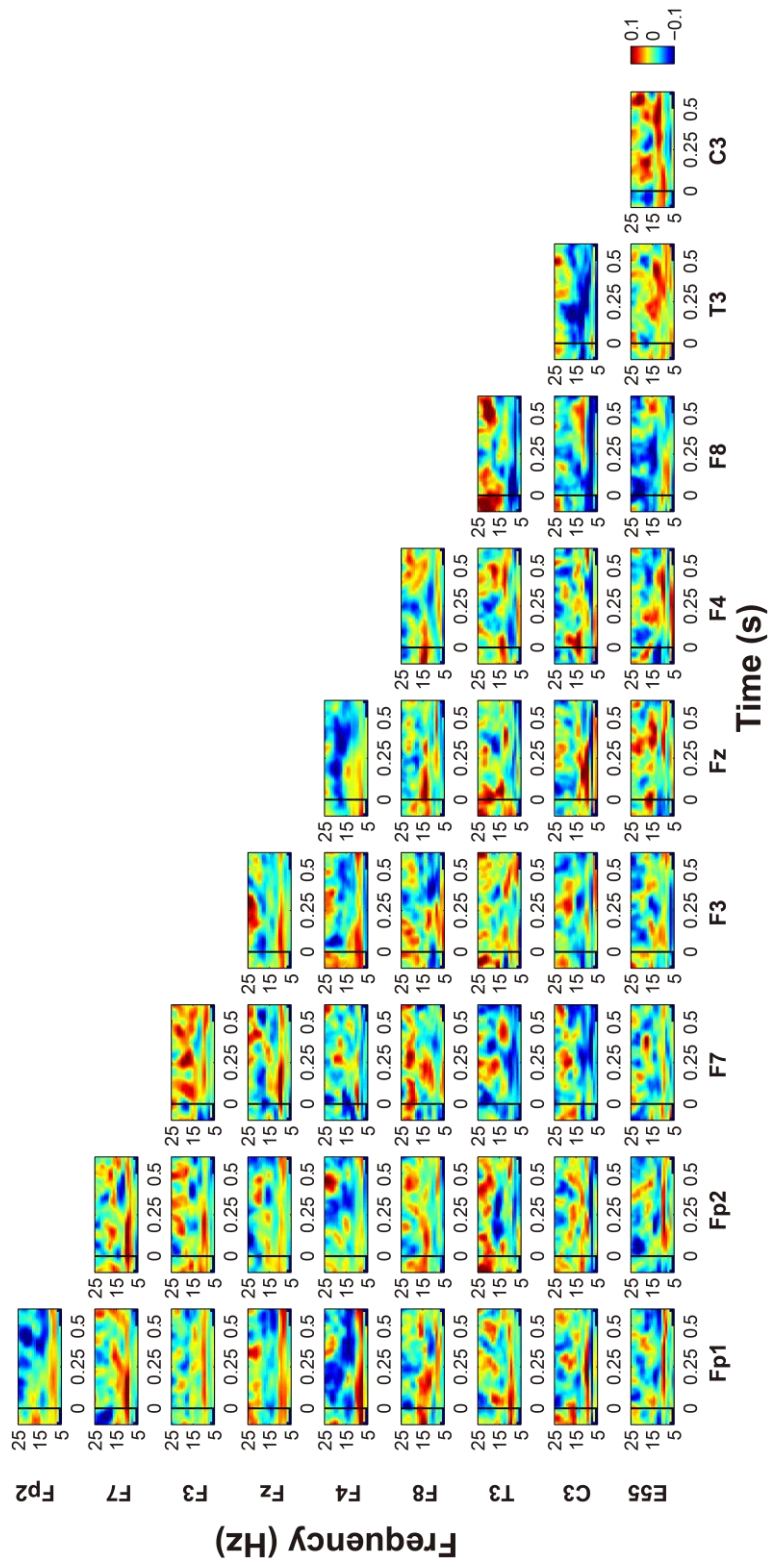


Figure S1a. The coherence of channels (stimulus locked epochs).
(To be continued.)

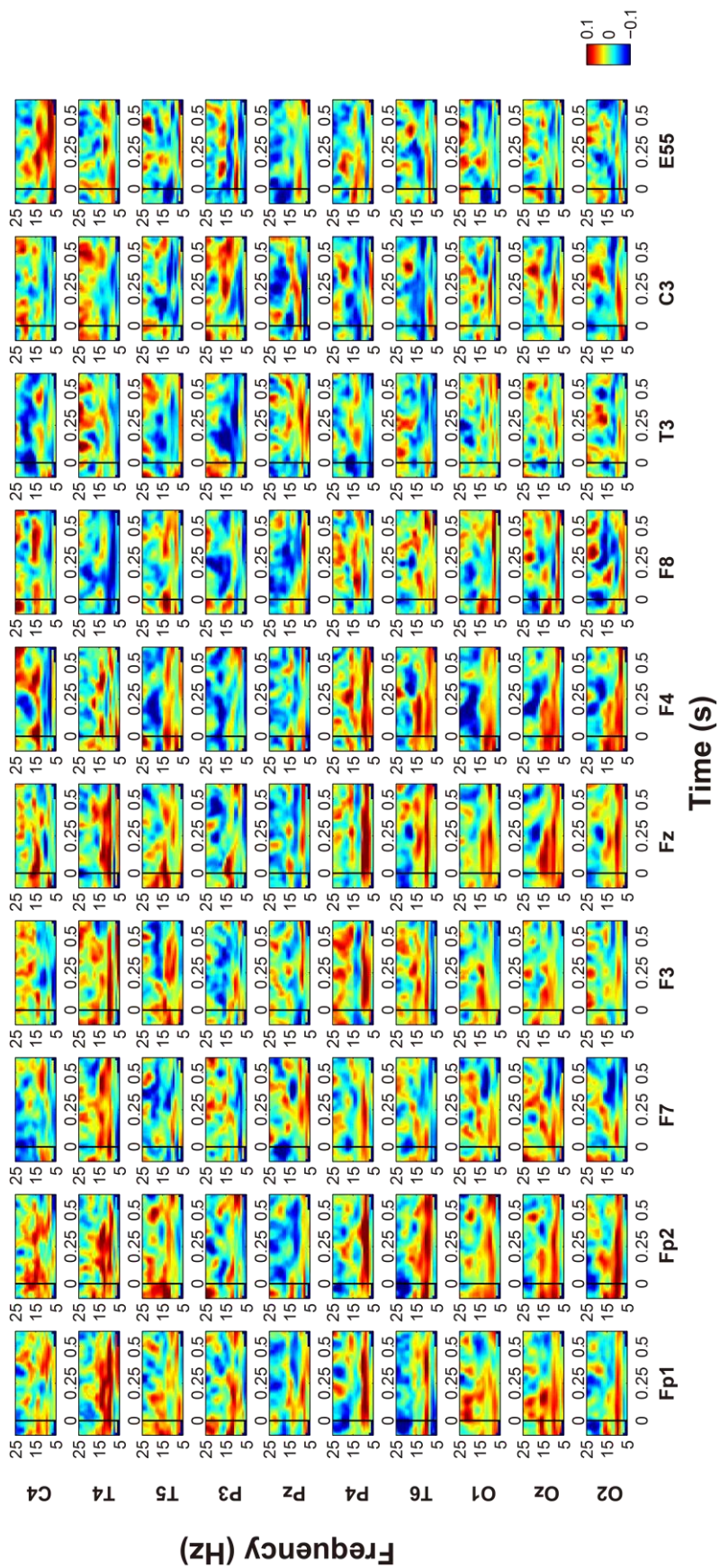


Figure S1b. The coherence of channels (stimulus locked epochs).
 (To be continued.)

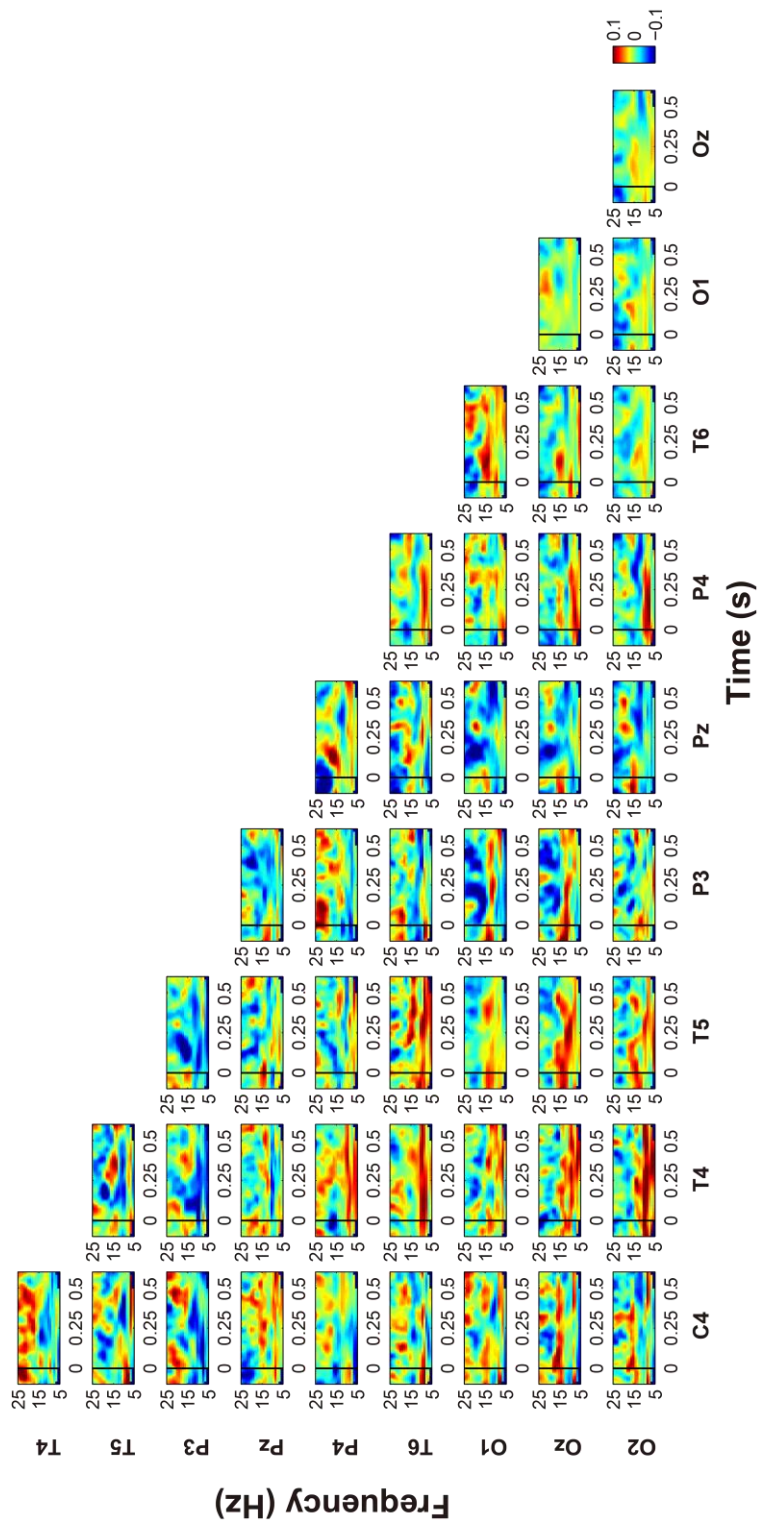


Figure S1c. The coherence of channels (stimulus locked epochs).

Figure S1 (a, b, c). The coherence of channels (stimulus locked epochs). Each panel represents the coherence values of low frequency band for channel pairs. The coherence values were calculated during the time window from 100 ms before stimulus onset to 600 ms after the onset. The black solid line at 0 on the time axis in each panel represents the stimulus onset. To show the figure in the limited space, we divided it into 3 parts: a, b and c.

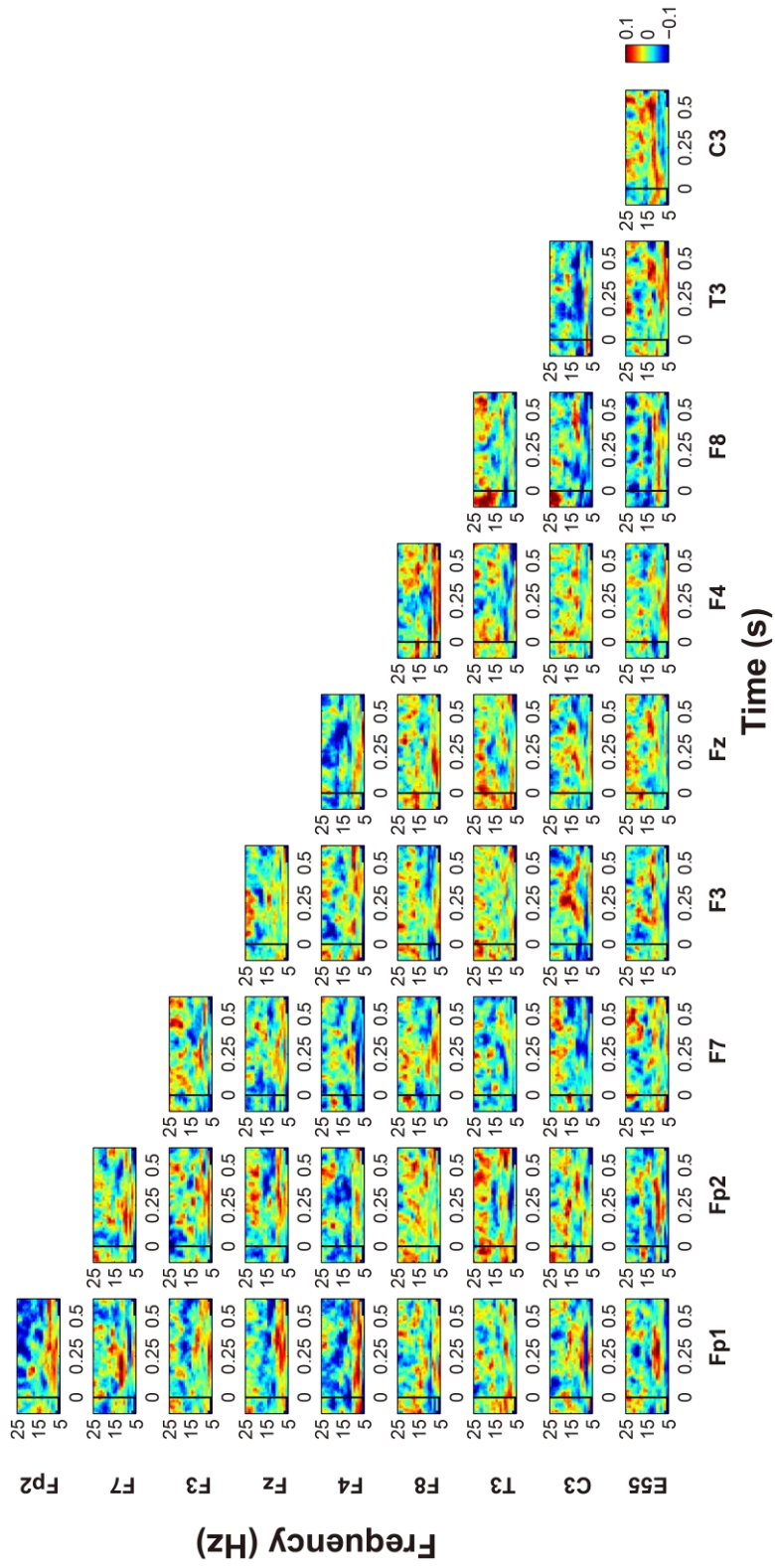


Figure S2a. The PLV of channels (stimulus locked epochs).
(To be continued.)

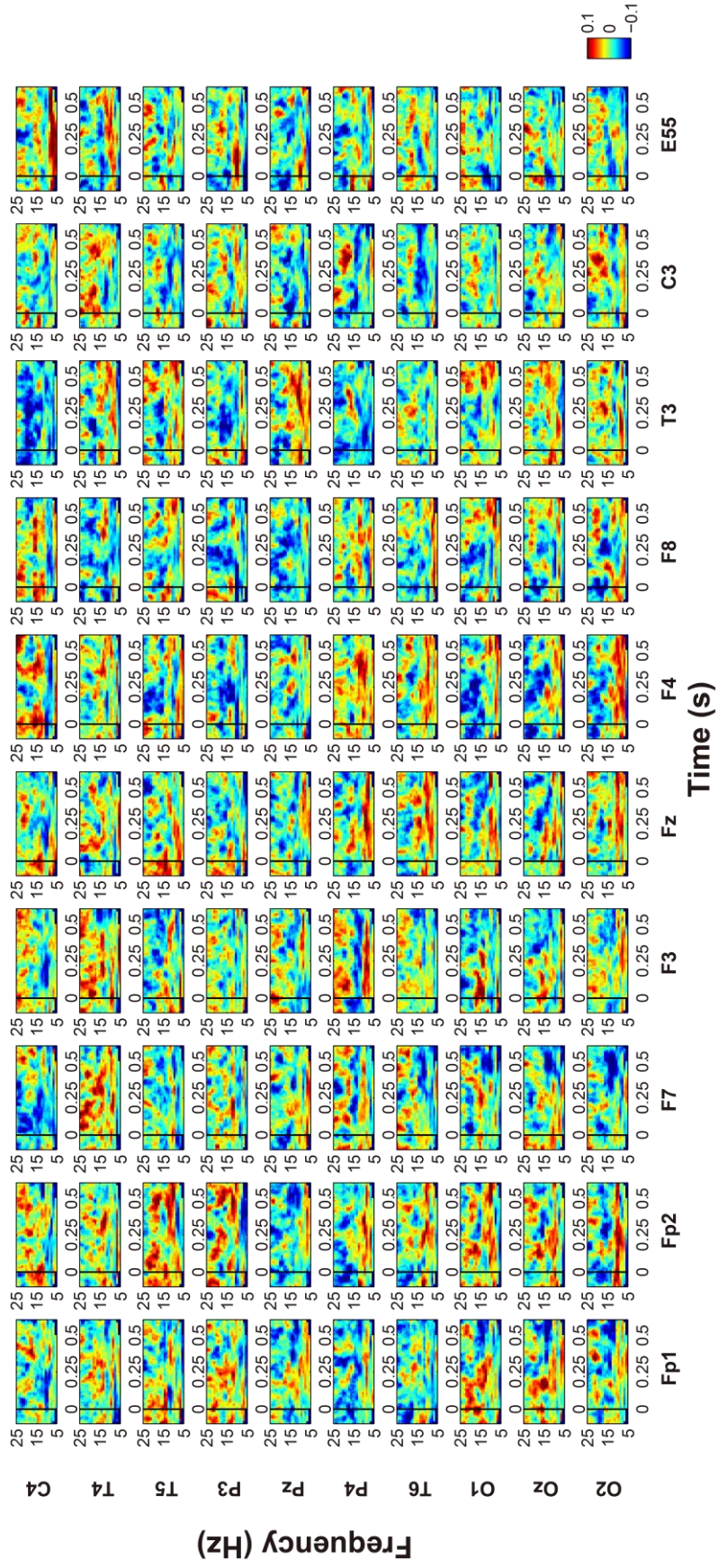


Figure S2b. The PLV of channels (stimulus locked epochs).
(To be continued.)

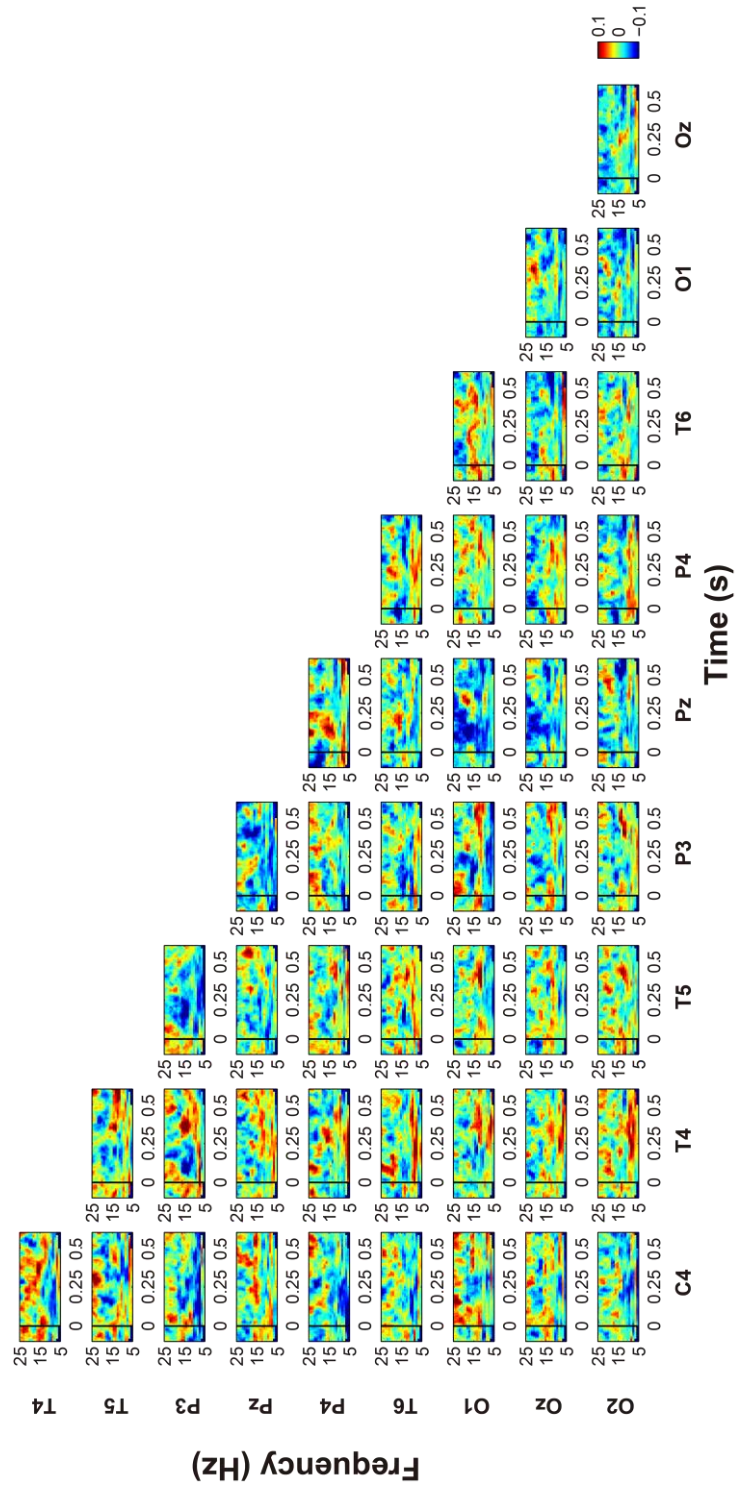


Figure S2c. The PLV of channels (stimulus locked epochs).

Figure S2 (a, b, c). The PLV of channels (stimulus locked epochs). Each panel represents the PLV of low frequency band for channel pairs. The PLV was calculated during the time window from 100 ms before stimulus onset to 600 ms after onset. The black solid line at 0 on the time axis in each panel represents the stimulus onset. To show the figure in the limited space, we divided it into 3 parts: a, b and c.

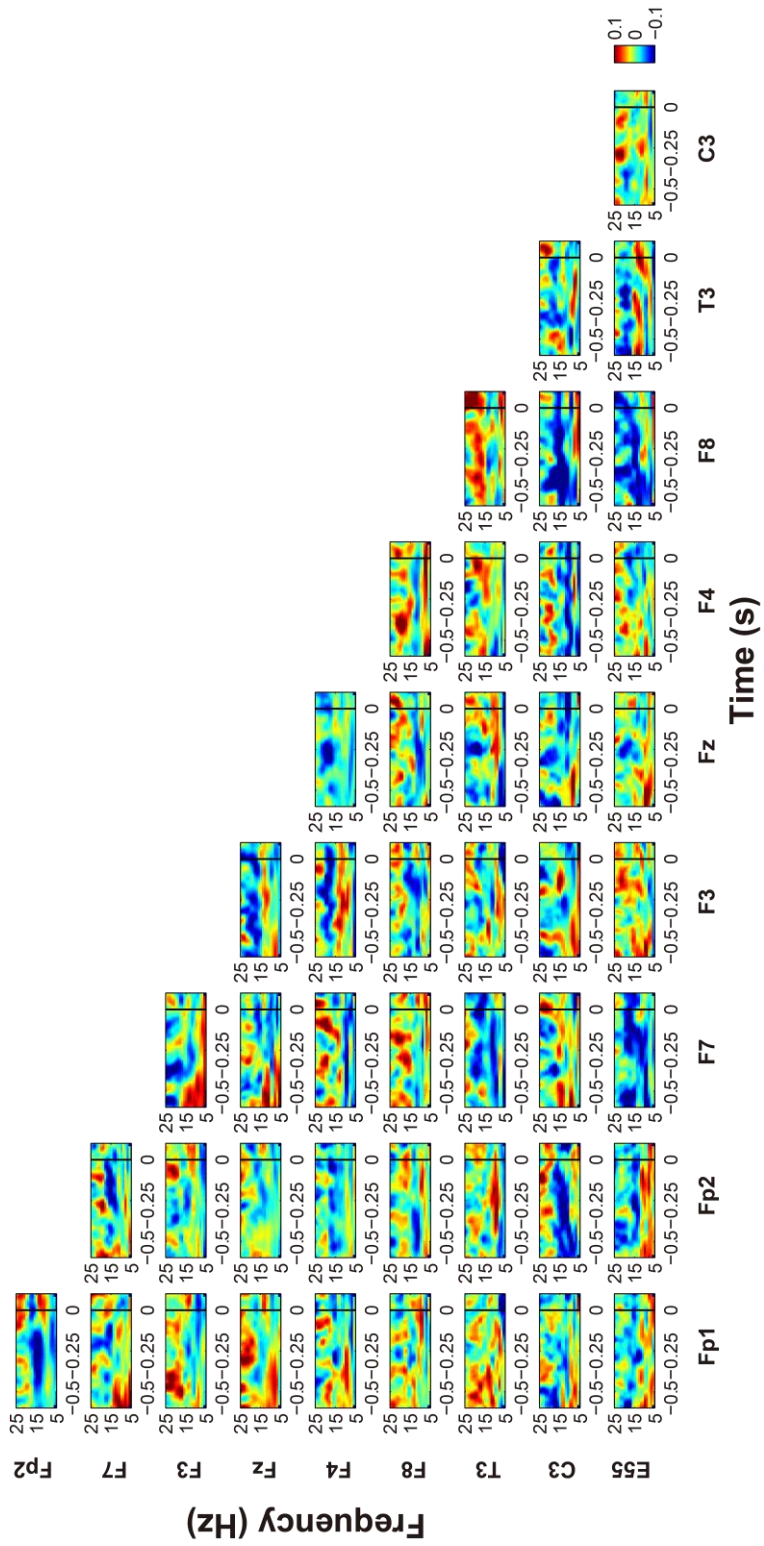


Figure S3a. The coherence of channels (response locked epochs).
(To be continued.)

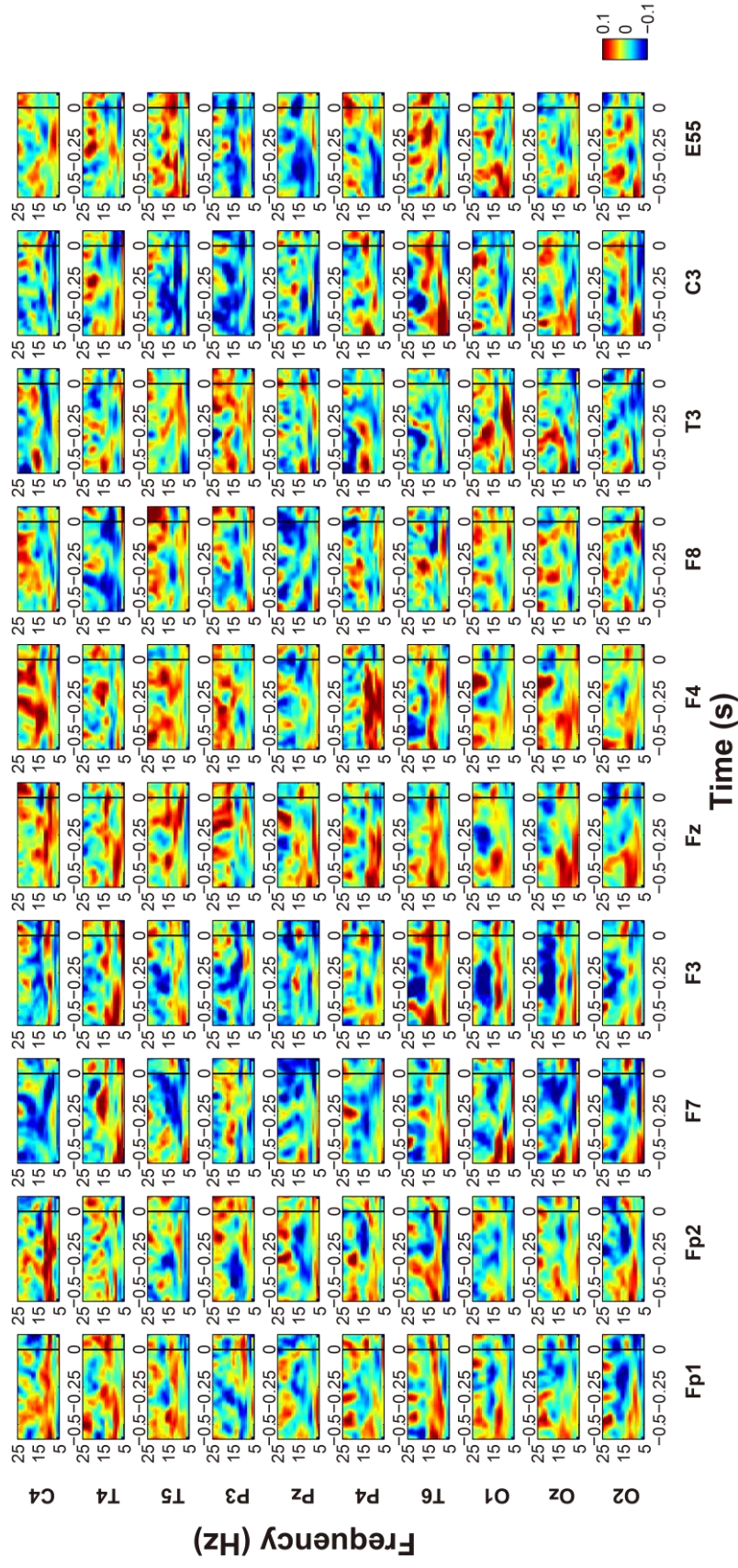


Figure S3b. The coherence of channels (response locked epochs).
(To be continued.)

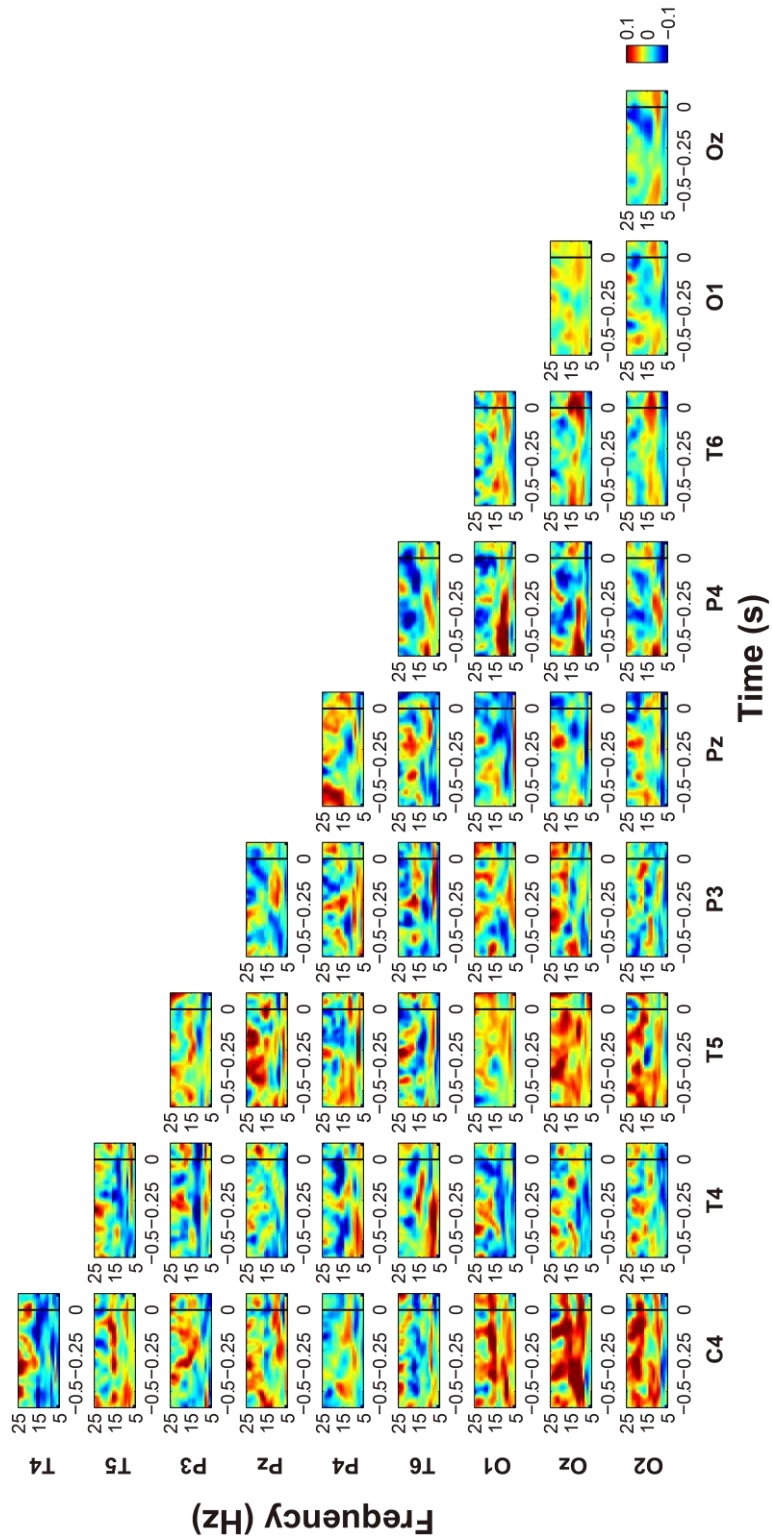


Figure S3c. The coherence of channels (response locked epochs).

Figure S3 (a, b, c). The coherence of channels (response locked epochs). Each panel represents the coherence values of low frequency band for channel pairs. The coherence was calculated during the time window from 600 ms before response to 100 ms after response. The black solid line at 0 on the time axis in each panel represents response. To show the figure in the limited space, we divided it into 3 parts: a, b and c.

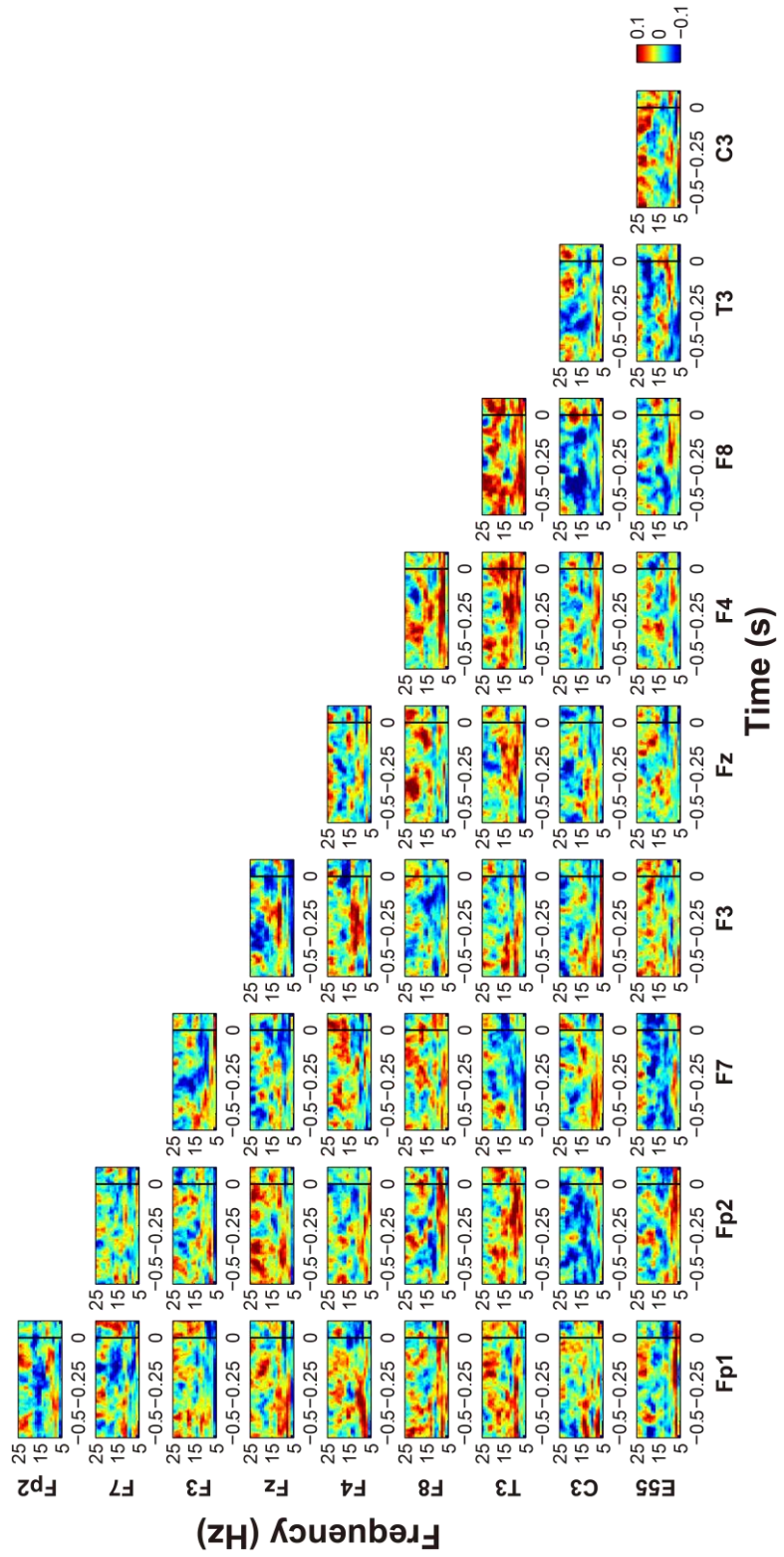


Figure S4a. The PLV of channels (response locked epochs).
(To be continued.)

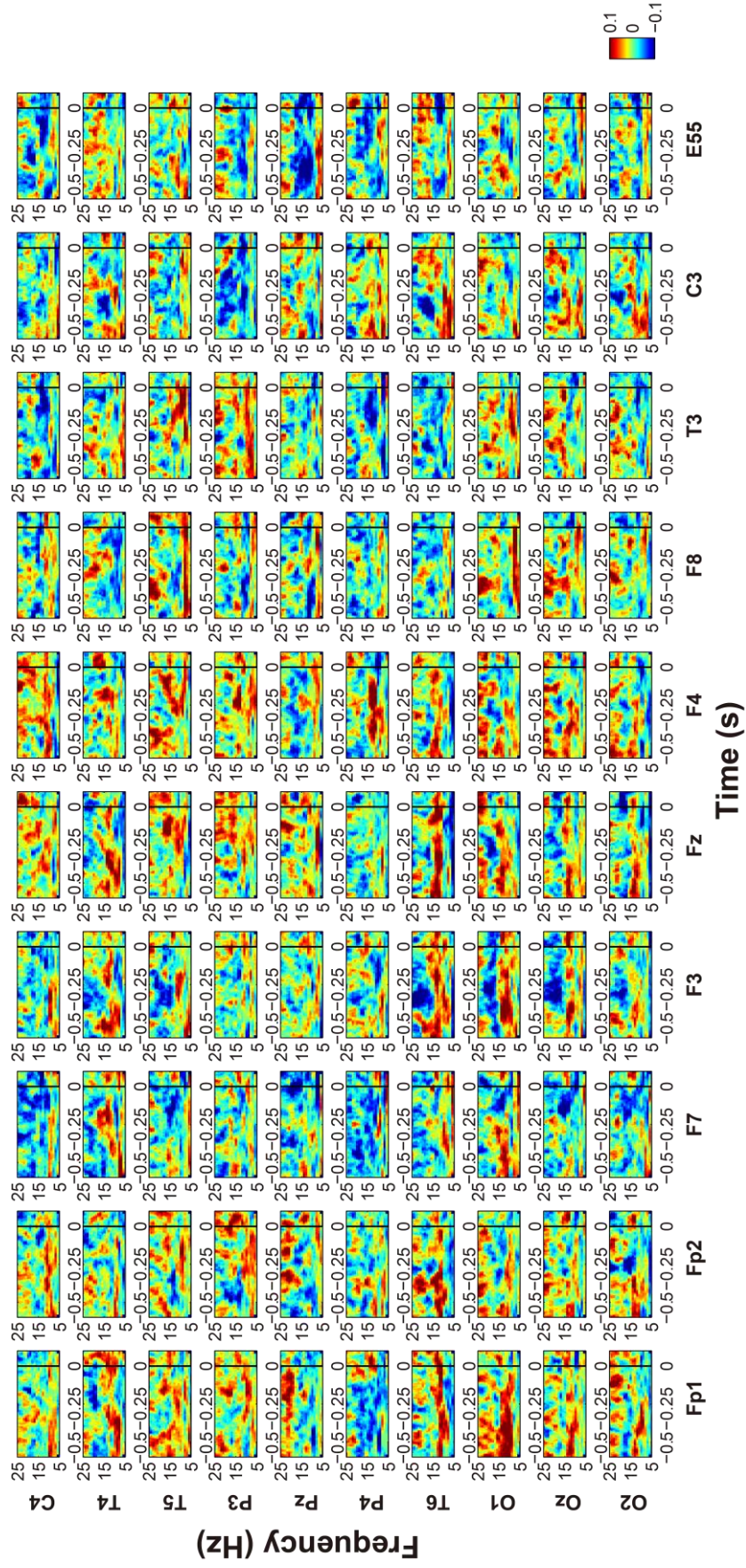


Figure S4b. The PLV of channels (response locked epochs).
(To be continued.)

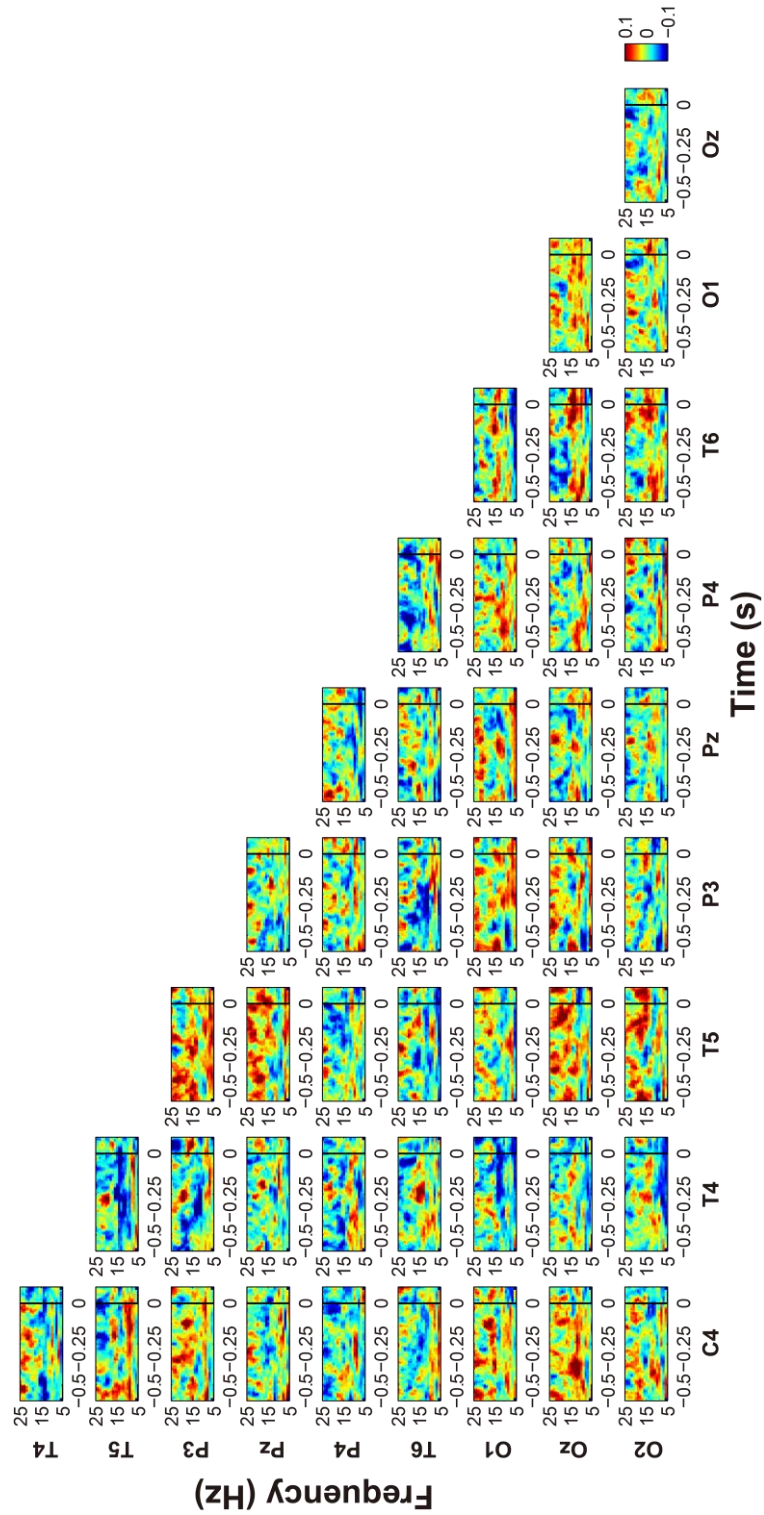


Figure S4c. The PLV of channels (response locked epochs).

Figure S4 (a, b, c). The PLV of channels (response locked epochs). Each panel represents the PLV of low frequency band for channel pairs. The PLV was calculated during the time window from 600 ms before response to 100 ms after response. The black solid line at 0 on the time axis in each panel represents response. To show the figure in the limited space, we divided it into 3 parts: a, b and c.

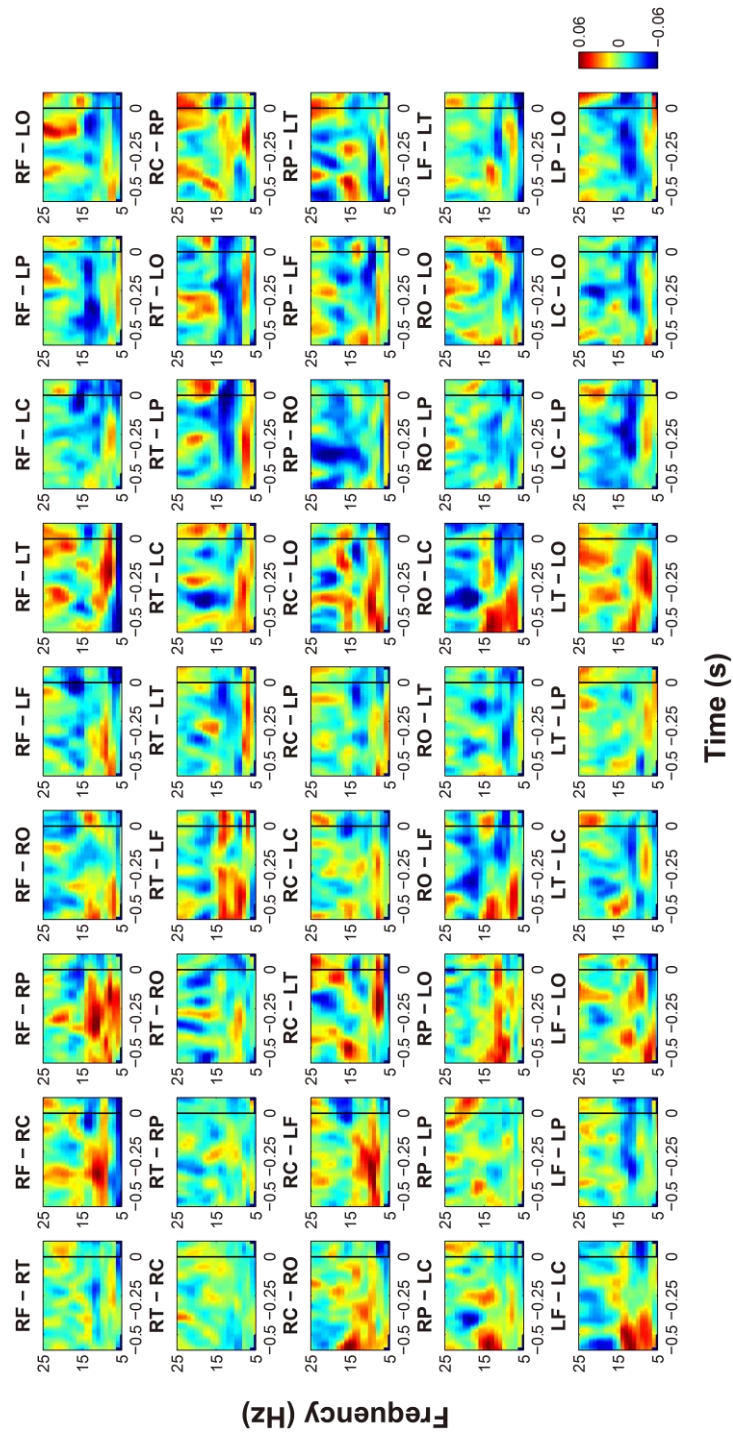


Figure S5. The coherence of channel clusters (response locked epochs). Each colored panel represents the coherence value between two clusters of channels. They were also calculated during the time window from 600 ms before response until 100 ms after response. The black solid line on 0 of the time axis in each panel shows response. The symbols of cluster pairs are marked on the top of corresponding panels.

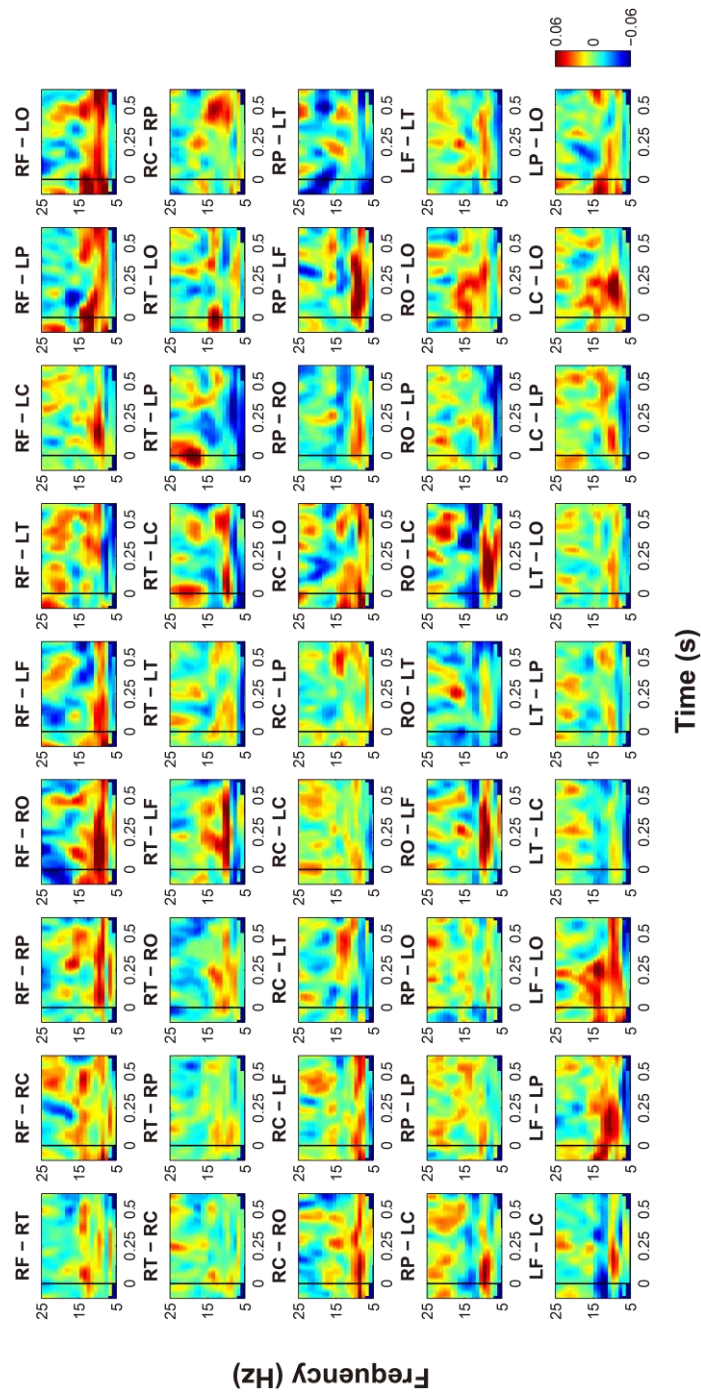


Figure S7. The coherence of channel clusters (stimulus locked epochs). Each colored panel represents the coherence value between two clusters of channels. They were also calculated during the time window from 100 ms before stimulus onset to 600 ms after onset. The black solid line on 0 of the time axis in each panel shows the onset. The symbols of cluster pairs are marked on the top of corresponding panels.

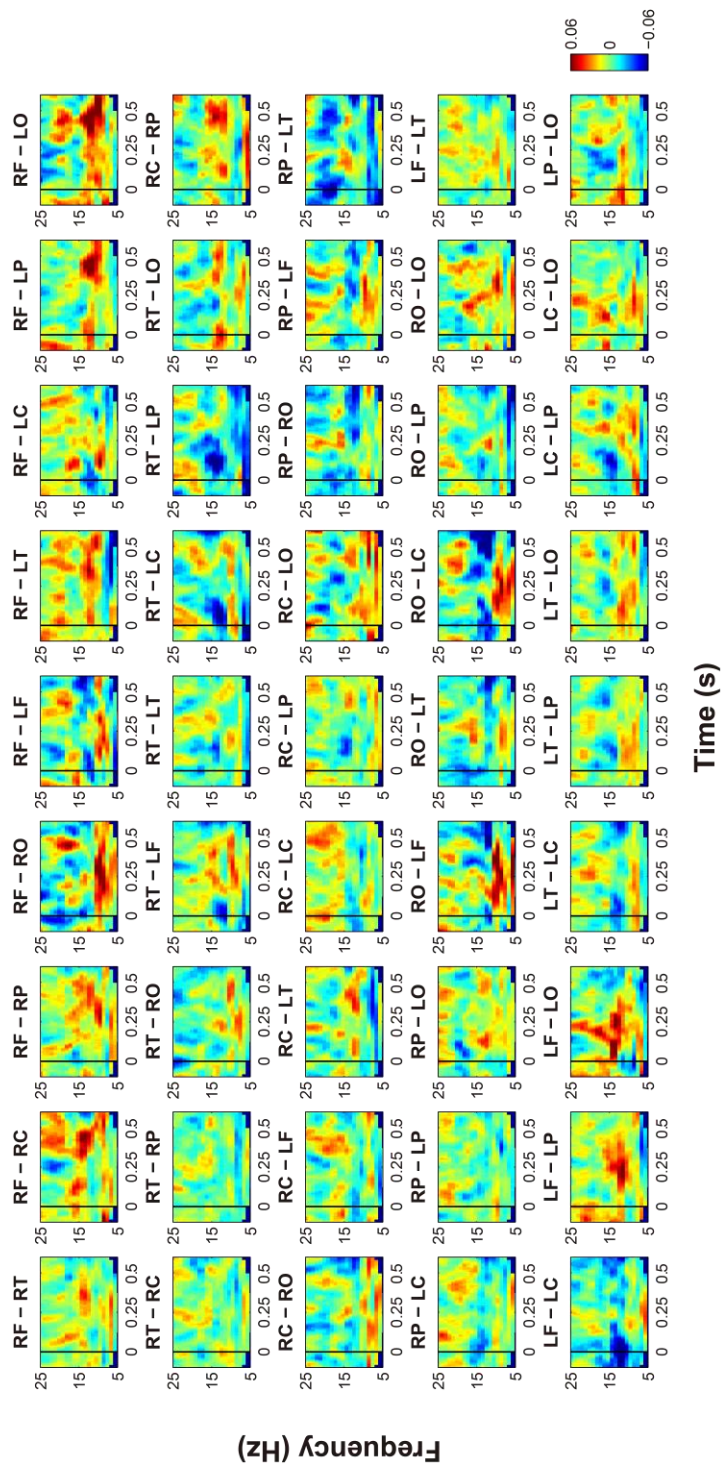


Figure S8. The PLV of channel clusters (stimulus locked epochs). Each colored panel represents the PLV between two clusters of channels. They were also calculated during the time window from 100 ms before stimulus onset to 600 ms after onset. The black solid line on 0 of the time axis in each panel shows the onset. The symbols of cluster pairs are marked on the top of corresponding panels.

4. Discussion

We investigated with EEG recordings brain activity during the Eureka effect, and found that oscillatory activity in the alpha and theta band exhibited right-hemisphere lateralized increases in coherence and phase locking, decreased power in the alpha band over frontal and occipital regions, and decreased power in the beta band over right parietal regions and the central gyrus, close to the midline. In addition we observed a reduction of dimensionality for activity recorded from the frontal and temporal region in the right hemisphere. We also measured pupillary responses as they reflect a large variety of central states related to alertness, attention, arousal, stress, cognitive load and emotions (Einhauser et al., 2008; Nassar et al., 2012; Reimer et al., 2016), but found Eureka related responses (dilations) only in trials with very long reaction times (> 2000 ms).

Methodological considerations

A crucial question is whether our paradigm reliably elicited a Eureka effect. As reviewed in the introduction, identification of neuronal correlates of the Eureka effect is hampered by the inability to precisely predict the time of its occurrence and to obtain sufficient trials per subject. Therefore, most of the classical conditions inducing Eureka effects are not suitable for neurobiological investigations. We have settled for a psychophysical task that allowed us to predict with some confidence, whether and when a stimulus would elicit a Eureka experience and to confirm its occurrence with a behavioural response. Subjects had to accomplish a difficult pattern

completion task that required flexible binding of features into a coherent gestalt and could be solved only in a minority of trials despite long inspection time when no additional cues were provided. However, by supplying additional information, subjects were enabled to solve the task promptly in the majority of trials, reporting sudden insight into the solution of the pattern completion problem. We are thus confident, that the paradigm allowed for comparison of neuronal responses to physically identical stimuli that did or did not induce the Eureka effect. In addition, our design allowed us to run a large number of trials in the same subject, which is a prerequisite for neurophysiological studies.

Although our paradigm allowed narrowing the time interval during which the Eureka effect was bound to occur, stimulus - response latencies were still variable. This could have been due to variable latencies of the Eureka effect or to variable lag times between the subjective Eureka experience and the motor response. In order to capture electrophysiological signatures of the Eureka state we therefore aligned for analysis neuronal responses to both stimulus and response onset. By adjusting the duration of the respective analysis window we made sure to cover the whole interval during which the Eureka effect was bound to occur. Because the results obtained for the two analysis windows were rather similar and located the effect to overlapping stretches of activity between stimulus and response onset, we are confident that the electrophysiological changes reflect processes associated with the Eureka experience.

Unexpectedly the measurements of pupil size gave less consistent results, showing dilatations only in the Eureka trials with long response latencies (> 2000 ms). Since these measurements showed interocular differences in the amount of dilatation, which should not have been the case given that pupillary responses are normally consensual, we did not pursue an in depth analysis of pupillary responses because we did not trust these measurements.

The Eureka effect and gamma band

Although processing of Mooney figures, or in a more general context, perceptual closure has been shown to be associated with enhanced power and phase synchronization of gamma oscillations (Uhlhaas et al., 2006; Uhlhaas et al., 2009; Castelhana et al., 2013; Moratti et al., 2014), our data did not reveal any significant changes in the gamma band in the eureka condition. This was unexpected as gamma synchronisation has been shown to be associated with binding operations (Singer, 1999) and the solution of the detection task in our experiments did require integration of sensory evidence with stored information. We propose as a likely reason for this negative evidence that the sudden insight into the solution of the perceptual problem did not require additional local binding operations such as are required for scene segmentation and perceptual closure, processes that are associated with gamma synchrony, but the matching of stored knowledge with sensory evidence.

Right-hemisphere lateralized alpha and theta activity

Our data indicate, that the Eureka effect is associated with distinct lateralized changes of coherence and power of oscillations in distinct frequency bands.

The most significant correlates of the Eureka effect were enhanced coherence and phase locking of alpha and theta oscillations over the right hemisphere. This enhanced synchronisation was not associated with amplitude changes and apparent both in measures applied to sensor pairs as well as to clusters of recording sites.

Alpha oscillations have been associated with many different functions. The fact that they tend to be suppressed when neuronal circuits engage in information processing and high frequency oscillations has been taken as indication that they represent an

idling rhythm (Pfurtscheller et al., 1996; Jensen et al., 2002). However, there are also abundant indications for an involvement of alpha oscillations in active processing. Alpha oscillations have been suggested to serve the suppression of irrelevant information in tasks requiring focusing attention (Clarke et al., 2008; Zanto et al., 2010; Zanto et al., 2011; Klimesch, 2012), to coordinate widely distributed processes by playing the role of a carrier frequency for the establishment of coherence across various frequency bands (cross frequency coupling) (Palva et al., 2005; Canolty and Knight, 2010), to be involved in the maintenance of contents in working memory (Palva et al., 2005; Freunberger et al., 2009; Zanto et al., 2014) and to mediate top down control (Klimesch et al., 2010; Benedek et al., 2011; Palva and Palva, 2011; Samaha et al., 2015). We suggest that the association of increased alpha coherence with the Eureka effect might be related to the maintenance and read out of contents from working memory and the top down mediation of this information to facilitate scene segmentation and perceptual binding.

An additional and non-exclusive possibility is that the enhanced right lateralized alpha and theta phase synchronization is related to the “creative” processes associated with the Eureka effect. Such electrographic signatures have been described in previous studies on creativity (Razumnikova, 2000; Jung-Beeman et al., 2004; Runco, 2004; Grabner et al., 2007; Freunberger et al., 2008; Sandkuhler and Bhattacharya, 2008; Kounios and Beeman, 2014). Although some of these studies used verbal tasks (Jung-Beeman et al., 2004; Grabner et al., 2007; Sandkuhler and Bhattacharya, 2008), the enhanced coherence in the alpha and theta range was lateralized to the right hemisphere. Even though our subjects were not asked to name the recognized objects, it is not excluded that (part of) the right hemisphere activity was related to covert verbalization.

Dissociation between alpha power and alpha phase locking

Somewhat unexpectedly there was a dissociation between alpha power and alpha phase locking, while power decreased, phase locking increased. A similar dissociation has been described by Freunberger et al., in an object recognition task with distorted colour pictures (Freunberger et al., 2008). Associated with the recognition of the objects alpha power (9 – 13 Hz) decreased in occipital and right centro-temporal areas while phase locking (10 – 12 Hz) increased in a right-hemispheric long-range anterior-to-posterior network. In a later study on working memory (Freunberger et al., 2009), found in posterior areas (parietal-occipital) reduced alpha power and at the same time enhanced phase locking. These observations add to the notion discussed above that alpha oscillations reflect heterogeneous processes. The decrease in alpha power associated with the Eureka effect is in line with the interpretation that alpha oscillations reflect an idling state and get reduced when cortical areas engage in functions (Pfurtscheller et al., 1996; Jensen et al., 2002). The regions exhibiting reduced alpha were most likely involved in the analysis of the visual stimuli used in the present study. The enhanced phase locking, by contrast, could be a reflection of the formation of large scale networks and the mediation of top-down effects, functions in which alpha oscillations have been proposed to serve as carrier frequency (Palva et al., 2005; Canolty and Knight, 2010). The increased alpha phase locking in the Eureka condition could thus be the reflection of the transient formation of a large scale coherent state comprising numerous areas in the right hemisphere. This interpretation agrees with the observation, that the dimensionality of the activity vector was also reduced over the right hemisphere in the Eureka condition.

Right-hemisphere lateralized reduction of dimensionality

Dimensionality is a measure of the complexity of dynamic states. If dimensionality is

high, coding space and the degrees of freedom are large but so is ambiguity. A reduction of dimensionality can be interpreted as a reduction of the number of possible states and hence as a reduction of ambiguity (Nikolic et al., 2008). In the present experiments we observed variable changes in dimensionality over frontal and occipital areas but these were small and reached significance only rarely. However, there was a robust reduction of dimensionality over frontal and temporal areas of the right hemisphere. This agrees with the finding that the “solution” state leading to the Eureka experience was associated with enhanced coherence in the alpha and theta frequency band, again over the right hemisphere. We interpret these changes as an indication that large cortical networks, in particular in the right hemisphere, converged towards a state identified as a solution state due to enhanced coherence and reduced variability.

Decrease of beta activity

These changes went in parallel with a decrease of the power of beta oscillations. A transient decrease of beta activity has been reported in association with the transition from the maintenance of posture to movement initiation (Schoffelen et al., 2008; Pogosyan et al., 2009; Allen and MacKinnon, 2010; Kilavik et al., 2013) but it is unlikely that the observed decrease was related to such motor functions because it should have been cancelled by subtraction of the control condition.. A more likely interpretation is that the beta decrease is related to memory retrieval and the switching of cognitive states. The present task required retrieval of information from memory (Sheth et al., 2009; Kounios and Beeman, 2014) and engaging memory has been found to be associated with decreased beta power in the parietal and parieto-occipital areas (Pesonen et al., 2007; Sheth et al., 2009). As described in the study of Sheth (Sheth et al., 2009) beta power also decreased in parietal, parieto-occipital, and centro-temporal areas in subjects solving verbal puzzles. Beta power also decreases

transiently with switches in cognitive states (Okazaki et al., 2008; Engel and Fries, 2010; Piantoni et al., 2010) and with the disambiguation of visual stimuli (Minami et al., 2014). As sudden switches in cognitive states are a hallmark of the Eureka effect we propose that the beta decrease observed in conjunction with the Eureka effect is related to such switches. To which extent the decrease in beta power is correlated to changes in neuronal activation cannot be inferred from EEG recordings. Two studies assessing neuronal activity with positron emission tomography (PET) and functional magnetic resonance imaging (fMRI) (Dolan et al., 1997; Eger et al., 2007) described an increase in activation in the parietal cortex associated with the Eureka experience. How this evidence relates to the transient decrease in beta power is unclear. As changes in neuronal dynamics such as increases and decreases of synchrony in particular frequency bands can occur without major changes in average firing rates, there need not be a conflict of these findings with our present results, both observations actually suggesting an involvement of parietal cortex in the Eureka effect.

5. Conclusions and future directions

In conclusion, our results suggest that the transition towards the solution of a perceptual task is mainly associated with a change of network dynamics towards a state of right-lateralized enhanced coherence and reduced complexity. Unfortunately the spatial and/or temporal resolution of non-invasive methods is too restricted in order to identify with more precision the underlying neuronal mechanisms. This would require invasive recordings and hence measurements in animals. However, it is unlikely that the Eureka effect can be studied in animals since the experience of the Eureka effect requires more than just perceiving or recognizing a stimulus. It depends in addition on the awareness of having solved a difficult cognitive problem and thus involves a form of meta-cognition that is only accessible from the first-person perspective. While animals with well developed cognitive functions such as non-human primates may be able to realize meta-cognitive functions it is unclear how one would assess whether and when they experience a Eureka effect. One attractive possibility for future investigations of the neuronal underpinnings of the Eureka effect would be to take advantage of intracranial recordings performed in patients for diagnostic purposes.

Bibliography

Ahissar M, Hochstein S (1997) Task difficulty and the specificity of perceptual learning. *Nature* 387:401-406.

Allen DP, MacKinnon CD (2010) Time-frequency analysis of movement-related spectral power in EEG during repetitive movements: a comparison of methods. *J Neurosci Methods* 186:107-115.

Amari S-i, Cichocki A, Yang HH (1996) A new learning algorithm for blind signal separation. In: *Advances in neural information processing systems*, pp 757-763.

Anemuller J, Sejnowski TJ, Makeig S (2003) Complex independent component analysis of frequency-domain electroencephalographic data. *Neural Netw* 16:1311-1323.

Ansburg PI, Dominowski RL (2000) Promoting insightful problem solving. *J Creative Behav* 34: 30-60

Aziz-Zadeh L, Kaplan JT, Iacoboni M (2009) "Aha!": The neural correlates of verbal insight solutions. *Hum Brain Mapp* 30:908-916.

Bell AJ, Sejnowski TJ (1995) An information-maximization approach to blind separation and blind deconvolution. *Neural Comput* 7:1129-1159.

Benedek M, Bergner S, Konen T, Fink A, Neubauer AC (2011) EEG alpha synchronization is related to top-down processing in convergent and divergent thinking. *Neuropsychologia* 49:3505-3511.

Biederman I (1987) Recognition-by-components: a theory of human image

understanding. *Psychol Rev* 94:115-147.

Bowden EM, Jung-Beeman M (2007) Methods for investigating the neural components of insight. *Methods* 42:87-99.

Bowden EM, Jung-Beeman M, Fleck J, Kounios J (2005) New approaches to demystifying insight. *Trends Cogn Sci* 9:322-328.

Bradley MM, Miccoli L, Escrig MA, Lang PJ (2008) The pupil as a measure of emotional arousal and autonomic activation. *Psychophysiology* 45:602-607.

Bullmore E, Sporns O (2012) The economy of brain network organization. *Nat Rev Neurosci* 13:336-349.

Canolty RT, Knight RT (2010) The functional role of cross-frequency coupling. *Trends Cogn Sci* 14:506-515.

Castelhano J, Rebola J, Leitao B, Rodriguez E, Castelo-Branco M (2013) To Perceive or Not Perceive: The Role of Gamma-band Activity in Signaling Object Percepts. *PLoS ONE* 8: e66363

Cerruti C, Schlaug G (2009) Anodal transcranial direct current stimulation of the prefrontal cortex enhances complex verbal associative thought. *J Cogn Neurosci* 21:1980-1987.

Chein JM, Weisberg RW, Streeter NL, Kwok S (2010) Working memory and insight in the nine-dot problem. *Mem Cognit* 38:883-892.

Chi RP, Snyder AW (2011) Facilitate insight by non-invasive brain stimulation. *PLoS ONE* 6:e16655.

Chu Y, MacGregor JN (2011) Human performance on insight problem solving: A review. *J Problem Solving* 3:119-150.

Clarke AR, Barry RJ, Heaven PC, McCarthy R, Selikowitz M, Byrne MK (2008) EEG coherence in adults with attention-deficit/hyperactivity disorder. *Int J Psychophysiol* 67:35-40.

Cranford EA, Moss J (2012) Is insight always the same? A protocol analysis of insight in compound remote associate problems. *J Problem Solving* 4:128-153

Cunningham JB, MacGregor JN, Gibb J, Haar J (2009) Categories of insight and their correlates: An exploration of relationships among classic - type insight problems, rebus puzzles, remote associates and esoteric analogies. *J Creative Behav* 43:262-280.

Delorme A, Makeig S (2004) EEGLAB: an open source toolbox for analysis of single-trial EEG dynamics including independent component analysis. *J Neurosci Meth* 134:9-21.

Dolan RJ, Fink GR, Rolls E, Booth M, Holmes A, Frackowiak RS, Friston KJ (1997) How the brain learns to see objects and faces in an impoverished context. *Nature* 389:596-599.

Dominowski RL, Dallob P (1995) Insight and problem solving. In: *The nature of insight*. pp 33-62.

Duncker K (1945) On problem-solving. *Psychol Monogr* 58:i-113.

Eger E, Henson RN, Driver J, Dolan RJ (2007) Mechanisms of top-down facilitation in perception of visual objects studied by fMRI. *Cereb Cortex* 17:2123-2133.

Einhauser W, Stout J, Koch C, Carter O (2008) Pupil dilation reflects perceptual selection and predicts subsequent stability in perceptual rivalry. *Proc Natl Acad Sci USA* 105:1704-1709.

Engel AK, Fries P (2010) Beta-band oscillations--signalling the status quo? *Curr Opin*

Neurobiol 20:156-165.

Fleck JJ, Weisberg RW (2004) The use of verbal protocols as data: an analysis of insight in the candle problem. *Mem Cognit* 32:990-1006.

Freunberger R, Klimesch W, Griesmayr B, Sauseng P, Gruber W (2008) Alpha phase coupling reflects object recognition. *Neuroimage* 42:928-935.

Freunberger R, Fellinger R, Sauseng P, Gruber W, Klimesch W (2009) Dissociation between phase-locked and nonphase-locked alpha oscillations in a working memory task. *Hum Brain Mapp* 30:3417-3425.

Fries P (2009) Neuronal gamma-band synchronization as a fundamental process in cortical computation. *Annu Rev Neurosci* 32:209-224.

Frigo M, Johnson SG (1998) FFTW: An adaptive software architecture for the FFT. In: *Acoustics, Speech and Signal Processing, 1998. Proceedings of the 1998 IEEE International Conference on*, pp 1381-1384: IEEE.

Giovannelli F, Silingardi D, Borgheresi A, Feurra M, Amati G, Pizzorusso T, Viggiano MP, Zaccara G, Berardi N, Cincotta M (2010) Involvement of the parietal cortex in perceptual learning (Eureka effect): an interference approach using rTMS. *Neuropsychologia* 48:1807-1812.

Goold JE, Meng M (2016) Visual Search of Mooney Faces. *Front Psychol* 7:155.

Gorlin S, Meng M, Sharma J, Sugihara H, Sur M, Sinha P (2012) Imaging prior information in the brain. *Proc Natl Acad Sci U S A* 109:7935-7940.

Grabner RH, Fink A, Neubauer AC (2007) Brain correlates of self-rated originality of ideas: evidence from event-related power and phase-locking changes in the EEG. *Behav Neurosci* 121:224-230.

Grassberger P, Procaccia I (1983) Measuring the strangeness of strange attractors. *Physica D: Nonlinear Phenomena* 9:189-208.

Gray CM, König P, Engel AK, Singer W (1989) Oscillatory Responses in Cat Visual-Cortex Exhibit Inter-Columnar Synchronization Which Reflects Global Stimulus Properties. *Nature* 338:334-337.

Griffin G, Holub A, Perona P (2007) Caltech-256 object category dataset. CIT

Grutzner C, Uhlhaas PJ, Genc E, Kohler A, Singer W, Wibral M (2010) Neuroelectromagnetic correlates of perceptual closure processes. *J Neurosci* 30:8342-8352.

Haddad RA, Akansu AN (1991) A class of fast Gaussian binomial filters for speech and image processing. *IEEE T Signal Proces* 39:723-727.

Hipp JF, Engel AK, Siegel M (2011) Oscillatory synchronization in large-scale cortical networks predicts perception. *Neuron* 69:387-396.

Hsieh PJ, Vul E, Kanwisher N (2010) Recognition alters the spatial pattern of fMRI activation in early retinotopic cortex. *J Neurophysiol* 103:1501-1507.

James TW, Humphrey GK, Gati JS, Menon RS, Goodale MA (2000) The effects of visual object priming on brain activation before and after recognition. *Curr Biol* 10:1017-1024.

Jansen A, Menke R, Sommer J, Forster AF, Bruchmann S, Hämlemp J, Weber B, Knecht S (2006) The assessment of hemispheric lateralization in functional MRI--robustness and reproducibility. *Neuroimage* 33:204-217.

Jensen O, Gelfand J, Kounios J, Lisman JE (2002) Oscillations in the alpha band (9-12 Hz) increase with memory load during retention in a short-term memory task.

Cereb Cortex 12:877-882.

Jung-Beeman M, Bowden EM, Haberman J, Frymiare JL, Arambel-Liu S, Greenblatt R, Reber PJ, Kounios J (2004) Neural activity when people solve verbal problems with insight. *PLoS Biol* 2:E97.

Kaplan CA, Simon HA (1990) In search of insight. *Cognitive Psychol* 22:374-419.

Kersten D, Mamassian P, Yuille A (2004) Object perception as Bayesian inference. *Annu Rev Psychol* 55:271-304.

Kilavik BE, Zaepffel M, Brovelli A, MacKay WA, Riehle A (2013) The ups and downs of beta oscillations in sensorimotor cortex. *Exp Neurol* 245:15-26.

Klimesch W (2012) alpha-band oscillations, attention, and controlled access to stored information. *Trends Cogn Sci* 16:606-617.

Klimesch W, Freunberger R, Sauseng P (2010) Oscillatory mechanisms of process binding in memory. *Neurosci Biobehav Rev* 34:1002-1014.

Knoblich G, Ohlsson S, Haider H, Rhenius D (1999) Constraint relaxation and chunk decomposition in insight problem solving. *J Exp Psychol: Learning, Memory, and Cognition* 25:1534-1555.

Kounios J, Beeman M (2014) The cognitive neuroscience of insight. *Annu Rev Psychol* 65:71-93.

Lachaux JP, Rodriguez E, Martinerie J, Varela FJ (1999) Measuring phase synchrony in brain signals. *Hum Brain Mapp* 8:194-208.

Lee T-W, Girolami M, Sejnowski TJ (1999) Independent component analysis using an extended infomax algorithm for mixed subgaussian and supergaussian sources. *Neural Comput* 11:417-441.

- Lim JS (1990) Two-dimensional signal and image processing. Englewood Cliffs, NJ, Prentice Hall. MIT, Cambridge, MA
- Luo J, Niki K, Phillips S (2004) Neural correlates of the 'Aha!' reaction'. *Neuroreport* 15:2013-2017.
- Maier NR (1930) Reasoning in humans. I. On direction. *J Comp Psychol* 10:115.
- Marie C, Trainor LJ (2013) Development of simultaneous pitch encoding: infants show a high voice superiority effect. *Cereb Cortex* 23:660-669.
- Maris E, Oostenveld R (2007) Nonparametric statistical testing of EEG- and MEG-data. *J Neurosci Meth* 164:177-190.
- Mayer A, Schwiedrzik CM, Wibral M, Singer W, Melloni L (2016) Expecting to See a Letter: Alpha Oscillations as Carriers of Top-Down Sensory Predictions. *Cereb Cortex* 26:3146-3160.
- McGinley MJ, David SV, McCormick DA (2015a) Cortical Membrane Potential Signature of Optimal States for Sensory Signal Detection. *Neuron* 87:179-192.
- McGinley MJ, Vinck M, Reimer J, Batista-Brito R, Zaghera E, Cadwell CR, Tolias AS, Cardin JA, McCormick DA (2015b) Waking State: Rapid Variations Modulate Neural and Behavioral Responses. *Neuron* 87:1143-1161.
- McKeeff TJ, Tong F (2007) The timing of perceptual decisions for ambiguous face stimuli in the human ventral visual cortex. *Cereb Cortex* 17:669-678.
- Mednick SA (1962) The Associative Basis of the Creative Process. *Psychol Rev* 69:220-232.
- Melloni L, Schwiedrzik CM, Muller N, Rodriguez E, Singer W (2011) Expectations change the signatures and timing of electrophysiological correlates of perceptual

awareness. *J Neurosci* 31:1386-1396.

Metcalf J (1986) Premonitions of insight predict impending error. *J Exp Psychol: Learning, Memory, and Cognition* 12:623.

Minami T, Noritake Y, Nakauchi S (2014) Decreased beta-band activity is correlated with disambiguation of hidden figures. *Neuropsychologia* 56:9-16.

Moca VV, Tincas I, Melloni L, Muresan RC (2011) Visual exploration and object recognition by lattice deformation. *PLoS ONE* 6:e22831.

Moratti S, Mendez-Bertolo C, Del-Pozo F, Strange BA (2014) Dynamic gamma frequency feedback coupling between higher and lower order visual cortices underlies perceptual completion in humans. *Neuroimage* 86:470-479.

Murphy PR, Robertson IH, Balsters JH, O'Connell R G (2011) Pupillometry and P3 index the locus coeruleus-noradrenergic arousal function in humans. *Psychophysiology* 48:1532-1543.

Nassar MR, Rumsey KM, Wilson RC, Parikh K, Heasley B, Gold JI (2012) Rational regulation of learning dynamics by pupil-linked arousal systems. *Nat Neurosci* 15:1040-1046.

Nikolic D, Moca VV, Singer W, Muresan RC (2008) Properties of multivariate data investigated by fractal dimensionality. *J Neurosci Meth* 172:27-33.

Ohlsson S (1984) Restructuring revisited: II. An information processing theory of restructuring and insight. *Scand J Psychol* 25:117-129.

Okazaki M, Kaneko Y, Yumoto M, Arima K (2008) Perceptual change in response to a bistable picture increases neuromagnetic beta-band activities. *Neurosci Res* 61:319-328.

Ollinger M, Jones G, Knoblich G (2008) Investigating the effect of mental set on insight problem solving. *Exp Psychol* 55:269-282.

Oostenveld R, Fries P, Maris E, Schoffelen JM (2011) FieldTrip: Open Source Software for Advanced Analysis of MEG, EEG, and Invasive Electrophysiological Data. *Comput Intel Neurosc.* 2011:1-9

Palva JM, Palva S, Kaila K (2005) Phase synchrony among neuronal oscillations in the human cortex. *J Neurosci* 25:3962-3972.

Palva S, Palva JM (2011) Functional roles of alpha-band phase synchronization in local and large-scale cortical networks. *Front Psychol* 2:204.

Partala T, Surakka V (2003) Pupil size variation as an indication of affective processing. *Int J Human-Comput St* 59:185-198.

Pesonen M, Hamalainen H, Krause CM (2007) Brain oscillatory 4-30 Hz responses during a visual n-back memory task with varying memory load. *Brain Res* 1138:171-177.

Pfurtscheller G, Stancak A, Jr., Neuper C (1996) Event-related synchronization (ERS) in the alpha band--an electrophysiological correlate of cortical idling: a review. *Int J Psychophysiol* 24:39-46.

Piantoni G, Kline KA, Eagleman DM (2010) Beta oscillations correlate with the probability of perceiving rivalrous visual stimuli. *J Vis* 10:18.

Pogosyan A, Gaynor LD, Eusebio A, Brown P (2009) Boosting cortical activity at Beta-band frequencies slows movement in humans. *Curr Biol* 19:1637-1641.

Razumnikova OM (2000) Functional organization of different brain areas during convergent and divergent thinking: an EEG investigation. *Brain Res Cogn Brain Res*

10:11-18.

Razumnikova OM (2007) Creativity related cortex activity in the remote associates task. *Brain Res Bull* 73:96-102.

Reimer J, Froudarakis E, Cadwell CR, Yatsenko D, Denfield GH, Tolias AS (2014) Pupil fluctuations track fast switching of cortical states during quiet wakefulness. *Neuron* 84:355-362.

Reimer J, McGinley MJ, Liu Y, Rodenkirch C, Wang Q, McCormick DA, Tolias AS (2016) Pupil fluctuations track rapid changes in adrenergic and cholinergic activity in cortex. *Nat Commun* 7:13289.

Rosenberg JR, Amjad AM, Breeze P, Brillinger DR, Halliday DM (1989) The Fourier approach to the identification of functional coupling between neuronal spike trains. *Prog Biophys Mol Biol* 53:1-31.

Runco MA (2004) Creativity. *Annu Rev Psychol* 55:657-687.

Samaha J, Bauer P, Cimaroli S, Postle BR (2015) Top-down control of the phase of alpha-band oscillations as a mechanism for temporal prediction. *Proc Natl Acad Sci USA* 112:8439-8444.

Sandkuhler S, Bhattacharya J (2008) Deconstructing insight: EEG correlates of insightful problem solving. *PLoS ONE* 3:e1459.

Schoffelen JM, Oostenveld R, Fries P (2008) Imaging the human motor system's beta-band synchronization during isometric contraction. *Neuroimage* 41:437-447.

Seghier ML (2008) Laterality index in functional MRI: methodological issues. *Magn Reson Imaging* 26:594-601.

Sehatpour P, Molholm S, Schwartz TH, Mahoney JR, Mehta AD, Javitt DC, Stanton

PK, Foxe JJ (2008) A human intracranial study of long-range oscillatory coherence across a frontal-occipital-hippocampal brain network during visual object processing. *Proc Natl Acad Sci USA* 105:4399-4404.

Shen W, Yuan Y, Liu C, Luo J (2016) In search of the 'Aha!' experience: Elucidating the emotionality of insight problem-solving. *Br J Psychol* 107:281-298.

Shen W, Liu C, Yuan Y, Zhang X, Luo J (2013) Temporal dynamics of mental impasses underlying insight-like problem solving. *Sci China Life Sci* 56:284-290.

Sheth BR, Sandkuhler S, Bhattacharya J (2009) Posterior Beta and anterior gamma oscillations predict cognitive insight. *J Cogn Neurosci* 21:1269-1279.

Singer W (1999) Neuronal synchrony: a versatile code for the definition of relations? *Neuron* 24:49-65, 111-125.

Singer W, Gray CM (1995) Visual feature integration and the temporal correlation hypothesis. *Annu Rev Neurosci* 18:555-586.

Sporns O, Chialvo DR, Kaiser M, Hilgetag CC (2004) Organization, development and function of complex brain networks. *Trends Cogn Sci* 8:418-425.

Sprugnoli G, Rossi S, Emmerdorfer A, Rossi A, Liew S-L, Tatti E, di Lorenzo G, Pascual-Leone A, Santarnecchi E (2017) Neural correlates of Eureka moment. *Intelligence* 62: 99-118

Srinath R, Ray S (2014) Effect of amplitude correlations on coherence in the local field potential. *J Neurophysiol* 112:741-751.

Sternberg RJ, Davidson JE (1995) *The nature of insight*. Cambridge, The MIT Press.

Tallon-Baudry C, Bertrand O (1999) Oscillatory gamma activity in humans and its role in object representation. *Trends Cogn Sci* 3:151-162.

Uhlhaas PJ, Roux F, Singer W, Haenschel C, Sireteanu R, Rodriguez E (2009) The development of neural synchrony reflects late maturation and restructuring of functional networks in humans. *Proc Natl Acad Sci USA* 106:9866-9871.

Uhlhaas PJ, Linden DE, Singer W, Haenschel C, Lindner M, Maurer K, Rodriguez E (2006) Dysfunctional long-range coordination of neural activity during Gestalt perception in schizophrenia. *J Neurosci* 26:8168-8175.

van Stijn S, Barnes WH, Singer W, Lee HS (2016) Neuronal dynamics related to figure-ground modulations in V1 and V4 of the macaque monkey. In: Society for Neuroscience. (abstract)

Vartanian O, Goel V (2005) Task constraints modulate activation in right ventral lateral prefrontal cortex. *Neuroimage* 27:927-933.

Vinck M, Batista-Brito R, Knoblich U, Cardin JA (2015) Arousal and locomotion make distinct contributions to cortical activity patterns and visual encoding. *Neuron* 86:740-754.

Volberg G, Wutz A, Greenlee MW (2013) Top-down control in contour grouping. *PLoS ONE* 8:e54085.

Wilke M, Schmithorst VJ (2006) A combined bootstrap/histogram analysis approach for computing a lateralization index from neuroimaging data. *Neuroimage* 33:522-530.

Zanto TP, Chadick JZ, Gazzaley A (2014) Anticipatory alpha phase influences visual working memory performance. *Neuroimage* 85 Pt 2:794-802.

Zanto TP, Rubens MT, Bollinger J, Gazzaley A (2010) Top-down modulation of visual feature processing: the role of the inferior frontal junction. *Neuroimage* 53:736-745.

Zanto TP, Rubens MT, Thangavel A, Gazzaley A (2011) Causal role of the prefrontal cortex in top-down modulation of visual processing and working memory. *Nat Neurosci* 14:656-661.

Zhao Q, Zhou Z, Xu H, Chen S, Xu F, Fan W, Han L (2013) Dynamic neural network of insight: a functional magnetic resonance imaging study on solving Chinese 'chengyu' riddles. *PLoS ONE* 8:e59351.

List of Abbreviations

Aha	Eureka (Aha) effect
Ctrl	control
Diff	difference between Aha and Ctrl (Aha minus Ctrl)
EEG	electroencephalography
FFT	fast Fourier transform
fMRI	functional magnetic resonance imaging
HCGSN	HydroCel Geodesic Sensor Net
ICA	independent component analysis
ITI	inter-trial intervals
LC	left central (area)
LF	left frontal (area)
LI	laterality index
LO	left occipital (area)
LP	left parietal (area)
LT	left temporal (area)
MCP	multiple comparisons problem
PET	positron emission tomography
PLV	phase locking value
RAT	remote associates test
RC	right central (area)
RF	right frontal (area)
RO	right occipital (area)
RP	right parietal (area)
RT	right temporal (area)
RTs	reaction times

List of Figures

Figure 1-1. Black and white image of a blurred stimulus.....	9
Figure 1-2. The grayscale image.....	11
Figure 1-3. Gabor elements without (left) and with (right) a figure closed contour. ..	11
Figure 2-1. The procedure of image manipulating.	14
Figure 2-2. The recognition task stimulus (Experiment 1).....	17
Figure 2-3. The procedure of Experiment 2.....	19
Figure 2-4. The position of ten clusters on HCGSN-128 EEG recording system.	23
Figure 3-1. Examples of images with different recognition difficulty in Experiment 1.	28
Figure 3-2. The response percentages per degradation level (per cut-off frequency).	29
Figure 3-3. The distribution of reaction times (RTs).....	30
Figure 3-4. The alpha coherence matrix of channels (stimulus locked epochs).....	32
Figure 3-5. The topographic distribution of alpha coherence of channels (stimulus locked epochs).	32
Figure 3-6. The laterality index (LI) of alpha coherence of channels (stimulus locked epochs).	33
Figure 3-7. The alpha PLV matrix of channels (stimulus locked epochs).....	34
Figure 3-8. The topographic distribution of alpha PLV of channels (stimulus locked epochs).	35
Figure 3-9. The laterality index (LI) of alpha PLV of channels (stimulus locked epochs).	35
Figure 3-10. The alpha power before response.....	38
Figure 3-11. The alpha coherence matrix of channels (response locked epochs).	39
Figure 3-12. The topographic distribution of alpha coherence of channels (response locked epochs).	39
Figure 3-13. The laterality index (LI) of alpha coherence of channels (response locked epochs).	40
Figure 3-14. The alpha coherence matrix of channel clusters (response locked epochs).	40
Figure 3-15. Topographic distribution of alpha coherence of channel clusters	

(response locked epochs).	41
Figure 3-16. Laterality index (LI) of alpha coherence of channel clusters (response locked epochs).	41
Figure 3-17. The alpha PLV matrix of the channel clusters (response locked epochs).	42
Figure 3-18. Topographic distribution of alpha PLV of channel clusters (response locked epochs).	43
Figure 3-19. Laterality index (LI) of alpha PLV of channel clusters (response locked epochs).	43
Figure 3-20. The theta coherence matrix of channels (stimulus locked epochs).....	45
Figure 3-21. The topographic distribution of theta coherence of channels (stimulus locked epochs).	45
Figure 3-22. The laterality index (LI) of theta coherence of channels (stimulus locked epochs).	46
Figure 3-23. The theta coherence matrix of channel clusters (stimulus locked epochs).	46
Figure 3-24. Topographic distribution of theta coherence of channel clusters (stimulus locked epochs).	47
Figure 3-25. The laterality index (LI) of theta coherence of channel clusters (stimulus locked epochs).	47
Figure 3-26. The theta PLV matrix of channels (stimulus locked epochs).	48
Figure 3-27. The topographic distribution of theta PLV of channels (stimulus locked epochs).	49
Figure 3-28. The laterality index (LI) of theta PLV of channels (stimulus locked epochs).	49
Figure 3-29. The theta PLV matrix of channel clusters (stimulus locked epochs).....	50
Figure 3-30. Topographic distribution of theta PLV of channel clusters (stimulus locked epochs).	50
Figure 3-31. The laterality index (LI) of theta PLV of channel clusters (stimulus locked epochs).	51
Figure 3-32. The beta power after stimulus onset.....	52
Figure 3-33. The beta power before response.....	53
Figure 3-34. The dimensionality for ten channel clusters, in the time window: 0 s – 0.5 s.	55
Figure 3-35. The dimensionality for ten channel clusters, in the time window: -0.5 s – 0 s.	56
Figure 3-36. The pupil size for trials with RTs > 0.5 s (stimulus locked epochs).....	57

Figure 3-37. The pupil size for trials with RTs > 1.0 s (stimulus locked epochs).....	58
Figure 3-38. The pupil size for trials with RTs > 1.5 s (stimulus locked epochs).....	58
Figure 3-39. The pupil size for trials with RTs > 2.0 s (stimulus locked epochs).....	58
Figure 3-40. The pupil size for trials with RTs > 0.5 s (response locked epochs).	59
Figure 3-41. The pupil size for trials with RTs > 1.0 s (response locked epochs).	59
Figure 3-42. The pupil size for trials with RTs > 1.5 s (response locked epochs).	60
Figure 3-43. The pupil size for trials with RTs > 2.0 s (response locked epochs).	60
Figure S1 (a, b, c). The coherence of channels (stimulus locked epochs).....	63
Figure S2 (a, b, c). The PLV of channels (stimulus locked epochs).....	66
Figure S3 (a, b, c). The coherence of channels (response locked epochs).	69
Figure S4 (a, b, c). The PLV of channels (response locked epochs).	72
Figure S5. The coherence of channel clusters (response locked epochs).....	73
Figure S6. The PLV of channel clusters (response locked epochs).....	74
Figure S7. The coherence of channel clusters (stimulus locked epochs).	75
Figure S8. The PLV of channel clusters (stimulus locked epochs).	76

Acknowledgements

I am extremely grateful to the many people who have helped me in this study.

I would like to thank my supervisor Prof. Wolf Singer, who provided me precious support to conduct this research. Thank you for your guidance, encouragement and advice you have provided in all the time of my research and writing of this thesis. You have been a great mentor for me. I appreciate your sharing of your vast knowledge in science, philosophy and art, which are invaluable for helping me grow as a scientist.

I am also grateful to my supervisors Prof. Ralf Galuske and Prof. Bodo Laube, for your guidance and assistance. Thank you for your support during my study. Without your support, it would not have been possible to finish this thesis.

I want to thank Prof. Michael Wibral, Prof. Danko Nikolic, Dr. Barbara Händel, and Prof. Lucia Melloni for your very helpful discussions, thank Dr. Gareth Bland for collaboration in the dimensionality analysis. I am also very grateful to Dr. William Barnes, Dr. Nina Merkel and Björn Mattes for your insightful comments for this thesis.

I must also acknowledge my colleagues from the Max Planck Institute for Brain Research, the Frankfurt Institute for Advanced Studies, and the Ernst Strüngmann Institute for Neuroscience in Cooperation with Max Planck Society, for your feedback, cooperation and friendship.

Finally, I must express my gratitude to my family, for providing me with continuous support and encouragement throughout my study.

Lebenslauf

Yiqing Lu

Date of Birth: August 28th, 1984

Nationality: China

Max Planck Institute for Brain Research

Deutschordenstr. 46

60528 Frankfurt am Main, Germany

Email: yiqing.lu@brain.mpg.de

- | | |
|----------------|--|
| 2013 - present | Fachbereich Biologie, Technische Universität Darmstadt |
| 2011 - present | Max Planck Institute for Brain Research; Ernst Strüngmann Institute for Neuroscience in Cooperation with Max Planck Society; Frankfurt Institute for Advanced Studies, Frankfurt am Main |
| 2008 - 2011 | Master, Pathology and Pathophysiology, School of Medicine, Zhejiang University |
| 2007 - 2011 | Center of Disease Modeling, School of Medicine, Zhejiang University |
| 2004 - 2006 | Undergraduate Research Programs, Department of Physiology and Department of Anatomy, School of Medicine, Zhejiang University |
| 2003 - 2008 | Bachelor, Basic Medical Sciences, School of Medicine, Zhejiang University |

Ehrenwörtliche Erklärung

Ich erkläre hiermit ehrenwörtlich, dass ich die vorliegende Arbeit entsprechend den Regeln guter wissenschaftlicher Praxis selbstständig und ohne unzulässige Hilfe Dritter angefertigt habe.

Sämtliche aus fremden Quellen direkt oder indirekt übernommenen Gedanken sowie sämtliche von Anderen direkt oder indirekt übernommenen Daten, Techniken und Materialien sind als solche kenntlich gemacht. Die Arbeit wurde bisher bei keiner anderen Hochschule zu Prüfungszwecken eingereicht.

Frankfurt am Main, den

.....